Development of subject-specific representations of neuroanatomy via a domain-specific language

Antonia Machlouzarides-Shalit

université
PARIS-SACLAY

Development of subject-specific representations of neuroanatomy via a domain-specific language

Thèse de doctorat de l'université Paris-Saclay

École doctorale n° 580, Sciences et technologies de l'information et de la communication (STIC)
Spécialité de doctorat: Informatique
Unité de recherche: Université Paris-Saclay, Inria, Inria Saclay-Île-de-France, 91120, Palaiseau, France.
Référent: faculté des sciences d'Orsay

Thèse présentée et soutenue en visioconférence totale, le 15-12-2020, par

Antonia Machlouzarides-Shalit

Composition du jury:

Olivier Coulon Directeur de Recherche, Aix-Marseille Université	Président
Roberto Toro Directeur de Recherche, Institut Pasteur	Rapporteur et Examinateur
Michel Dojat Directeur de Recherche, Grenoble Institute des Neuro-sciences	Rapporteur et Examinateur
Stephanie Forkel Postdoc avancé/jeune chercheur, Université de Bordeaux	Examinatrice
Philippe Ciuciu Chercheur expert senior, CEA, Université Paris-Saclay	Examinateur
Demian Wassermann Chargé de Recherche, INRIA Paris-Saclay	Directeur de thèse

Thèse de doctorat

NNT: 2020UPASG041

ABSTRACT

The field of brain mapping is rapidly expanding, providing further insights into the spatial organisation of the brain and the relationships of cortical features. The development of brain mapping tools is dependent on the profound grasp of the anatomy of the brain. We identified the need for the development of a brain mapping tool which is grounded in the detailed knowledge of individual sulci. In this thesis, we develop a new brain mapping tool called NeuroLang, which utilises the spatial geometry of the brain to demonstrate subject-specific representations of sulcal morphology.

We approach this challenge with two perspectives: firstly, we situate our theory firmly in the comprehensive characterisations of sulci from the literature, or 'classical neuroanatomy'. We survey the wealth of information on neuroanatomical characterisation, consider the organisation of cortical features, and examine brain-mapping techniques in neuroimaging and their capabilities. Secondly, we design and implement methods for sulcus-specific queries in our domain-specific language, NeuroLang. We lay out the theoretical bases for NeuroLang in terms of the representation of the brain as a 3D object and of the foundation of a domain-specific language grounded in first-order logic. We test our method on 52 subjects of the Human Connectome Project dataset and evaluate the performance of NeuroLang for population and subject-specific representations of neuroanatomy. Then, we interpret the quantification of the results of sulcal identification as an evaluation of sulcal stability, and establish a novel, data-driven hierarchical organisation of sulci.

Finally, we review the relevance of using sulci as cortical markers, and the implication of a subject-specific sulcal mapping tool for representing cortical anatomy. We relate the significance of sulcal patterns as associative measures to other cortical features such as cytoarchitectonics. We examine the implications of NeuroLang, its applications and its limitations. To conclude, we summarise the implication of our method within the current field, as well as our overall contribution to the field of brain mapping. Our work paves the way for future development of neuroimaging tools which prioritise individual variability and neuroanatomical inference.

ACKNOWLEDGMENTS

This work would not be possible without the invaluable contributions of my supervisor, Demian Wassermann. I thank him for his endless guidance, patience, and availability. I strive to improve skills I have learned from him, both directly and indirectly.

I thank the members of the jury: Roberto Toro, Michel Dojat, Olivier Coulon, Stephanie Forkel, and Philippe Ciuciu for taking the time to review this thesis and for their supportive and constructive comments.

I extend my gratitude to our collaborator, Nikos Makris at Harvard University, for insightful conversations and sharing the complex and beautiful world of classical neuroanatomy with me.

Science is a collaborative journey, and I thank all the members of the Parietal team at Inria Paris-Saclay and the Athena team at Inria Sophia-Antipolis for their help and friendship these past few years.

I owe a lifetime of gratitude to my parents, my family and my friends.

Finally, I thank ANR NeuroRef for funding my thesis.

CONTENTS

1 OVERVIEW

The development of brain mapping tools is grounded in the extensive grasp of the anatomy of the brain. The ability for brain mapping tools to accurately and efficiently capture the individual variability of neuroanatomical morphology, while remaining relevant for every brain, is a particularly difficult balance to strike. Typically, the most reliable way of conserving detailed individual morphology of sulci is through manual labelling, which is tedious, time-consuming work which requires extensive knowledge of classical neuroanatomy. This body of knowledge is also notoriously inconsistent in terms in naming and morphology, and therefore could manifest as inconsistencies depending on who is doing the labelling and according to which framework. To combat this, extensive work has been carried out on template-based brain mapping methods, which focus on the identification of landmarks relative to which a predetermined set of brain regions are superimposed. We identified the need for the development of a brain mapping tool which is grounded in the detailed knowledge of individual variability of sulci.

In this thesis, we develop a new brain mapping tool called NeuroLang, which utilises the spatial geometry of the brain to demonstrate subject-specific representations of sulcal morphology. We approach this challenge with two perspectives: firstly, we ground our theory firmly in the comprehensive characterisations of sulci from the literature, or 'classical neuroanatomy'. Secondly, we design and implement methods for sulcus-specific queries in the domain-specific language NeuroLang. We evaluate the performance of NeuroLang for population and subject-specific representations of neuroanatomy. From our results, we determine a data-driven hierarchical organisation of sulci. In this chapter, we outline the structure of this manuscript.

In the introductory part, we survey the wealth of information on neuroanatomical characterisation, consider the organisation of cortical features, and examine brain-mapping techniques in neuroimaging and their capabilities. We establish a literature-based hierarchical organisation of the sulci which provide the framework for our sulcal atlas, and establish the rules of spatial geometry and first-order logic which act as a framework for NeuroLang.

In the next part, we present our work on the design and implementation of NeuroLang. Firstly, we present our collaborative work on administering anatomical names to images in a dictionary of functional modes. Next,

we demonstrate how we design and construct sulcus-specific queries and evaluate their performances. We present the results of our experiment using NeuroLang. We demonstrate how we validate the sensitivity of our results, the results on the population level, and subject-specific outcomes. Lastly, we interpret the quantification of the results of sulcal identification as an evaluation of sulcal stability, and determine a novel, data-driven method for the hierarchical organisation of sulci.

Finally, we review and discuss the relevance of using sulci as cortical markers, and the implication of a subject-specific sulcal mapping tool for representing cortical anatomy. We relate the significance of sulcal patterns as associative measures to other cortical features such as cytoarchitectonics. We examine the implications of NeuroLang, its applications and its limitations.

To conclude, we summarise the implication of our method within the current field, as well as our overall contribution to the field of brain mapping. Our work paves the way for future development of neuroimaging tools which prioritise individual variability and neuroanatomical inference.

2 RÉSUMÉ

La cartographie cérébrale est un domaine actif de recherche, en croissance rapide, apportant de plus en plus de données sur l'organisation spatiale du cerveau. Le développement des outils de cartographie cérébrale repose sur une compréhension approfondie de l'anatomie du cerveau. De fait, il est essentiel de comprendre les caractéristiques corticales communes d'une population, ainsi que les sources et degrés de variabilité qui contribuent aux spécificités individuelles. En règle générale, le moyen le plus fiable de conserver la morphologie individuelle détaillée des sulci est l'étiquetage manuel. Ce travail fastidieux et chronophage nécessite une connaissance approfondie de la neuroanatomie classique. De plus, cet ensemble de connaissances est notoirement incohérent en termes de dénomination et de morphologie. Ainsi, l'étiquetage peut dépendre de son auteur et de son cadre d'utilisation. Pour lutter contre cela, des travaux approfondis ont été menés sur des méthodes de cartographie cérébrale basées sur des modèles, qui se concentrent sur l'identification de points de repère par rapport auxquels un ensemble prédéterminé de régions cérébrales se superpose. Nous avons identifié la nécessité de développer un outil de cartographie cérébrale qui repose sur la connaissance détaillée de la variabilité individuelle des sulci.

Dans cette thèse, nous développons un nouvel outil de cartographie cérébrale: le language NeuroLang, reposant sur les spécificités géométriques individuelles des sulci et la logique du premier ordre. Nous avons abordé cette question avec deux approches. Premièrement, nous ancrons fermement notre théorie dans la caractérisation complète des sulci de la littérature en neuroanatomie classique. Deuxièmement, nous concevons et implémentons des composants et des requêtes spécifiques au sulcus dans le langage NeuroLang. Nous avons évalué les performances de NeuroLang pour les représentations de la neuroanatomie spécifiques à la population et au sujet. Dans ce chapitre, nous décrivons la structure de ce manuscrit.

Dans la partie introductive, nous passons en revue la richesse des informations sur la caractérisation neuroanatomique, considérons l'organisation des caractéristiques corticales et examinons les techniques actuelles de cartographie cérébrale en neuroimagerie et leurs capacités. Nous établissons une organisation hiérarchique des sulci basée sur la littérature qui a fourni le cadre de notre atlas sulcal, et établissons des règles de géométrie

spatiale et de logique de premier ordre qui agissent comme un cadre pour NeuroLang.

Dans la partie suivante, nous présentons nos travaux sur la conception et la mise en œuvre de NeuroLang. Premièrement, nous présentons notre travail collaboratif sur l'attribution de noms anatomiques aux images dans un dictionnaire de modes fonctionnels.Ensuite, nous montrons comment nous concevons et construisons des requêtes spécifiques aux sulcus et évaluons leurs performances. Nous présentons les résultats de notre expérience utilisant NeuroLang. Nous démontrons comment nous validons la sensibilité de nos résultats, les résultats au niveau de la population et les résultats spécifiques à la matière. Enfin, nous utilisons la quantification des résultats de l'identification des sulci comme un critère d'évaluation de stabilité, et établissons une nouvelle méthode guidée par les données pour l'organisation hiérarchique des sulci.

Enfin, nous passons en revue et discutons de la pertinence de l'utilisation des sulci comme marqueurs corticaux, et de l'implication d'un outil de cartographie sulcal spécifique au sujet pour représenter l'anatomie corticale. Nous relions l'importance des modèles sulcaux en tant que mesures associatives à d'autres caractéristiques corticales telles que la cytoarchitectonique. Nous examinons les implications de NeuroLang, ses applications et ses limites.

Pour conclure, nous résumons l'implication de notre travail dans le domaine, ainsi que notre contribution globale au domaine de la cartographie cérébrale. Nos travaux ouvrent la voie au développement futur d'outils de neuroimagerie qui donnent la priorité à la variabilité individuelle et à l'inférence neuroanatomique.

Part I

NEUROANATOMY IN NEUROIMAGING ANALYSES

3 THE STUDY OF NEUROANATOMY

Form and function of the human brain are inextricably linked. An open and ongoing question in neuroscience is which is more dependent on the other. When it comes to deciphering the actions and outputs of the brain, it is vital to be able to locate oneself within its space; not only to give an output a dimension, but to associate a location with other brain characteristics such as structural relationships and connectivity with other regions.

3.1 THE CORTEX

The brain is composed of white matter and grey matter. White matter is composed of the axons of neurons, which connect different brain regions to each other. They appear white due to the fatty myelin sheaths surrounding them as insulation for better conduction of electrical signals. Grey matter is largely comprised of the rest of the neuronal cell parts, the somas, dendrites and terminal endings. These appear grey because they do not have myelin (Catani and Schotten, 2013).

The cerebral cortex is the outermost layer of the brain. A very thin layer of about only 2.5mm, it is composed primarily of grey matter (Heuer and Toro, 2019). The cortex (plural, cortices) is necessary for carrying out numerous functions and actions, both directly and indirectly. Constituting the majority of the corticocortical connection terminals, the arrangement of the cortex is imperative to the deduction of structural and functional connectivity in neuroimaging analyses (Toro, Fox, and Paus, 2008). Across mammalian species, the surface area of the cortex varies greatly and the variable folding patterns reflect this property (Heuer et al., 2019; Heuer and Toro, 2019). During the course of human evolution, human brain size has remained relatively stable while the lobes expanded and connectivity increased (Rilling, 2014). As a compensatory mechanism, the human cortex is among the most highly folded from all the species (Heuer et al., 2019), with a vast collection of sulcal labels with varying stability.

The types of cortices which exist are dependent on the organisation of the cell types which make them up, and the neocortex is the largest one (Kennedy et al., 1998). The cortex is made up of outer, concave protrusions called gyri (single, gyrus) and inner, convex indentations, called sulci

(single, sulcus). We can think of the cortex of the brain as a 2D surface if we unfold and flatten this outer layer of elevations and valleys, much like flattening a tablecloth (Fischl, Liu, and Dale, 2001; Lohmann, Von Cramon, and Colchester, 2008). The cortex is so highly convoluted that 2/3 of the surface of the brain is actually hidden within the sulci (Van Essen and Drury, 1997; Zilles et al., 1988). This folding process begins during gestation and only slows significantly during young adulthood (Chi, Dooling, and Gilles, 1977). There is a general folding pattern which serves as a draft for the overlap of sulcal arrangements in the general population. This is because the first sulci to develop during gestation and infancy are among the deepest sulci and are the most stable and reliable in their location, depth and shape (Chi, Dooling, and Gilles, 1977; Pizzagalli et al., 2019). These sulci are dictated chiefly by genetics and driven by earlier mechanical movements and are thus less susceptible to change over the course of neurodevelopment (Chi, Dooling, and Gilles, 1977; Heuer and Toro, 2019; Pizzagalli et al., 2019).

THE HISTORY OF NEUROANATOMY For centuries brains were analysed only *ex vivo* (Catani and Schotten, 2013). Gross neuroanatomy, on the macroscale, consisted of identification and labelling of brain regions visible to the naked eye. Soon, patterns began emerging of visible landmarks which delineated the brain into functional territories defined as *lobes*. Anatomists used these landmarks, soon to be characterised as *primary sulci*, to orientate themselves in the topography of the brain (Auzias et al., 2013). From these landmarks, relations implying relativity to the primary landmarks provided a method for characterising the remaining gyri and sulci. The directional terms developed in classical neuroanatomy refer to relative location in space without a precise coordinate system, much like north, south, east, west in cartography. Due to the lack of systematisation, there were eventually many terms to designate the same relation, such as anterior/rostral, posterior/caudal, superior/dorsal, and inferior/ventral (Catani and Schotten, 2013). The English and Latin terms designate the same relationship in the central nervous system, but the Latin terms do not necessarily correspond to the same relationship when in reference to the body. For this reason and to conserve simplicity, we henceforth utilise only the English directional terms.

3.1.1 Importance of sulci in neuroscience

Sulci form landmarks on the cortex visible to the naked eye. Descriptive anatomy provides names for sulci based on their location on the cortex (Catani and Schotten, 2013). The classification of sulci is based on characteristics including location, depth and relationship to other brain regions

(Duvernoy, 1999; Ono, Kubik, and Abernathey, 1990; Rademacher et al., 1992).

Primary sulci are among the first to develop during gestation and are the least variable across individuals, due largely to their dependence on genetics and their relationship to primary functional areas (Duvernoy, 1999; Ono, Kubik, and Abernathey, 1990). The further away a region is from primary functional areas, the more variable and unreliable the morphology of a region becomes due to the integrative nature of the functional area and the dependence of the region's development on environmental factors, as well as genetic (Rademacher et al., 1993). This 'distance' of a region can be both functional and physical. As an example, Margulies et al. (2016) showed how gradients of functionality are evenly dispersed across the cortex, where 'hubs' of the default mode network are found at equidistant points from the primary functional areas.

Though still not fully understood, the relevance of cortical folding to other aspects of neurobiology are becoming increasingly clear with the evolution of advanced brain imaging techniques. It is postulated that folding patterns give rise to connectivity patterns (Toro, Fox, and Paus, 2008; Van Essen, 1997), act as cytoarchitectonic markers and boundaries (Amunts et al., 1999; Eickhoff et al., 2005b; Kujovic et al., 2013; Vogt et al., 1995), and correlate with functional regions (Amunts et al., 2004; Eichert et al., 2020; Sprung-Much and Petrides, 2020). Variability exists for all sulci, to varying degrees. A number of factors contribute to the morphology of sulci, with varying ratios. Typically, the first sulci to form during foetal life are landmarks in cortical development and anatomy, and are considered by many as 'primary sulci.' These sulci exhibit certain characteristics which make them good contenders as cortical landmarks for atlases. The following characteristics are favourable in primary sulci and thus make them excellent landmarks and reference points in atlases:

- **Location:** Primary sulci are used to chart the lobes of the hemispheres into frontal, temporal, parietal and occipital. Their locations do not fluctuate enough to not be discernible by eye as lobe delineators. They are considered as the most stable and reliable sulci of the brain in terms of their location (Duvernoy, 1999).

- **Depth**: The first sulci to develop during gestation are among the deepest across the cortex (Chi, Dooling, and Gilles, 1977; Ono, Kubik, and Abernathey, 1990). With advanced neuroimaging techniques, it is common to 'inflate' the cortex, to make deeper sulci clearer to distinguish and thus view lobular differences more clearly. The primary sulci retain their places on the cortex even when very inflated, acting as lobular partitions, while the surrounding shallower sulci

which are more susceptible to inter-individual differences are mostly smoothed out (Fischl, Sereno, and Dale, 1999).

- **Shape:** Most of the surface of a sulcus is hidden within itself, in the folds. On the surface, the fold creates a line shape which is distinguishable by eye. Beneath the surface, the sulcus may have a different shape, branching, or connections with surrounding sulci. Ono, Kubik, and Abernathey (1990) have extensively catalogued the various morphologies of sulci on the surface, while more advanced techniques have been used to model the shape of primary sulci within the folds (Cykowski et al., 2008). The reliable depth of primary sulci also suggests that there is less variability of the inner sulcus shape.

- **Relationships to surrounding sulci:** Supposing that primary sulci are used as primary localisers for cortical navigation, the cartography of the brain is charted relative to these landmarks. Other sulci typically develop later and are shallower or more irregular, which generates larger variability in their morphologies. Despite this, what remains stable is their relative spatial location to the primary sulci. Regardless of their absolute location, size and shape, their characterisation in relation to the primary sulci remains unchanged, and a defining feature of a sulcus.

- **Susceptibility to influences:** All sulci are subject to genetic, environmental, and mechanical influences to varying degrees. The ratio of influence is different for sulci which appear at different stages of life and at different locations on the cortex. The earliest appearances of evidence of cortical folding begins in the first trimester of gestation, but formed sulci do not appear until the last trimester (Chi, Dooling, and Gilles, 1977). During brain growth, the cortical folding patterns are also susceptible to the mechanical properties of the brain; that is, the constrained volume and shape (Heuer and Toro, 2019). The order in which the sulci form affects how susceptible the formation of the sulcus is to mechanical influences on morphogenesis. This susceptibility is another element which factors in to how stable and reliable the sulcus is on the cortex.

- **Existence in all healthy brains:** There exists a group of sulci which are always localised in humans. Across numerous literature sources, a group of about 20 sulci on the neocortex are consistently reported. They always include the interlobular, 'primary' sulci, and include a subset of all the sulci found in each lobe. Typically, the sulci described in each lobe are the most continuous, deepest, and reliable in terms of their location. The most 'stable' sulci are an embodiment of the properties mentioned here. A representation of the hierarchical

organisation of sulcal stability in 3 literature sources is depicted in Figure 3.1.

3.1.1.1 *Importance of sulci in cytoarchitectonics*

Sulci have long been used as visual cues to delineate various boundaries on the cortex. Those boundaries may be defined functionally, anatomically, cytoarchitectonically or myeloarchitectonically (Catani and Schotten, 2013; Lohmann, Von Cramon, and Colchester, 2008). Cytoarchitecture tells us a lot about how the composition of the layers of the cortex are structured. The cortex is composed of 6 layers, with varying cell types which dictate their functions (Amunts, Schleicher, and Zilles, 2007; Brodmann, 2007; Fischl et al., 2008). The cell types and their arrangements of their layers make up a large portion of the microstructural organisation of the brain. The functional anatomy of the brain is closely linked to the structural anatomy (Lohmann, Von Cramon, and Colchester, 2008). The microstructure, in turn, is closely linked to the functional organisation and connectivity of brain regions (Amunts et al., 2020).

It has been established that sulci can act as borders for cytoarchitectonic areas or functional territories (Rademacher et al., 1992), but the concept is still debated (Fischl et al., 2008). However, it is difficult to determine the cytoarchitectonic organisation of the cortex without invasive methods. Probabilistic atlases, like the JulichBrain Cytoarchitectonic Atlas help (Amunts et al., 2020), but the identification of cytoarchitectonic regions of interest still heavily relies on the macroanatomical features (Amunts, Schleicher, and Zilles, 2007; Auzias, Coulon, and Brovelli, 2016). Mapping the macroanatomical features on the individual level may complement atlases for cytoarchitectonics. But first, it's important to ensure a comprehensive understanding of sulcal morphology and their relationships to other cortical features.

3.2 LITERATURE REVIEW OF SULCI

A comprehensive overview of the anatomical traits of each sulcus is necessary in order to construct queries which are loyal to their classical neuroanatomy descriptions. Prior to designing the queries which search for sulci, or even the descriptors or relationships for the basis of our tool, we must gather information on sulcal characterisations from the literature.

In this section, we present our extensive literature review of each sulcus included in Figure 3.1. We cover sulcal position on the cortex, development, relationships to surrounding sulci, segmentation, branching, and relationships to cytoarchitectonic areas, where relevant.

We refer the reader more interested in the application of this review to our organisation of the cortex to the next section, Organisation of Sulci, 3.3.

3.2.1 Primary sulci

LATERAL FISSURE The lateral, or Sylvian, fissure is the most characteristic, constant feature of the lateral surface, and is therefore regarded as the most reliable anatomical landmark (Ono, Kubik, and Abernathey, 1990; Rademacher et al., 1992). It is distinctively one of the most deep fissures of the entire brain, and the first to appear in each hemisphere during gestation, at 14-19 weeks (Chi, Dooling, and Gilles, 1977; Ono, Kubik, and Abernathey, 1990). It has a general longitudinal trajectory, coursing from the frontal opercula to the superior parietal lobule, acting as the main demarcator between the frontal, parietal and temporal lobes, the insula and the opercula (Catani and Schotten, 2013; Destrieux et al., 2010). It exists as a main fissure with numerous extensions and side branches, many of which possess reliable appearances and have thus been characterised and others which have contrasting nomenclatures and appearances and are broadly described as generic side-branches (Ono, Kubik, and Abernathey, 1990; Rademacher et al., 1992). Anatomists have generally divided the lateral fissure between three and 10 parts (Destrieux et al., 2010; Ono, Kubik, and Abernathey, 1990; Rademacher et al., 1992). The posterior horizontal ramus is the main trunk of the fissure, and the deepest segment. It runs posteriorly and terminates posterior to the postcentral sulcus, between the parietal and temporal lobes (Rademacher et al., 1992). Here, the fissure may extend superiorly or inferiorly at an angle, and may possess side branches such as the terminal ascending segment (Ono, Kubik, and Abernathey, 1990; Rademacher et al., 1992).

ANTERIOR ASCENDING AND HORIZONTAL RAMI OF THE LATERAL FISSURE The anterior projections of the lateral fissure are the anterior ascending, anterior horizontal and sometimes the diagonal rami of the lateral fissure (Catani and Schotten, 2013; Destrieux et al., 2010; Ono, Kubik, and Abernathey, 1990). These project superiorly and supero-anteriorly from the lateral fissure into the inferior frontal gyrus of the frontal lobe (Catani and Schotten, 2013; Destrieux et al., 2010; Duvernoy, 1999; Ono, Kubik, and Abernathey, 1990; Rademacher et al., 1992). They may connect with the surrounding sulci, the inferior frontal sulcus or the inferior segment of the precentral sulcus (Ono, Kubik, and Abernathey, 1990). Their locations are consistent as being anterior of the inferior portion of the precentral sulcus and inferior of the inferior frontal sulcus. The rami themselves act as boundaries to delineate the frontal operculum subdivisions into the

posterior pars opercularis, the middle pars triangularis and the anterior pars orbitalis (Brodmann, 2007; Rademacher et al., 1992). The positioning of these rami is fundamental in the placement of Brodmann areas 44 and 45, constituting Broca's area (Amunts et al., 1999).

CENTRAL SULCUS The central sulcus, or the fissure of Rolando, is a defining landmark on the lateral surface of the brain. Extending from the superior margin to the lateral fissure, it courses antero-ventrally in a continuous manner (Ono, Kubik, and Abernathey, 1990; Rademacher et al., 1992). It ends near the superior aspect of the circular sulcus of the insula, where it often, but not always, meets the lateral fissure, where the frontal, temporal and parietal lobes converge like tectonic plates (Destrieux et al., 2010; Duvernoy, 1999). It often, but not always, extends onto the medial surface (Duvernoy, 1999; Ono, Kubik, and Abernathey, 1990; Rademacher et al., 1992). The central sulcus is among the first sulci to develop in the embryonic brain, usually between 4 and 6 months/20-23 weeks of gestation (Chi, Dooling, and Gilles, 1977; Cykowski et al., 2008; Toi, Lister, and Fong, 2004). Chi, Dooling, and Gilles, 1977 observed its initial development first in the right hemisphere, followed by its appearance in the left hemisphere approximately a week later. Its early appearance in the foetal brain reflects its characteristic depth and continuity. Its depth may present asymmetrically according to various features, such as gender, age (Cykowski et al., 2008), handedness (Amunts et al., 2000) or musical abilities (Zilles et al., 1997). The central sulcus acts as a landmark to distinguish the frontal from the parietal lobes, as well as a cytoarchitectonic boundary between the giant pyramidal cells without an inner granular layer of the precentral gyrus (Brodmann area 4), and the apyramidal granular layer of the postcentral gyrus (Brodmann areas 3, 1, 2) (Brodmann, 2007; Pandya et al., 2015).

PARIETO-OCCIPITAL SULCUS The parieto-occipital sulcus is one of deepest sulci and one of the landmark sulci of the medial surface (Rademacher et al., 1992). Chi, Dooling, and Gilles, 1977 observed its appearance at the 16th gestational week. On the medial surface, the sulcus itself separates the parietal from the occipital lobes, and on the lateral surface, to which it almost always extends onto, its hypothetical line to the pre-occipital notch separates the occipital lobes from the parietal and temporal lobes (Catani and Schotten, 2013; Duvernoy, 1999; Ono, Kubik, and Abernathey, 1990). It cleaves the medial surface, starting at the postero-superior junction of the superior hemispheric margin and coursing antero-inferiorly, terminating just inferior of the posterior part of the callosal sulcus (Ono, Kubik, and Abernathey, 1990). Oftentimes, this inferior termination meets, or almost meets, the anterior termination of the calcarine sulcus, named the cuneal point (Duvernoy, 1999; Ono, Kubik, and Abernathey, 1990; Rademacher

et al., 1992). Here, the parieto-occipital sulcus separates the cingulate gyrus, and thus the limbic lobe, from the cuneus, and the cuneus from the precuneus (Catani and Schotten, 2013; Desikan et al., 2006; Margulies et al., 2009).

CALLOSAL SULCUS A distinctive reference landmark on the medial surface, the callosal sulcus gives reference to the location of the corpus callosum, separating it from the outer cingulate gyrus (Catani and Schotten, 2013; Chi, Dooling, and Gilles, 1977; Destrieux et al., 2010; Duvernoy, 1999). It is among the first sulci to develop during gestation, forming at the same time as the lateral fissure (Chi, Dooling, and Gilles, 1977).

CALCARINE SULCUS Among the first distinguishable sulci during neurodevelopment is the calcarine sulcus (Chi, Dooling, and Gilles, 1977). It forms a deep, frequently continuous sulcus which reaches from the occipital pole to just anterior and inferior of the splenium of the corpus callosum (Ono, Kubik, and Abernathey, 1990; Rademacher et al., 1992). This conjunction point is referred to as the cuneal point, where the calcarine sulcus often meets the parieto-occipital sulcus (Duvernoy, 1999; Ono, Kubik, and Abernathey, 1990; Rademacher et al., 1992). This is a principal landmark on the medial surface (Rademacher et al., 1992). Brodmann, 2007 correlates the calcarine sulcus with the primary visual cortex (Brodmann's area 17), remarking how much larger this area is than it appears due to the depth of the calcarine sulcus. It has been further distinguished cytoarchitecturally by the stripe of Gennari, a thick strip of horizontal fibres (Pandya et al., 2015).

3.2.2 Frontal lobe

FRONTOMARGINAL SULCUS The frontomarginal sulcus is a short sulcus located on or near the frontal pole (Duvernoy, 1999). Ono, Kubik, and Abernathey, 1990 reports it as mostly continuous (80% right hemisphere, 76% left hemisphere), but sometimes interrupted into two or three segments. Often, it manifests as a continued stem of other frontal lobe sulci, namely the superior, middle or inferior frontal sulci (Duvernoy, 1999; Ono, Kubik, and Abernathey, 1990) . Bludau et al., 2014 describe it as part of the "Fp1" or frontal pole 1, area. Fp1 is on the lateral surface and has cytoarchitectonic features which distinguish it from surrounding and medial areas (Bludau et al., 2014).

INFERIOR FRONTAL SULCUS The inferior frontal sulcus emanates anteriorly from the precentral sulcus in a longitudinal manner, mirroring its superior counterpart. It acts as the limit between the middle and inferior

frontal gyri (Catani and Schotten, 2013; Destrieux et al., 2010; Duvernoy, 1999; Rademacher et al., 1992). The junction with the precentral sulcus is generally perpendicular (Duvernoy, 1999; Ono, Kubik, and Abernathey, 1990). The inferior frontal sulcus often has a true connection with the inferior part of the precentral sulcus, though Ono, Kubik, and Abernathey, 1990 reported no junction at all in 12% of 50 hemispheres. They also reported frequent segmentation and branching of the inferior frontal sulcus, presenting as 2-4 segments in 44% and 60% of right and left hemispheres, respectively, and most commonly 2 upward side branches in the right hemisphere, 3 in the left hemisphere, and 2 downward side branches in the right and left hemispheres (Ono, Kubik, and Abernathey, 1990). It can also connect with surrounding sulci, including the middle and superior frontal sulci, frontomarginal sulcus and the rami of the lateral fissure (Ono, Kubik, and Abernathey, 1990).

SUPERIOR FRONTAL SULCUS The superior frontal sulcus anteriorly projects from the precentral sulcus in a longitudinal manner, mirroring its inferior counterpart. It acts as the limit between the superior and middle frontal gyri (Catani and Schotten, 2013; Destrieux et al., 2010; Duvernoy, 1999; Rademacher et al., 1992). The junction with the precentral sulcus is generally perpendicular, shown by Ono, Kubik, and Abernathey, 1990 in 32% and 48% of right and left hemispheres, respectively, and no junction at all in 8% of right hemispheres. They also reported frequent segmentation and branching of the superior frontal sulcus, presenting as 2-4 segments in 60% and 68% of right and left hemispheres, respectively, which sometimes overlapped (Ono, Kubik, and Abernathey, 1990). Furthermore, they reported many upward and downward side branches of this sulcus. The superior frontal sulcus can also connect with surrounding sulci, including the middle and inferior frontal sulci, and the frontomarginal sulcus (Ono, Kubik, and Abernathey, 1990).

MIDDLE FRONTAL SULCUS The middle, or intermediate, frontal sulcus is located inferiorly of the superior frontal sulcus and superiorly of the inferior frontal sulcus, coursing through the middle frontal gyrus (Destrieux et al., 2010). Its appearance varies from long and continuous to short and segmented (Destrieux et al., 2010; Ono, Kubik, and Abernathey, 1990). It may be independent or connected to surrounding sulci, including the precentral, superior frontal, inferior frontal and frontomarginal sulci (Catani and Schotten, 2013; Destrieux et al., 2010; Duvernoy, 1999; Ono, Kubik, and Abernathey, 1990).

OLFACTORY SULCUS The olfactory sulcus is a constant landmark on the ventral surface of the frontal lobe (Rademacher et al., 1992). It first forms

as a shallow depression around 16 weeks of gestation, around the same time as primary sulci such as the parieto-occipital sulcus, and deepens gradually (Chi, Dooling, and Gilles, 1977). It has a longitudinal trajectory, parallel and just lateral of the interhemispheric fissure, medial of the orbital sulci, and separates the orbital gyrus, gyrus rectus and olfactory gyrus (Catani and Schotten, 2013; Chi, Dooling, and Gilles, 1977; Destrieux et al., 2010; Rademacher et al., 1992).

ORBITAL SULCI The orbital sulci are a collection of several short sulci located on the ventral surface of the frontal lobe, including what Destrieux et al., 2010 have referred to as the medial and lateral orbital sulcus and what Ono, Kubik, and Abernathey, 1990 and Rademacher et al., 1992 have referred to as the transverse orbital sulcus. Though Ono, Kubik, and Abernathey, 1990 have recorded it as always present, its originations and terminations seem arbitrary, as it has been often recorded as a continuation of the frontomarginal, inferior frontal or olfactory sulci (Duvernoy, 1999; Ono, Kubik, and Abernathey, 1990). The configuration of these short sulci can form an 'H' or 'X' shape (Catani and Schotten, 2013; Destrieux et al., 2010; Ono, Kubik, and Abernathey, 1990).

PARACENTRAL SULCUS The marginal sulcus of the cingulate sulcus reaches the superior hemispheric fissure, which also acts as the posterior boundary of the paracentral lobule (Catani and Schotten, 2013). The paracentral sulcus anteriorly separates this lobule from the medial posterior superior frontal gyrus (Desikan et al., 2006; Destrieux et al., 2010). The paracentral sulcus may arise as various manifestations, including as a superior projection of the cingulate, or an extension from the lateral surface (Catani and Schotten, 2013; Destrieux et al., 2010; Ono, Kubik, and Abernathey, 1990). It has been described as not always distinguishable enough (Destrieux et al., 2010).

PARACINGULATE SULCUS The paracingulate sulcus presents as an outer – more anterior and more superior – parallel of the cingulate sulcus (Fornito et al., 2006; Paus et al., 1996). First described as a "double parallel" of the cingulate sulcus, first by Weinberg, 1905 and later by Ono, Kubik, and Abernathey, 1990, further investigation has correlated its existence with a relative expansion of the paracingulate cortex (Fornito et al., 2006; Paus et al., 1996). Its existence is infrequent. Ono, Kubik, and Abernathey, 1990 reported its existence in 24% of 50 hemispheres, while Paus et al., 1996 reported its existence in 37% and 54% in right and left hemispheres, respectively, in 494 hemispheres. Other notable findings of theirs were paracingulate asymmetry skewing towards the left hemisphere, with more prominent appearance, and more regular appearance in males (Fornito

et al., 2006; Paus et al., 1996). This asymmetry mirrors earlier findings by Weinberg, 1905, who reported the existence of a "doubling of the cingulate sulcus in its anterior part" in 40% and 84% of right and left hemispheres, respectively.

PRECENTRAL SULCUS The precentral sulcus is a consistent sulcus on the lateral surface of the brain, lying just anterior to the central sulcus and with a roughly parallel, antero-inferior course (Ono, Kubik, and Abernathey, 1990). Superiorly, it crosses over the superior hemispheric margin and is always present on the medial surface (Ono, Kubik, and Abernathey, 1990). It is frequently discontinuous, most often into two parts, generally designated as the superior and inferior segments of the precentral sulcus (Destrieux et al., 2010; Duvernoy, 1999; Germann et al., 2005; Ono, Kubik, and Abernathey, 1990).

SUPERIOR/INFERIOR ROSTRAL SULCI / SUBORBITAL SULCUS The anterior projections of the cingulate sulcus in the medial frontal lobe are the superior and inferior rostral sulci. The superior rostral sulcus, always present, originates at either the anterior subcallosal region, anterior cingulate sulcus or anterior paracingulate and extends anteriorly towards the frontal pole where it may or may not reach the anterior hemispheric margin (Ono, Kubik, and Abernathey, 1990; Paus et al., 1996; Rademacher et al., 1992). Its posterior termination may be continuous with the anterior parolfactory sulcus (Ono, Kubik, and Abernathey, 1990; Spasojević et al., 2011). Additionally, this sulcus was described by Brodmann, 2007 as the infero-medial border of Brodmann Area 10. Its inferior counterpart, the inferior rostral sulcus, is less constant (Ono, Kubik, and Abernathey, 1990; Rademacher et al., 1992). Ono, Kubik, and Abernathey, 1990 showed that while the superior rostral sulcus is continuous, the inferior rostral sulcus can present as either continuous or segmented into multiple sulci (20% of 50 hemispheres), as well as connections with the anterior parolfactory sulcus.

3.2.3 Temporal lobe

COLLATERAL SULCUS The name collateral sulcus is used interchangeably with medial occipitotemporal sulcus by some (Catani and Schotten, 2013; Destrieux et al., 2010; Duvernoy, 1999). This alternative name indicates its position more clearly: as medial of the lateral occipitotemporal sulcus, another landmark sulcus of the ventral surface. The collateral sulcus is frequently identified, but its various branches and connections with the lateral occipitotemporal sulcus make it not easily discernible from the surrounding sulci (Destrieux et al., 2010). The collateral sulcus usually

gives rise to other ventral sulci, including the transverse collateral sulci such as the rhinal and lingual sulci, and the parahippocampal ramus (Destrieux et al., 2010; Duvernoy, 1999; Ono, Kubik, and Abernathey, 1990).

INFERIOR TEMPORAL SULCUS The inferior temporal sulcus is located on the lateral surface of the temporal lobe, inferior to the superior temporal sulcus and supero-lateral to the occipitotemporal sulcus, with a general longitudinal trajectory (Catani and Schotten, 2013; Destrieux et al., 2010; Rademacher et al., 1992). It acts as the boundary between the middle and inferior frontal gyri (Catani and Schotten, 2013; Destrieux et al., 2010). It is a discontinuous sulcus, with reports of between 2 and 7 segments (Destrieux et al., 2010; Duvernoy, 1999; Ono, Kubik, and Abernathey, 1990). These segments can also have antero-posterior extensions to the temporal tips and parietal and occipital lobes and frequently have connections with surrounding sulci, including the superior temporal sulcus, anterior occipital sulcus, lateral occipital sulcus, inferior occipital sulcus, preoccipital notch, occipitotemporal sulcus or intraparietal sulcus (Catani and Schotten, 2013; Destrieux et al., 2010; Duvernoy, 1999; Ono, Kubik, and Abernathey, 1990; Rademacher et al., 1992).

OCCIPITOTEMPORAL SULCUS The occipitotemporal sulcus is a major landmark of the ventral occipito-temporal lobes (Chau, Stewart, and Gragnaniello, 2014). Though its presence is widely regarded as constant, it is characterised as a frequently discontinuous sulcus, extending from the temporal to occipital lobes but without reaching as far anterior as the temporal pole (Chau, Stewart, and Gragnaniello, 2014; Destrieux et al., 2010; Ono, Kubik, and Abernathey, 1990). This sulcus is found between the inferior temporal sulcus, laterally, and collateral sulcus, medially, acting as the division between the inferior temporal gyrus, laterally, and the fusiform gyrus, medially (Catani and Schotten, 2013; Chau, Stewart, and Gragnaniello, 2014; Destrieux et al., 2010; Ono, Kubik, and Abernathey, 1990). Ono, Kubik, and Abernathey, 1990 describes this sulcus as more discontinuous than continuous, observing up to 4 segments. Notably, they also rarely observed (8% of right hemispheres, 4% of left hemispheres) a "double parallel type", with segments running parallel to each other, in an overlapping fashion. These segments often have side branches, or connections with surrounding sulci, such as the rhinal sulcus, inferior temporal sulcus or collateral sulcus (Ono, Kubik, and Abernathey, 1990).

RHINAL SULCUS The rhinal sulcus is a short, constant sulcus of the ventral temporal lobe (Chau, Stewart, and Gragnaniello, 2014). Its position is often correlated with that of the collateral sulcus and the anterior

boundary of the limbic lobe (Destrieux et al., 2010; Duvernoy, 1999; Ono, Kubik, and Abernathey, 1990). It is described as a antero-medial sulcus usually projecting from the anterior end of the collateral sulcus, with which it is sometimes continuous–28% by Ono, Kubik, and Abernathey, 1990, 50% by Chau, Stewart, and Gragnaniello, 2014–and sometimes overlapping (Ono, Kubik, and Abernathey, 1990 documented overlapping in 52% and 40% of right and left hemispheres, respectively).

SUPERIOR TEMPORAL SULCUS The superior temporal sulcus is inferior to the lateral fissure and runs in a parallel course (Duvernoy, 1999). It extends from the temporal pole to the posterior end of the lateral fissure, where it turns superiorly and continues as the angular sulcus. The angular sulcus is sometimes a true continuation of the superior temporal sulcus, and sometimes a segmented branch (Duvernoy, 1999). Another horizontal posterior segment can be the anterior occipital sulcus. Frequently presenting with such branching, segmentation is more common in the left hemisphere than the right (Ochiai et al., 2004). Asymmetries extend to depth as well; the right superior temporal sulcus is deeper than the left, complementing the earlier appearance by 1 to 2 weeks of the superior temporal sulcus in the right than the left hemispheres during gestation. It has been suggested that this depth asymmetry, since it does not extend to other mammals, is unique to the human cortical development, acting as a "species-specific perisylvian anatomical marker" (Leroy et al., 2015).

TEMPOROPOLAR SULCUS The temporopolar sulcus is described by Catani and Schotten, 2013 as a variable sulcus at the ventral tip of the temporal lobe, separating the fusiform gyrus from the temporal polar region. Destrieux et al., 2010 describe the separation of the temporal pole by the convergence of the antero-lateral planum polare, the superior, middle, inferior temporal sulci, anterior collateral sulcus and occipitotemporal sulcus.

3.2.4 Parietal lobe

ANGULAR SULCUS The angular sulcus is aptly named as a descriptor of its trajectory beginning from the posterior segment of the superior temporal sulcus, which can be a true continuation of it or an independent segment of it (Duvernoy, 1999). It is collectively described as a superiorly-curving posterior branch of the superior temporal sulcus, angling around the posterior part of the lateral fissure, to bisect the angular gyrus (Catani and Schotten, 2013; Ono, Kubik, and Abernathey, 1990; Rademacher et al., 1992).

INTERMEDIATE PRIMUS OF JENSEN The intermediate primus of Jensen is a inferiorly-projecting orthogonal sulcus from the intraparietal sulcus (Destrieux et al., 2010). It is one of many downward-projecting branches of the intraparietal sulcus (Catani and Schotten, 2013; Destrieux et al., 2010; Ono, Kubik, and Abernathey, 1990). We characterise the intermediate primus of Jensen in particular because of its distinction in bisecting the inferior parietal lobule, acting as the border between the supramarginal (anteriorly) and angular (posteriorly) gyri (Destrieux et al., 2010).

INTRAPARIETAL SULCUS A landmark of the lateral surface of the parietal lobe, the intraparietal sulcus courses in a loosely longitudinal manner from the postcentral sulcus to the hemispheric margin, just superior of the lateral notch of the parieto-occipital sulcus (Duvernoy, 1999). Its nature is concave, and can be distinguished by up to three segments: an anterior, ascending segment, which may begin from the base of the postcentral sulcus, the horizontal intermediate segment, which clearly delineates the superior and inferior parietal gyri, and the posterior descending route which crosses over into the occipital lobe, continuing as the superior occipital sulcus (Destrieux et al., 2010; Duvernoy, 1999; Ono, Kubik, and Abernathey, 1990). It separates the superior and inferior parietal lobules (Catani and Schotten, 2013).

CALLOSOMARGINAL SULCUS The callosomarginal or simply 'marginal' sulcus, is consistently defined as the continued posterior segment of the cingulate sulcus which extends superiorly to reach the interhemispheric fissure, just posterior of the superior termination of the central sulcus. At this position, it lies between the often-bifurcated superior termination of the postcentral sulcus (Ono, Kubik, and Abernathey, 1990; Rademacher et al., 1992).

POSTCENTRAL SULCUS The postcentral sulcus is located in the parietal lobe. It is the first sulcus posterior to the central sulcus and follows a generally similar antero-inferior trajectory (Rademacher et al., 1992). While the central sulcus is almost always a single continuous sulcus, the postcentral sulcus has been reported as either continuous and segmented into 2 or 3 segments (Destrieux et al., 2010; Ono, Kubik, and Abernathey, 1990). Alternatively, a "double parallel" type has been reported by Ono, Kubik, and Abernathey, 1990, though not commonly. It is frequently connected to surrounding sulci, most notably the intraparietal sulcus, and frequently has side branches projecting into the surrounding gyri (Ono, Kubik, and Abernathey, 1990; Rademacher et al., 1992). A noteworthy characteristic of the postcentral gyrus is its common Y-shaped bifurcation

at its superior termination, which may or may not extend over the superior hemispheric margin into the medial surface (Ono, Kubik, and Abernathey, 1990; Rademacher et al., 1992).

SUBPARIETAL SULCUS The subparietal sulcus is a landmark sulcus of the medial parietal lobe (Ono, Kubik, and Abernathey, 1990). On the medial surface, it is located postero-inferiorly to the posterior end of the cingulate sulcus, from which it is occasionally a continuation of, and limits the precuneus from the cingulate gyrus (Destrieux et al., 2010; Rademacher et al., 1992). It is composed of several branches, and usually appears as an H-shape or Y-shape which extends inferiorly (Destrieux et al., 2010; Ono, Kubik, and Abernathey, 1990; Rademacher et al., 1992).

SUPERIOR PARIETAL SULCUS The superior parietal sulcus is located in the superior parietal lobule, posterior of the postcentral sulcus, anterior of the parieto-occipital sulcus, and superior of the intraparietal sulcus (Ono et al, 1990; Destrieux et al, 2010). It is described as inconstant or supplementary (Ono et al, 1990; Destrieux et al, 2010). It can arise as a branch of the intraparietal sulcus (Destrieux et al., 2010), and reported by Ono et al (1990) as having between 0 and 2 branches.

3.2.5 Occipital lobe

ANTERIOR OCCIPITAL SULCUS A rather elusive sulcus, the anterior occipital sulcus nonetheless appears in many studies but with varying lobular positions. Some place it as a posterior branch of either the superior temporal sulcus (Ono, Kubik, and Abernathey, 1990) or the inferior temporal sulcus (Duvernoy, 1999). Its position is ambiguously located in the area where the temporal, parietal and occipital lobes converge. Some localise it to the parietal lobe (Rademacher et al., 1992), some to the temporal lobe (Ono, Kubik, and Abernathey, 1990) and others to the occipital lobe (Duvernoy, 1999).

CUNEAL SULCUS Brodmann, 2007 remarks the presence of the cuneal sulcus when describing it as a landmark for the V1 striate area, though not necessarily a boundary of it. Its existence and location is consistent, though its appearance is not. It is a short, shallow sulcus on the medial surface of the cuneus, wedged between the parieto-occipital and calcarine sulci.

INFERIOR OCCIPITAL SULCUS The inferior occipital sulcus is the sulcus which limits the lateral occipital lobe from the ventral (Destrieux et al., 2010). Its delineation can be arbitrary, and its descriptions are synonymous

with other occipital sulci such as the lateral or transverse occipital sulci (Rademacher et al., 1992).

LATERAL OCCIPITAL SULCUS The lateral occipital sulcus, sometimes referred to as the middle occipital sulcus or prelunatus sulcus, is a constant sulcus which lies in the arbitrary junction between the occipital, temporal and parietal lobes (Bailey and Urbana, 1951; Destrieux et al., 2010; Ono, Kubik, and Abernathey, 1990). It acts as the limit between the superior and inferior occipital gyri (Rademacher et al., 1992). It may arise as a posterior projection of the superior temporal sulcus and may be connected to surrounding sulci including the anterior occipital sulcus, inferior temporal sulcus or lunate sulcus (Destrieux et al., 2010; Duvernoy, 1999).

LINGUAL SULCUS The lingual, or intralingual, sulcus is so named because it courses through the lingual gyrus (Destrieux et al., 2010). It is commonly found and described as a sulcus emerging from the posterior third of the collateral sulcus, reaching postero-medially into the occipital lobe (Chau, Stewart, and Gragnaniello, 2014; Destrieux et al., 2010; Ono, Kubik, and Abernathey, 1990).

LUNATE SULCUS Though a characteristic feature of the macaque brain, the lunate sulcus proves rather elusive in the human brain (Martin and Bowden, 2000; Ono, Kubik, and Abernathey, 1990). When present in humans, it is positioned at a much more posterior location, and is much less prominent than in the great ape brain (Allen, Bruss, and Damasio, 2006; Brodmann, 2007). It is described as a short sulcus on the posterior medial surface of the occipital lobe, near the occipital pole, separating Brodmann areas 17 and 18/primary and secondary visual cortices (Brodmann, 2007; Rademacher et al., 1993). Contrary to some other cortical functional areas, the architectonic transition between the primary and secondary visual cortices is abrupt (Brodmann, 2007) . Eickhoff, Yeo, and Genon, 2018 have demonstrated how, at particular locations such as this, cyto- or myeloarchitectonic transitions represent the border of different cortical areas. The lunate sulcus may act as this border. Ono, Kubik, and Abernathey, 1990 noted its presence only in 40% and 36% of the right and left hemispheres, respectively. Allen, Bruss, and Damasio, 2006 reported its variability, with asymmetries within the same brain to variations in shape.

RETROCALCARINE SULCUS The retrocalcarine sulcus is not always present (Ono, Kubik, and Abernathey, 1990), but when it is it exists as a separate small sulcus posterior of the calcarine sulcus, on the occipital pole (Iaria and Petrides, 2007). It can often be included as part of the calcarine sulcus as posterior ascending or descending rami (Destrieux et al.,

2010; Duvernoy, 1999; Iaria and Petrides, 2007). Elliot Smith, 1902 gave emphasis to this sulcus in the posterior occipital cortex for its relevance in comparative anatomy and relationship to the primary visual cortices.

SUPERIOR OCCIPITAL SULCUS The superior occipital sulcus often arises as a postero-inferior continuation of the intraparietal sulcus almost reaching the occipital pole (Catani and Schotten, 2013; Destrieux et al., 2010; Duvernoy, 1999).

3.2.6 Limbic lobe

ANTERIOR PAROLFACTORY SULCUS The parolfactory region lies inferior to the genu of the corpus callosum (Catani and Schotten, 2013; Rademacher et al., 1992). Here there exists a sulcus called the anterior parolfactory sulcus, which may not be easily distinguishable from its surrounding sulci because it often exists as a branch or continuation of other medial sulci, including the cingulate or superior and inferior rostral sulci (Ono, Kubik, and Abernathey, 1990). It has been postulated that the anterior parolfactory sulcus may act as an anterior border to Brodmann area 25, a region implicated in depression (Hamani et al., 2011).

CINGULATE SULCUS The cingulate sulcus is present on the medial surface, separating the frontal lobe from the limbic lobe (Ono, Kubik, and Abernathey, 1990). It is the outer boundary of the cingulate gyrus, separating it from the superior frontal gyrus and paracentral lobule (Catani and Schotten, 2013). It begins in the subcallosal area and follows the course of the pericallosal sulcus, in a concentric manner, following the trajectory of the corpus callosum (Duvernoy, 1999). Posterior to the central and paracentral sulci, it curves superiorly, turning into the marginal sulcus, and terminates at the superior hemispheric margin, corresponding to the position of the postcentral sulcus on the lateral surface (Duvernoy, 1999). On the lateral surface, oftentimes the postcentral sulcus bifurcates just prior to its termination at the superior hemispheric margin. When this occurs, the termination of the marginal sulcus usually lies between these postcentral terminal bifurcations (Ono, Kubik, and Abernathey, 1990; Rademacher et al., 1992).

HIPPOCAMPAL SULCUS The hippocampal sulcus is located on the edge of the limbic lobe, separating the hippocampus from the parahippocampal gyrus on the ventral temporal lobes (Duvernoy, 2005; Duvernoy, 1988; Rademacher et al., 1992). It can be seen from the ventral surface, medial to the collateral sulcus and with a similar, longitudinal trajectory but more convex (Ono, Kubik, and Abernathey, 1990).

INTRALIMBIC SULCUS The intralimbic sulcus, rarely present nor prominent, exists within the intralimbic gyrus, surrounding the Callosal sulcus (Destrieux et al., 2010; Duvernoy, 1999; Paus et al., 1996)

3.3 ORGANISATION OF SULCI

In section 3.2, we covered the morphology of individual sulci as reviewed in numerous classical neuroanatomy sources. From a literature standpoint, we ascertain degrees of variability or instability of a sulcus. We gather this knowledge and infer the organisation of the cortex using sulci.

There exists a set of sulci in addition to the primary sulci which can be expected to be identified in all healthy brains, and have overlapping definitions in many neuroanatomy sources. These are referred to as the 'secondary' sulci, or, more ambiguously, the 'major' sulci. Folding patterns during neurodevelopment follow basic trajectories which form a rudimentary pattern for the ontogenesis of sulci and gyri on the macroscale. The folding patterns govern the cortical organisation, and the development of the primary sulci influence subsequent sulcal developments (Ono, Kubik, and Abernathey, 1990; Toro and Burnod, 2003).

We compiled sources of sulcal characterisation dating back centuries until present day, which included a vast array of anatomical techniques for identification and labelling. We identified a large proportion of overlap among the sources as well as an equally large proportion of inconsistencies in the identification of sulci and their namings. In many cases, sulci had multiple names across sources but the characterisation was the same. In the case of multiple names, we chose to include the name which is most reflective of its structural anatomy, as opposed to its functional relationship.

We present the NeuroLang atlas which has a universal set of 42 sulci. The schematic presented in Figure 3.2 is a representation of the accumulation of sulcal characterisations in a form which reflects the pattern of organisation of the sulci on the cortex in the literature. The positions of the sulci within each lobe are characterised in relation to the primary sulci, but are not dependent on sulci within other lobes. For this reason we distinguish the lobe to which the sulcus belongs in addition to assigning it a position on the hierarchical organisation. This representation suggests that there exists a gradient of stability within each lobe, in relation to the primary sulci. Therefore, the group of the 'secondary' sulci have a vertical relationship to the 'tertiary' sulci, but there are also 4 vertical relationships within the group of the secondary sulci, within each lobe. From the order in which sulci are identified per lobe, we derive a semi-hierarchical organisation of secondary and tertiary sulci, and this is what we depict in Figure 3.2.

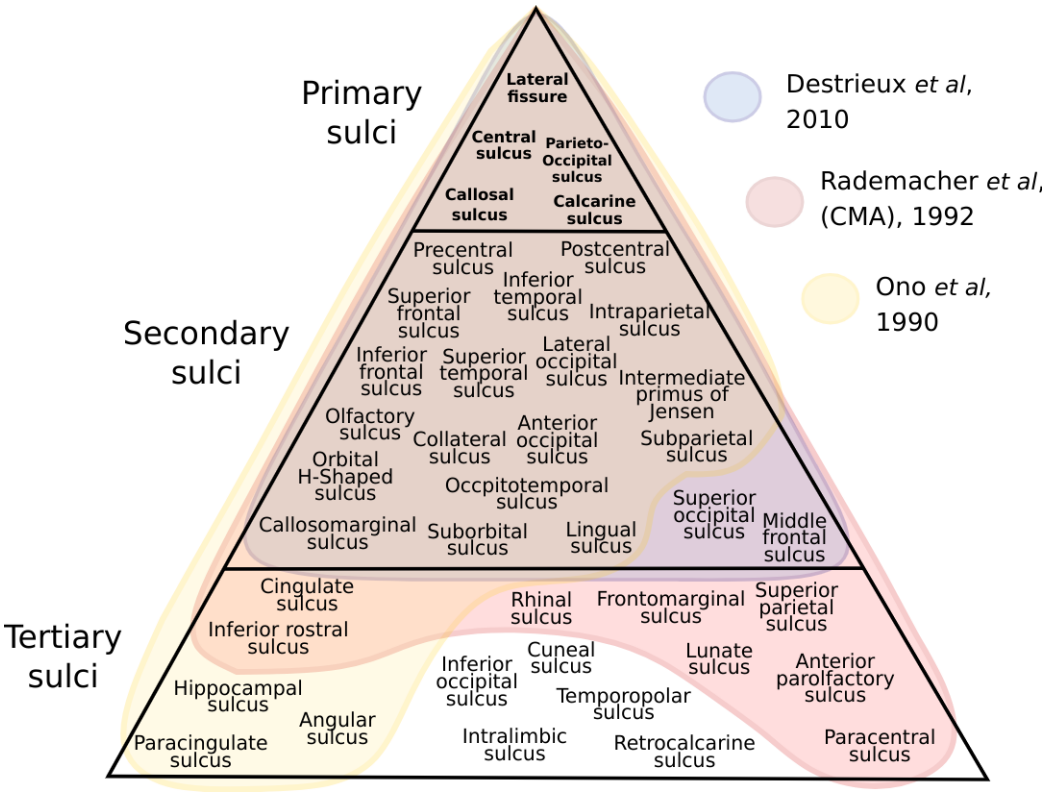

Figure 3.1: Schematic depicting the overlap and disagreement in the sulci of 3 gold-standard sulcal atlases (Destrieux et al., 2010; Ono, Kubik, and Abernathey, 1990; Rademacher et al., 1992). The primary sulci are interlobular markers (except the calcarine) and are the most stable in their morphology and location. The secondary sulci were chosen are those represented independently in the Destrieux atlas, and the tertiary were included in at least one of the sources, or existed in the Destrieux atlas as sulci merged with their surrounding gyri. Tertiary sulci are more variable in their existence, morphology, location, relationships to other sulci, and relationships with other brain features.

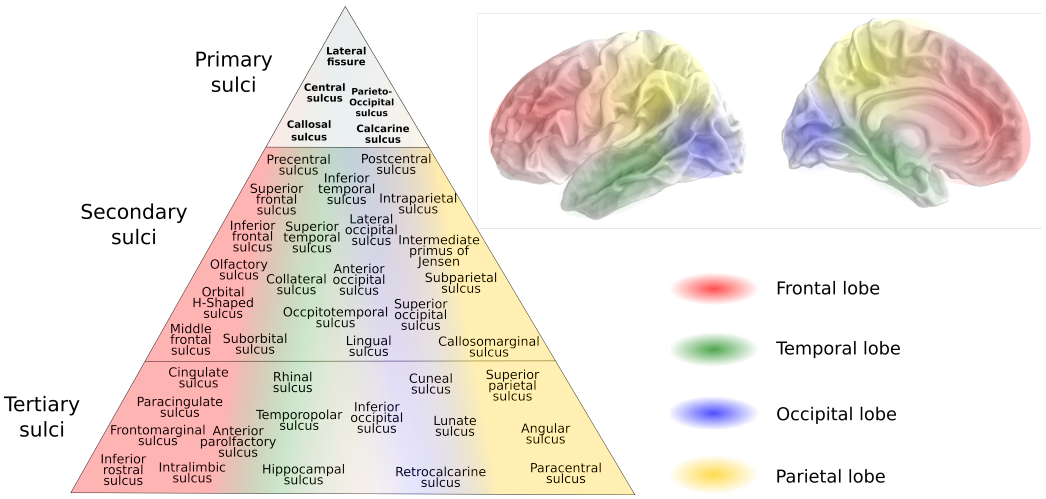

Figure 3.2: Schematic depicting our semi-hierarchical organisation of the universal set of sulci in NeuroLang. The position of the sulcus in the pyramid corresponds to its lobular location. The semi-hierarchical organisation signifies how the identification of a sulcus within a lobe may or may not be dependent on a previous identification of a different sulcus within the same lobe, but not necessarily on the identification of a sulcus in a different lobe, even if they are in the same tier or above. The primary sulci were manually selected, the secondary sulci are those included as independent regions in the Destrieux atlas template and could be verified with their Destrieux atlas counterparts, as we show in Appendix A.1 (Destrieux et al., 2010). The tertiary sulci comprise the remaining sulci, including those with irregular existence, morphology or location.

This semi-hierarchical organisation of sulci reflects the way in which classical neuroanatomists would navigate their way across the cortex in localising decreasingly reliable sulci. It therefore reflects the intuitive methodology for sulcal localisation based on the spatial geometry of the surface. It is this property of classical neuroanatomy descriptions we use in this work to devise a method for progressively localising cortical sulci. However, our literature-based semi-hierarchical ordering proves that characterisations of the sulci and sulcal reliability are quite arbitrary. To combat this, we would need our own set of 'ground truth' neuroanatomy in which to base our own sulcal neuroanatomy localisation on and for the validation of our sulcal mapping queries in NeuroLang. While automated identification of sulci is a necessary step for the investigation of large populations, 'tedious anatomy' provides the necessary accuracy and inter-individuality, a case neatly put forth by Devlin and Poldrack, 2007.

4 BRAIN MAPPING IN NEUROIMAGING

4.1 IMAGING THE BRAIN

4.1.1 Templates

Before the advent of advanced neuroimaging tools, cortical anatomy took place largely on the gyral surface as the sulci were, for the most part, hidden (Zilles and Amunts, 2010). Modern neuroscience has unlocked the prominence and relevance of the sulcal features for anatomical landmarking and correlations with structure and function. Brain atlases bridge the gap between information on and within the surface (Evans et al., 2012).

Modern brain mapping originated in the 1960s with the seminal work of Jean Talairach who introduced 'Talairach space', the transformation of brain images into 3D coordinates (Talairach et al., 1967). This system was based on two landmark points on the sagittal plane of the brain, the anterior commissure (AC) and the posterior commissure (PC). This work culminated in the widely used anatomical spatial reference system described in Talairach and Tournoux (1988). The line between the two of these is the ACPC line and is the foundational reference point for linear alignment between brain images. Efforts to create standard 'templates' for neuroanatomy through MRI blossomed across North America and Europe in parallel, as groups gathered data from various sources to try to build a standard model for brain mapping (Evans et al., 2012). Some of the difficulties and obstacles they encountered they overcame, others remain as drawbacks to this day. For example, the identification of the AC and PC points are not standard (Nowinski, 2020). Among these are the extrapolation of cerebral morphology from a lack of sufficient data, such as mirroring the hemispheres, when it is commonly accepted that there are considerable left-right asymmetries which should be taken into consideration. It is a challenge to create a template which is based on a diverse enough dataset of human cerebral morphology but still applicable to the mass population.

The creation of a template in Talairach space paved the way for further standardisation techniques in the brain mapping field. An atlas derived from a single adult subject was created by Talairach and Tournoux in Talairach space (Talairach and Tournoux, 1988). However, it posed its own limitations, such as its lack of anatomical variability (Iaria and Petrides,

2007; Talairach and Tournoux, 1988). Soon, *MNI space* followed. Beginning with a template from manually labelled anatomical landmarks in the 1990s, images from a large set of young, healthy subjects were aggregated and averaged to a template, correcting for brain size and orientation, and resulted in the original MNI305 atlas (Evans et al., 1994). This evolved and was updated in the next decade to become the MNI 152 atlas, which remains a gold-standard anatomical tool today.

The benefits of a stereotaxic template system abound. It is incredibly practical to have a universal set of coordinates which groups working on different datasets, using different methods or pipelines can agree upon and understand each other (Nowinski, 2020). It also allows for replication of studies with different subjects, a branch of neuroimaging studies which is consistently lacking (Poldrack et al., 2017).

4.1.2 Spaces in neuroimaging

There are many different coordinate spaces which can be used in neuroimaging analyses. Brain images are represented using *voxels*, the 3-dimensional equivalent of pixels for 2-dimensional images. The voxel dimensions can vary but are typically 1mm x 1mm x 1mm, and are spaced equally on a 3-dimensional grid. Each voxel can be described in a data array by its index or by its coordinates. There are some spaces, including MNI space and ACPC space, which have their coordinates as stereotaxic locations in the form (x, y, z), relative to the origin point (0, 0, 0), fixed as the intersection of the anterior commissure with the interhemispheric fissure (Eickhoff et al., 2005a; Talairach and Tournoux, 1988). The mapping between these two forms is by carried out by an affine transformation. The orientation is in the RAS form; the x-axis points to the *r*ight, the y-axis points to the *a*nterior, and the z-axis points to the *s*uperior.

A subject's MRI T1 (T1) scan without any correction or processing done to it is referred to as being in native volume space. Native space conserves individual head size and shape. T1 and T2 are pulse sequences commonly used in MRI acquisition. T1 images are used to identify cortical structures as they appear appear grey in T1, with the white matter lighter grey, and liquid such as cerebrospinal fluid appearing black.

These two types of images, generated by altering the relaxation (ET) and repetition (TR) times, can be used separately but also together. The contrast of the images can elucidate features of cortical anatomy otherwise unfounded, as well as revealing relative underlying cytoarchitecture and myeloarchitecture (Cohen-Adad, 2014; Glasser and Essen, 2011; Shams, Norris, and Marques, 2019). This feature is particularly useful due to the difficulty in acquiring exhaustive and flexible cytoarchitectonic and

myeloarchitectonic maps (Eickhoff et al., 2005a; Eickhoff et al., 2005b; Zilles and Amunts, 2010).

We can see how templates inherently lack anatomical sensitivity. While the main landmarks of the brain are typically preserved in their location, shape and depth, much of the particularities of lesser-known sulci which are not regarded as landmarks are either somewhat or completely glossed over.

As previously mentioned, sulcal morphological variability is closely linked with architectonic variability of the underlying neuronal makeup. A significant hindrance in the cortical parcellation community is the difficulty in capturing the wide inter-individuability which exists in cortical morphology (Evans et al., 2012; Mangin, Jouvent, and Cachia, 2010; Nowinski, 2020; Roland and Zilles, 1994).

4.1.3 Atlases

As brain mapping techniques gained traction over the last 40 years, surface neuroanatomy became increasingly relevant for precise alignment in neuroimaging. The characterisation of sulci became crucial for the establishment of reliable sulci as reference landmarks (Auzias et al., 2013). Brain templates and coordinate systems relied on accurate anatomical landmark localisation as a basis (Destrieux et al., 2010; Talairach et al., 1967; Van Essen and Drury, 1997). As presented in chapter 3.1, sulcal landmarks are typically reliable in terms of their position, orientation and relative location to other cortical regions. They are thus critical for the development of dependable atlases or templates which must be general enough to be fit onto any brain but accurate enough to reliably label all brain regions.

Brain atlases have been developed on the basis of probability. While many brain regions exhibit large variability between subjects in their location and size, a considerable subset of brain regions are relatively stable in their locations relative to regional landmarks such as the ACPC line or sulcal landmarks such as the Central sulcus or the Lateral fissure. Probabilistic brain atlases for the cortex per hemisphere are subdivided into various numbers of regions (48 in the Harvard-Oxford Atlas (Caviness et al., 1996), 37 in the Destrieux atlas (Destrieux et al., 2010), 45 in the Anatomical Labeling atlas (Tzourio-Mazoyer et al., 2002)) (Figure 4.1).

Templates for atlases are created by averaging a set of brain images to create a model image of the population and developing a deformation algorithm which will allow for the transformation of the template image to be warped onto any new brain image. Human cortical templates work by aligning template images voxel by voxel to a brain image (Diedrichsen, 2006). This is achieved via a deformation transformation

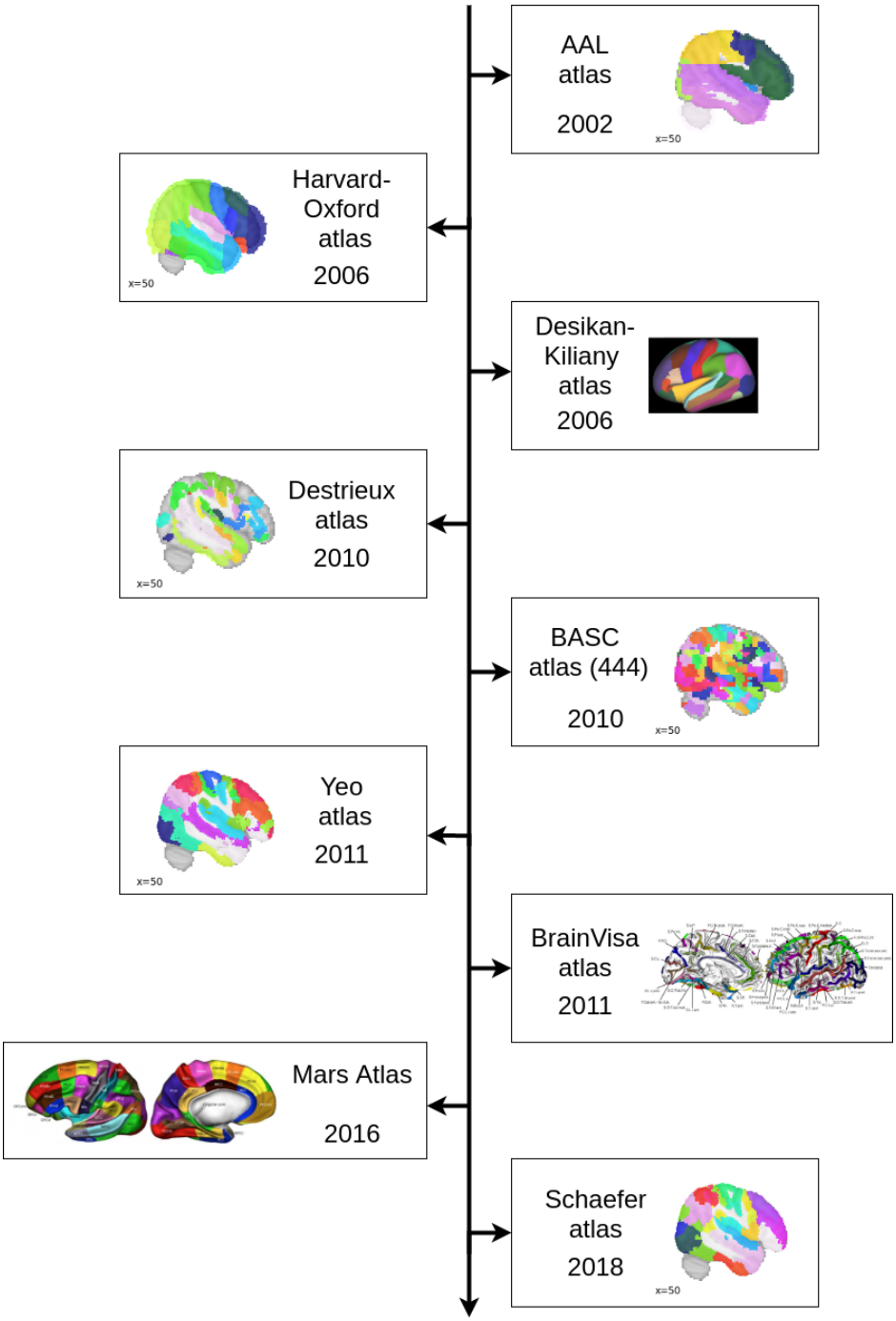

Figure 4.1: Timeline of the development of some notable cortical atlases. Current atlases incorporate vast anatomical and functional information, but there exists great discrepancy in anatomical nomenclature and definitions. Atlases encompass a large overlap of cortical features in humans but tend to lack the ability to express individual variation (Auzias, Coulon, and Brovelli, 2016; Bellec et al., 2010; Caviness et al., 1996; Desikan et al., 2006; Destrieux et al., 2010; Rivière et al., 2009; Schaefer et al., 2018; Thomas Yeo et al., 2011; Tzourio-Mazoyer et al., 2002).

which can take into account factors including inter-individual variability of sulci (Diedrichsen, 2006; Mangin, Jouvent, and Cachia, 2010). Cortical landmarks can be manually predetermined (Diedrichsen, 2006; Talairach and Tournoux, 1988) or automatically (Desikan et al., 2006; Destrieux et al., 2010). By necessity, a template ends up smoothing out much of the variability which is exhibited between any set of subjects, and relies on inter-subject matching on the coarse scale.

With surface neuroanatomy as a basis, atlases can rely upon the intrinsic geometrical organisation of the cortex. For example, Toro and Burnod, 2003 conveyed the organisation of the cortex as a geometrical atlas. Auzias, Coulon, and Brovelli, 2016 constructed the Mars Atlas on the basis of the anterior/posterior and superior/inferior designation of the sulci (shown in Figure 4.1).

4.1.4 Sulcal parcellations

Surface-based registration techniques depend on the reliability of cortical landmarks (Yun et al., 2019). Extensive work has been carried out to accurately extract sulci to be used for brain mapping. One of the most widely-used tools for the analysis of neuroimaging data is Freesurfer, developed in 2012 (Fischl, 2012). Freesurfer carries out automated volume-based and surface-based analysis of brain features from T1 images. It includes tools for inter-subject alignment from cortical folding patterns (Fischl et al., 1999), sulcal parcellations (Desikan et al., 2006; Destrieux et al., 2010), and probabilistic estimation of cytoarchitectonic regions (Fischl et al., 2008, 2004). Freesurfer was essential to the processing pipeline of the Human Connectome Project dataset, which we use in our analysis (Glasser et al., 2013).

Templates depend on the reliability of sulcal landmarks to spatially delineate the brain, because of their uniformity across subjects (Desikan et al., 2006; Im et al., 2010; Yun et al., 2019). Sulcal extraction is often carried out on the basis of its defining characterisation: depth. The maximum depth measure of a sulcus, described as its 'basin' or 'pit', provides a reliable measure for extracting sulci (Auzias et al., 2015a; Yun et al., 2019). Many approaches rely on the depth of a sulcus as a measure between its deepest point and the external surface of the cortex, where the curvature is either flat or convex (Im et al., 2010), or the local depth measured by average convexity (Fischl, Sereno, and Dale, 1999).

Auzias et al., 2015a extracted sulcal pits without the need of an external surface reference point, but rely on a Freesurfer-based surface template. Alternatively, Klein et al., 2017 compute their own shape measures for each labelled region, then extract cortical features such as 'folds' based on the shape measures. The 'folds' are grouped vertices which are connected and

convex, and are extracted on the basis of their depth. The folds can then be segmented according to an *a priori* atlas labelling protocol. Labelling of folds into sulci resolves the lack of correspondence of fold shapes across subjects (Klein et al., 2017).

While sulcal parcellation and labelling techniques are currently successful in distinguishing sulci based on both their location and their morphologies, we recognise the opportunity to carry this function out on an individual level. By harnessing existing sulcal extraction techniques such as the one mentioned by Klein et al., 2017, and applying the concepts of sulci as spatial regions and interval algebra (Dameron, Musen, and Gibaud, 2007; Dylla et al., 2017; Navarrete et al., 2013), we utilise the individual geometry of each person's sulcal arrangements to identify and label them in a subject-specific manner. We add our method to existing sulcal parcellation techniques, notably in the pertinence of taking tertiary sulcal variability into account.

4.1.5 Spatial geometry of the cortex

The geometry of the cortex is the mathematical study of its shape and its space. Spatial geometry refers to the structure and relationships of objects in a space in terms of points, lines, boxes or other geometric shapes. Terms used in spatial language utilise the vocabulary of spatial relations to relate objects in space to each other.

For our purposes of identification and labelling, we consider the qualitative relationships of pairs of sulci to each other of higher importance than the morphology of the sulci. We apply spatial geometry to the sulci of the cortex to consider each sulcus as a brain region and relate it to the primary sulci.

To determine relativity of sulci to the primary sulci, we will apply the concept of interval algebra, as introduced by Allen, 1983, reviewed in Dylla et al., 2017 and expanded upon by Navarrete et al., 2013. Navarrete et al., 2013 focus specifically on rectangular cardinal relation calculus, and lay out all the possibilities of spatial relationships between two rectangles using cardinal relations. For two rectangles, one is taken as the *'primary region'* and the other as the *'reference region'*, with their *'minimum bounding rectangle'* determining their place in space in relation to each other.

4.1.6 Representing sulci as spatial regions

In response to feedback from the jury, we also look at how sulci have been represented using spatial regions within the space of the brain. The formalisation of the ontology of anatomical brain regions has been studied

before, with the aim to capture the concepts of the characterisations of and relationships between brain regions (Dameron, Musen, and Gibaud, 2007; Rosse et al., 1998). Conceptually, representing sulci as distinguishable spatial regions with distinct relationships to other sulci spatial regions is intended as the ontological formalisation of existing anatomical knowledge bases, such as the extensive sulcal atlas by Ono, Kubik, and Abernathey, 1990. The formalisation acts as standardising neuroanatomical references, and such a knowledge base is useful in fields including neuroimaging and neurosurgery (Mangin et al., 2004b; Rosse et al., 1998).

Sulci as spatial regions can be represented on either the 2D or 3D plane. On the 2D plane, sulci as longitudinal or latitudinal orientations were explored as reference points on a 2D coordinate system by Auzias et al., 2013 and Mangin et al., 2004b. Auzias et al., 2013 used a coordinate-based system to assign sulci to either a longitudinal or latitudinal orientation, which served as the basis for the Mars Atlas (Auzias et al., 2015b; Auzias, Coulon, and Brovelli, 2016). This was also investigated by Mangin et al., 2004b, using the longitude/latitude system as a 2D reference system for anatomy in neuroimaging analyses. However, due to the simplification of the morphological variabilities of sulcal patterns, such representations lack the ability to be used in conjunction with the investigation of other cortical features such as integrative functional regions or cytoarchitectonic areas (Mangin et al., 2004b).

The ontological model proposed by Dameron, Musen, and Gibaud, 2007 comprises sulci as concepts, and describes their characterisations and relationships to other sulci. For the definition of sulci as concepts, morphological and topological information are used to define sulci. Such constraints can apply to any candidates which fulfill the conditions ('all reality'), or specific conditions, ('only reality'). In this way, logical interpretations of anatomical characterisations of sulci are used to model the possible variabilities of both sulcal morphologies and sulcal relationships. They also subsume lobular regions into lobes. The known anatomy and relationships of sulci can then be grouped and organised into a taxonomic hierarchy, from which dependencies between topological relationships can be inferred.

This work provided inspiration for our method for building upon sulcal representation using spatial geometry. The work of Dameron, Musen, and Gibaud, 2007 extend spatial regions of sulci but do not use relative spatial relationships for navigation, with the purpose of identifying and labelling unknown sulci. We show how the representation of sulci as spatial regions has been used for the coordination of sulcal landmarks as the basis for sulcal-labelling techniques (Auzias et al., 2013; Auzias, Coulon, and Brovelli, 2016; Rosse et al., 1998), and the formalisation of anatomical descriptions (Dameron, Musen, and Gibaud, 2007). We propose

to expand upon this body of work to add the use of representations of sulci using spatial regions for the purposes of navigating across the cortex according to cerebral spatial geometry. By representing sulci as spatial regions in relation to landmarks, we propose a sulcal labelling technique which identifies and labels sulci according to individual morphology and relationships, allowing for wider inter-individual variability of sulcal mapping.

4.1.7 Domain-Specific Languages

A domain-specific language (DSL) is a type of language used in computer programming as a way to formalise and represent knowledge. It is developed to solve problems existing within a certain *domain*, therefore specific to a particular field of knowledge. The advantage in using a DSL as opposed to a general-purpose programming language is that it increases the expressability of complex concepts within a field (Davison, Hines, and Muller, 2009; Tian et al., 2006). DSLs exist in many different fields, such as mathematical modelling (Louboutin et al., 2019), video game development (González García et al., 2019), or music programming (Rauber, Bois, and Ribeiro, 2019). They are useful for allowing a user to interface with a large amount of relevant data. This is particularly useful in neuroimaging, where the last few decades have seen a huge influx of neuroscience data (Dockès et al., 2020). To accommodate this, researchers have been developing tools for dealing with large databases of neuroscientific data, such as Neurosynth (Yarkoni et al., 2011), a large-scale meta-analystic neuroimaging database, NeuroQuery, a reverse-inference neuroimaging prediction tool based on the meta-analytic data of Neurosynth (Dockès et al., 2020), and NeuroQL. NeuroQL is a DSL proposed for neuroscientists to work with a vast array of neuroscience databases. NeuroQL integrates concepts specific to neuroscience, such as neuronal structures and properties, with simple operators which increase interpretability, and complex operators which allow for the descriptions of complex relationships (Tian et al., 2006).

In the case of brain mapping, using a DSL is advantageous because the language, features, and concepts of anatomy can be integrated directly into the structure of the programming language. NeuroLang is a DSL, but it is not the first DSL to exist for solving neuroanatomical queries. The White Matter Query Language (WMQL) was introduced in 2013 as a query-based tool for defining and identifying the major white matter tracts of the brain, with a near-to-English syntax (Wassermann et al., 2013). Acting as a bridge between white matter anatomy and computer science, the queries were translations of classical neuroanatomy descriptions taken from the literature. The parameters defined within this domain are parameters used

by anatomists to describe the anatomy of white matter tracts: 'endpoints in', 'traverses through', 'anterior of' (Wassermann et al., 2013, 2016).

We develop a tool which stems from the same idea. The formalisation of the definitions of brain regions in the literature and in brain mapping tools is an ongoing process. One complexity in the process is the difficulty in agreeing on definitions. We explore the capacity of the field to accommodate a flexible tool for anatomical identification, where the directional terms of neuroanatomy are integrated directly into the structure for composing sentences, and properties and relations can be layered to create complex characterisations of sulci which are changeable. We build descriptors of cortical anatomy directly into the back-end of our domain-specific language. The syntax is the set of rules which govern the structure of well-formed expressions in a language. In our language, the well-formed expressions are composed of the descriptors of cortical anatomy. We use the syntax of first-order logic to translate the language of classical neuroanatomy in our DSL.

5 FIRST ORDER LOGIC

To construct a domain-specific language (DSL) for the characterisation of the cortex, we need a method for representing the knowledge of classical neuroanatomy. We sought to include a system which reflects this consequence of logic which the characterisation of sulci in the literature follows. The syntax of our DSL is independent, and can be implemented using the rules of first-order logic.

First-order logic (FOL) is a type of logic used in mathematics and philosophy for representing knowledge. It is flexible and has a near-English syntax (Jurafsky and Martin, 2019; Van Harmelen and Lifschitz V, 2008). FOL is used to convey knowledge and communicate relationships of its elements. FOL is particularly favourable for representing *declarative* knowledge, meaning statements which are either true or false (Van Harmelen and Lifschitz V, 2008).

Like English, the two main components of structuring the language are *syntax* and *semantics*. The *syntax* of a language is the study of the elements and rules which make up the language (Chomsky, 2002). The term's etymological roots in the Greek words συν and ταξη, meaning *with order*, describe how the syntax of a language is meant to provide the structure and regulations to give a language meaning through its *semantical* output, coming from the Greek word for significant (σημαντικο). Information is communicated by the construction of basic phrases (syntax) which designate information about an object (semantics). Phrases can then be incrementally layered to create added layers of complexity to describe objects in the world and their relationships to each other. FOL is widely used in this way in various fields involving logistics to formalise knowledge representation (Van Harmelen and Lifschitz V, 2008).

The use of FOL allows for the development of an independent language with its own syntax. Therefore, FOL can act as an intermediary for a DSL. First we go over the syntactical components necessary to construct expressions in FOL, and then the semantic interpretation of these expression.

In FOL, the world is represented using *objects*. Knowledge of objects is conveyed through their properties and their relations, which are represented using *predicates*. Describing an object or its relations are a way of declaring information about the object. We call these declarations *formulae*, and the formulae with the status of the formula *statements*.

When working in FOL, the world is represented in a specific *domain*, which can change according to what is being represented. The domain is a set of objects being represented. The objects can be known or unknown, single elements or grouped, but all exist within the same domain. The words object and elements are used interchangeably to indicate an individual entity within the domain. The domain can be include constants, variables, terms, functions, properties, and relations.

- Objects are things within the domain with individual identities. They are represented by either a *constant* or a *variable*, depending on how they are to be used (Jurafsky and Martin, 2019).
- *Constants* refer to single objects which remain unchanged.
- *Variables* refer to either a single unknown object alone or within a group of other unknown objects.

All the objects included in a model, constants and variables, are unique and together compose the domain (Jurafsky and Martin, 2019). *Terms* can also be used to describe elements of the domain, as constants, variables or functions:

- A *function*, typically denoted by f, is used to map objects to each other. It is is a predetermined action to execute on a non-empty set of objects. Therefore if x is a variable, then x can also be a term, and $f(x)$ is also a term.

Within this section, we will represent two constants as A and B where $A \neq B$, and two variables x and y, where $x \neq y$.

Predicates are symbols which provide information about the objects, denoted by P. Predicates can define relationships of n objects, where $n \geqslant 0$. Predicates relating to single objects are called one-place predicates (e.g. $P(x)$) and those relating two or more objects are called two-place predicates (e.g. $P(x_1,...,x_n)$) (Jurafsky and Martin, 2019). Defining characteristics to indicate relationships are ways to semantically represent knowledge.

Quantifiers are operators in FOL which dictate how many objects in the domain the formula refers to.

- $\forall$: If a formula is applicable to any object, it is denoted by the symbol $\forall$, which is read as 'for all'.
- $\exists$: If the formula can apply to at least one object in the domain, the quantifier $\exists$ declares that 'there exists' at least one object of the domain which satisfies the formula (Jurafsky and Martin, 2019).

Quantifiers are used in FOL semantics to state the status of an object in a formula, e.g. $\exists x P(x)$, where the quantifier $\exists$ states the existence of x within the formula $P(x)$.

A variable can be *bound* or *free*. It is bound if it is attached to a predicate within the formula and a free variable is not attached to a subformula (Abiteboul, Hull, and Vianu, 1995). In the example $\forall x\ P(x, y)$, x is a bound variable and y is a free variable.

A *formula* is an expression which can refer to several situations using FOL. It can refer to the relationship between two objects, or it can evaluate the relationship of a predicated or non-predicated object or objects (Smullyan, 1968). Suppose P is a predicate and x and y are variables where $x \neq y$. A formula can refer to either a singular predicated object or multiple predicated or non-predicated objects. The predicate P can act upon a single object (e.g. $P(x)$) or more than one object (e.g. $P(x, y)$ or $P(x_1,...,x_n)$). A formula can also refer to the combination of more than one formula. For example, $P(x)$ and $P(y)$ are each a formula, and $P(x) \wedge P(y)$ is also a formula. A formula can be represented with the symbol φ or ψ. Below are examples of each type of possible formula:

- $P(x_1,...x_n)$
- $x \neq y$
- φ
- $\neg\varphi$
- $\varphi \wedge \psi$
- $\varphi \vee \psi$
- $\forall$ x φ (For all x, φ holds)
- $\exists$ x φ (There exists x in which φ is satisfied)

The outcome of a formula can be true or false, and these are called *truth values* (Van Harmelen and Lifschitz V, 2008). Logical connectives are used within FOL to join, add or negate formulas. The logical connectives are a part of *propositional logic*, a subset of FOL (Van Harmelen and Lifschitz V, 2008). A more basic form of logic, it proposes relationships between objects which can join, intersect or exclude them, and allows for conditional statements. The same operators are used in both propositional logic and FOL. Nevertheless, propositional logic is limited in its capacity to formally express complex knowledge (Abiteboul, Hull, and Vianu, 1995). There are four logical operators which carry out the above tasks:

1. Between two formulas, the symbol $\wedge$ denotes a conjunction, creating the intersection of the two, indicating that *both* conditions must be satisfied.

2. The symbol $\vee$ is called a disjunction, and indicates the union of the two formulas, so that what is to be considered must be satisfied by *either* of the formulae.

3. The symbol $\neg$ is called a negation and contradicts a formula, reversing its truth value.

4. The symbol $\rightarrow$ is called an implication. It indicates the outcome, or consequence, of a conditional statement or formula. If $p \rightarrow q$, read as "if p, then q", p is the *antecedent* of the statement, and q is the *consequence*.

5. The symbol $\leftrightarrow$ demonstrates a *biconditional implication*. If $p \leftrightarrow q$, it implies that p is only true if q is true, and q is only true as long as p is true. This statement is read as "p if and only if q".

The truth values of an expression are part of the semantics of FOL. For example, there are 8 implications of truth values from the combination of 2 expressions. Construction of formulae in FOL are based on the above formula types, and can stand alone or as combinations. A well-formed formula can be proven by deducing it into its basic formulae.

For example, supposing φ and ψ are both formulae, the formula $\varphi \rightarrow \psi$ is an implication, and we can symbolise it with Φ. It can be broken down and rewritten as combinations of the basic formulae listed above, and retain its meaning, called an *equivalence* (Van Harmelen and Lifschitz V, 2008). If φ is true, then ψ holds true. If φ is false, ψ is false. We can rewrite Φ as $(\varphi \wedge \psi) \vee (\neg \psi)$. We say that:

$$\varphi \rightarrow \psi \equiv (\varphi \wedge \psi) \vee (\neg \varphi) \tag{5.1}$$

is an equivalence. The equivalent formula can be further simplified into $\neg\varphi \vee \psi$, but for pedagogical purposes to show their equivalence, we show it as it is in equation 5.1.

We can prove this is true by showing that their truth tables for $\varphi \rightarrow \psi$ and $(\varphi \wedge \psi) \vee (\neg \varphi)$ are the same:

The truth table of Table 5.1 for this implication are such because they are defined, conditionally, purely in terms of the truth values of the constituents of the formula, φ and ψ. Therefore, if both φ and ψ are true, then Φ must be true. If φ is true and ψ is false, Φ is false. For a true implication, the truth of ψ is implied by the truth of φ. If φ is true, ψ should be true. A true φ would not imply a false ψ, therefore in the second

φ	ψ	$\varphi \rightarrow \psi$
T	T	**T**
T	F	**F**
F	T	**T**
F	F	**T**

Table 5.1: Truth table for the implication of $\varphi \rightarrow \psi$, where φ and ψ are unique formulae, T=true and F=false.

case, Φ is false. The third case can be proven by looking at the inverse problem: $\varphi \not\rightarrow \psi$ is false because even if φ is true, ψ is nevertheless false. Therefore if $\varphi \not\rightarrow \psi$ is false, then $\varphi \rightarrow \psi$ is true when φ is false and ψ is true. Finally, when φ and ψ are both false, the implication is true: it is true that when φ is false, ψ is also false.

In Table 5.2, we demonstrate how the equivalent formula has the same truth value table as the implication formula

φ	ψ	$\varphi \wedge \psi$	$\neg\phi$	$(\varphi \wedge \psi) \vee (\neg\varphi)$
T	T	T	F	**T**
T	F	F	F	**F**
F	T	F	T	**T**
F	F	F	T	**T**

Table 5.2: Truth table for the equivalence of $\varphi \rightarrow \psi$, where φ and ψ are unique formulae, T=true and F=false.

Furthermore, as stated in number 5 of the logical operators above, the biconditional formula $\varphi \leftrightarrow \psi$ states that φ holds if and only if ψ holds. They are conditions of each other. We can rewrite this as:

$$\varphi \leftrightarrow \psi \equiv (\varphi \rightarrow \psi) \wedge (\psi \rightarrow \varphi) \tag{5.2}$$

where $\psi \ \varphi$ has the reverse truth table of $\varphi \rightarrow \psi$ (Table 5.4). We obtain the truth tables of the biconditional formula and of the equivalence formula to show how they match, in Tables 5.3 and 5.4.

The truth tables match for both, and the semantics are the same. When either φ and ψ, or $\varphi \rightarrow \psi$ and $\psi \rightarrow \varphi$, are both true or both false, the biconditional formula of the two is true.

A *tautology* is a formula, but not all formulae are tautologies. From the Greek work ταυτος meaning identical, it denotes the expression of a self-serving formula, or a formula which is true in every possible outcome

φ	ψ	$\varphi \leftrightarrow \psi$
T	T	**T**
T	F	**F**
F	T	**F**
F	F	**T**

Table 5.3: Truth table for the biconditional formula $\varphi \rightarrow \psi$, where φ and ψ are unique formulae, T=true and F=false.

$\varphi \rightarrow \psi$	$\psi \rightarrow \psi$	$(\varphi \rightarrow \psi) \wedge (\psi \rightarrow \varphi)$
T	T	**T**
F	T	**F**
T	F	**F**
T	T	**T**

Table 5.4: Truth table for the equivalence of $\varphi \leftrightarrow \psi$, where φ and ψ are unique formulae, T=true and F=false.

(Van Harmelen and Lifschitz V, 2008). The laws of tautology declare that if $\varphi \rightarrow \psi$, then $\neg\varphi \rightarrow \neg\psi$ also. Another example of a tautology is:

$$P(x) \vee \neg P(x) \tag{5.3}$$

In the case where an expression can be true or false, the outcome is always true. In the case of equation 5.3, regardless of the truth values of the formulae $P(x)$ and $\neg P(x)$, the truth value of the formula of the union of the two will always be true, and that makes it a tautology.

An axiom is a formula which is considered to hold within a given theory. Its intention is to capture foundational statements and concepts within a given domain. An axiom which is considered to be true must hold true for all logical consequences of the axiom (Abiteboul, Hull, and Vianu, 1995). The semantics of the symbols in an axiom must be defined within the theory. Therefore, axioms can be used within the domain to prove theorems.

The semantics of subsequent formulae within the theory are derived from the axioms. In the case of the above tautology, it can be used as an axiom if we rewrite it as:

$$\forall x \; P(x) \tag{5.4}$$

where $x \in$ Objects and P is a predicate stating "is an unlabelled sulcus". As an axiom, all logical consequences of the axiom hold true as well, such as:

$$\forall x \; P(x) \equiv \neg \exists x \; \neg P(x) \tag{5.5}$$

If we add to the theory another axiom:

$$\forall y \; Q(y) \tag{5.6}$$

where $y \in$ Objects and Q is a predicate stating "is a primary sulcus", we can deduce the following information from axioms 5.4 and 5.6:

$$\forall x \forall y \; (P(x) \wedge \neg \; Q(x)) \vee (Q(y) \wedge \neg \; P(y)) \tag{5.7}$$

This axiom states the statuses of all the variables and constants within our set, by declaring that for all x where x is a variable, x is not a constant, and for all y, y is a constant and not a variable. All logical consequences of this axiom can be formulated as well, such as:

$$\begin{aligned} &\forall x P(x) \equiv \neg \forall x Q(x) \\ &\forall y Q(y) \equiv \neg \forall y P(y) \end{aligned} \tag{5.8}$$

Using FOL, the world can be broken down into constituents and be pieced together, choosing the objects and relationships we want to conserve. The combination of predicates and connectives allow for the logical deduction of knowledge about the objects. The deduction is by interpreting the truth values of the formulae (Van Harmelen and Lifschitz V, 2008). Deductions formed from two or more true propositions are deemed *syllogisms*. From the Greek word meaning conclusion (συλλογισμος) and first coined by Aristotle, it indicates a deduction of knowledge by logical reasoning. For example:

All Primary sulci are sulci

Not all sulci are Primary sulci.

Therefore, there exists at least one sulcus which is not a Primary sulcus.

We use the rules of First-Order Logic to construct sulcus-specific queries in NeuroLang. As domain-specific predicates, we use translations of neuroanatomy, and translations of English descriptors to conjoin or disjoin characterisations of sulci for sulcus-specific mapping on the cortex.

Our domain consists of a resolution of a finite set of elements. Constructing a query language for a finite database is the common adopted practice, and first-order logic can be a good system to represent relational algebra (Abiteboul, Hull, and Vianu, 1995). In subsection 7.1, we will describe how we utilise FOL for the translation of relational algebra for sulcal mapping.

6 HYPOTHESIS OF THIS WORK

Definitions of brain regions occupy the space at the intersection between classical and automated anatomy. In this part, we have demonstrated how sulci are one aspect of brain anatomy, and a vital one. Ranging from boundaries of lobes to boundaries of cytoarchitectonic areas, from associations between function and connectivity, the localisation and identification of sulci continues to be critical to the increasingly interdisciplinary field of computational neuroscience.

The aim of this work is to translate what has been achieved in classical neuroanatomy for centuries into a domain-specific language using first-order logic and sulcal characterisations, to harness the classical method in order to label sulci based on individual topography. From classical neuroanatomy, we have identified a method for anatomical labelling. This method allows for orientating oneself in the brain and navigating oneself across the topography using spatial geometry relations. Using this as a basis, we developed 35 sulcus-specific queries, within their own domain-specific language, NeuroLang. The queries were tested on 52 healthy subjects of the Human Connectome Project dataset, and the query performances were assessed. The results of the queries and their implications on the population and individual levels were reviewed. The significance of our method and findings are examined in the last part, Implications of sulcal mapping using queries, III. We provide a method for bridging the gap between classical neuroanatomy and computational neuroscience for the localisation, identification and labelling of primary, secondary and tertiary sulci in neuroscience.

The contributions of this work are three-fold:

1. Firstly, we establish a sulcal atlas with a semi-hierarchical structure based on an extensive literature review of sulci dating back centuries. Gathering sulcal information on naming, characterisation of the properties and location, existence on the cortex, neurodevelopment and relationships to surrounding cytoarchitectonic regions, we systematised the data to demonstrate our proposed literature-based semi-hierarchical organisation of sulci on the neocortex.

2. Secondly, we carried out the manual segmentation of 10 brains, implementing our sulcal atlas. With an average of 39 sulci per hemisphere, we provide a thorough, verified sulcal dataset which stands

independently from the rest of our work. This dataset can act as ground truth sulcal neuroanatomy for future studies.

3. Lastly, we develop 35 sulcus-specific queries as translations of classical neuroanatomy descriptions of sulci. Tested on a dataset of HCP subjects, we present the results on the population level and individually. We consider the impact of the use of NeuroLang on large-scale sulcal identification as a method for population-level analyses and subject-specific investigations into neuroscientific pursuits. We implement our method are propose a novel, data-driven hierarchical organisation of sulci derived from the quantification of sulcal stabilities.

Part II

DESIGN AND IMPLEMENTATION OF NEUROLANG

7 DEVELOPMENT OF NEUROLANG

Sulcal taxonomy allows for the determination of the cortical regions we seek and a semi-hierarchical order in which to localise them. NeuroLang's goal is to map the cortex in this order. Within our language, the universal set of sulci are the objects. The primary sulci are initially identified using the Destrieux atlas for established consistency, while the remaining objects are unlabelled folds extracted by Mindboggle.

7.1 FIRST ORDER LOGIC FOR THE CONSTRUCTION OF QUERIES

In the field of classical neuroanatomy, locations and morphologies of brain regions do not have precise coordinates interchangeable between subjects. Their traits and associations to neighbouring or non-neighbouring areas exhibit patterns of consistency, but are nonetheless subject to individual variability which is dependant on varying ratios of genetics and environmental influences, depending on the brain region.

By transcribing brain regions into objects which can be described and contrasted, the combination of using predicates for asserting the characteristics of objects and for describing any relationships they may have to each other allows us to transcribe the nature of classical neuroanatomy.

First-order logic (FOL) is applicable to our query-based language because it is the best representation of the syntax and semantics of the language of classical neuroanatomy for the translation into queries, with minimum loss of knowledge. Using FOL in a domain-specific language means we layer formulations of the language of anatomy. In classical neuroanatomy, definitions of sulci vary greatly across sources and are largely dependent on numerous factors. Nonetheless, a few fundamental considerations can be taken into account when assessing how to transcribe classical neuroanatomy into FOL for queries. The computer can then solve queries based on the statements or phrases. As a result of this, it is a good tool to use to translate the nature of neuroanatomy, which largely revolves around the properties and relationships of regions of the brain. Such objects, individually distinct, have key features and relationships with each other which define them. These features are either true or false, and can thus be well represented using FOL.

In our NeuroLang domain, the sulci are the objects. In classical neuroanatomy we name 5 primary sulci. In NeuroLang, the lateral fissure is split into 3 geometrically unique segments: the posterior lateral fissure, the anterior horizontal ramus and the anterior vertical ramus of the lateral fissure. Therefore, the 7 primary sulci segments are predetermined and labelled to begin with, and the unlabelled sulci extracted by Mindboggle are the unlabelled objects. Table 7.1 displays the predicates for characterising the objects. These predicates are used within the queries to bound variables for the identification process. Objects which are not primary sulci, begin as belonging to the predicate Unlabelled sulci, then once they are localised they are added as members to Found sulci. The Found sulci predicate is used in subsequent queries to omit the already labelled sulci. These are examples of one-place predicates.

Two-place predicates represent the relationship of one object to another. In this domain, we design predicates which indicate the relationships of objects to each other in relative space. If we want to convey that a variable x is in front of, or *anterior to* a variable y, we can represent this as

$$\text{anterior to}(x, y) \tag{7.1}$$

Predicates were designed specifically to characterise the objects and their relationships to the primary sulci objects. The full list of predicates to indicate relative relationships is given in Table 7.2, and a description of how we calculate each predicate of relativity is found in section 7.2.1.

Plane	**Sulcus category**
medial sulci	Primary sulci
lateral sulci	Unlabelled sulci
superior sulci	Found sulci
ventral sulci	

Table 7.1: Predicates for characteristics in NeuroLang

We use axioms to define the basis of classical neuroanatomy. Sulci are the extracted objects from the cortex. They are used to distinguish relationships and navigate across the surface, composed of sulci and gyri. The NeuroLang domain is comprised of objects of only sulci. The primary sulci are labelled manually, and are used as landmarks for which we examine the relationships of all the other unlabelled sulci against. Set notations designate the inclusion of an object in a group, and the status of that group, with the symbols $\in$ for 'is in', $\notin$ for 'is not in'. A proper subset, where all the members of a set are also members of another set, is expressed with the symbol $\subseteq$.

Absolute relativity	Partial relativity	Dominant relativity
anatomical anterior of	anterior of	anterior dominant of
anatomical posterior of	posterior of	posterior dominant of
anatomical superior of	superior of	superior dominant of
anatomical inferior of	inferior of	inferior dominant of
		medial dominant of
		lateral dominant of
		overlapping anteriorly dominant
		overlapping superiorly dominant
		overlapping medially dominant

Table 7.2: Predicates for relative relationships in NeuroLang

We begin with definition of the objects:

$$\mathrm{S} \neq \emptyset \tag{7.2}$$

where S refers to the non-empty set of objects with unique elements to be used within our domain.

$$P \subseteq \mathrm{S} \text{ and } |P| = 7 \tag{7.3}$$

In NeuroLang, the initially labelled objects are the primary sulci, so P refers to the set of pre-labelled primary sulci in our model. Seven segments have been predetermined and are manually selected, so P is a subset of S and contains 7 elements.

$$s \in \mathrm{S} \text{ and } s \notin P \text{ and } |s| = n \tag{7.4}$$

where s refers to an object within S, s is not a primary sulcus, and S has a flexible number of elements within it, depending on the subject. Therefore, s is a constant which represents an unlabelled sulcus in S.

$$e \in \mathrm{S} \tag{7.5}$$

where e is a unique element in S, and can refer to either a primary sulcus (an element in P) or an unlabelled sulcus (an element in S, not in P).

$$p \in P \tag{7.6}$$

where p refers to any object within P.

$$\mathrm{CS} \in P \tag{7.7}$$

where CS is a labelled element of P. We denote the Central sulcus as CS.

For the sake of simplicity and clarity, we maintain these definitions of the elements s, e, and p for the rest of this section. These axioms in equations 7.2 to 7.7 provide the general rules for how to define or group the objects in the NeuroLang domain. We can deduce information about objects, such as $s \neq \text{CS}$. We've demonstrated how s is an object in S but does not belong to the subset P. If the CS belongs to P, s cannot be equal to the CS.

Next, we can devise axioms for the predicates which designate relationships between the elements of S. The predicates can specify properties of e, or relations of e to p. Table 7.1 displays the one-place predicates which describe the relations of elements of S. Table 7.2 displays the two-place predicates which describe the possible relations of e to p.

Some properties and relations in Tables 7.1 and 7.2 can be described as implications of each other and some as biconditional formulae. The following formulae adhere to the first-order logic rules of implication and biconditional formulae defined in chapter 5. For the purposes of clarity, the following axioms describe in equations 7.8 to 7.21, the variables s, e and p are used as defined in the above equations 7.4, 7.5, and 7.6, respectively. The axioms for the predicates are the following:

$$\forall e \text{ medial sulcus}(e) \leftrightarrow \neg \text{ lateral sulcus}(e) \tag{7.8}$$

$$\forall s \; \forall p \text{ anatomical anterior of}(s, p) \leftrightarrow \neg \text{ posterior of}(s, p) \tag{7.9}$$

$$\forall s \; \forall p \text{ anatomical superior of}(s, p) \leftrightarrow \neg \text{ inferior of}(s, p) \tag{7.10}$$

$$\forall s \; \forall p \text{ anatomical anterior of}(s, p) \rightarrow \text{anterior of}(s, p) \tag{7.11}$$

$$\forall s \; \forall p \text{ anatomical posterior of}(s, p) \rightarrow \text{posterior of}(s, p) \tag{7.12}$$

$$\forall s \; \forall p \text{ anatomical superior of}(s, p) \rightarrow \text{superior of}(s, p) \tag{7.13}$$

$$\forall s \; \forall p \text{ anatomical inferior of}(s, p) \rightarrow \text{inferior of}(s, p) \tag{7.14}$$

$$\forall s\ \forall p \text{ anterior dominant of}(s, p) \rightarrow \text{anterior of}(s, p) \tag{7.15}$$

$$\forall s\ \forall p \text{ posterior dominant of}(s, p) \rightarrow \text{posterior of}(s, p) \tag{7.16}$$

$$\forall s\ \forall p \text{ superior dominant of}(s, p) \rightarrow \text{superior of}(s, p) \tag{7.17}$$

$$\forall s\ \forall p \text{ inferior dominant of}(s, p) \rightarrow \text{inferior of}(s, p) \tag{7.18}$$

$$\forall s\ \forall p \text{ medial dominant of}(s, p) \rightarrow \neg \text{ lateral dominant of}(s, p) \tag{7.19}$$

$$\forall s\ \forall p \text{ overlapping anteriorly dominant of}(s, p) \rightarrow \neg \text{ anterior dominant of}(s, p) \tag{7.20}$$

$$\forall s\ \forall p \text{ overlapping anteriorly dominant of}(s, p) \rightarrow \text{anterior of}(s, p) \tag{7.21}$$

All logical consequences of the above axioms are true within our model as well. The axiom 7.8 with the biconditional implication implies that the sulci on the medial and lateral surfaces are mutually exclusive; the predicates do not both hold true for an object e. However, e can be both medial and ventral or both lateral and ventral, shown below in equations 7.22 and 7.23. The predicate 'ventral sulci', shown in Table 7.1, is non-mutually exclusive with the other plane predicates, medial sulci and lateral sulci. This is a deduction of the above axioms 7.8 and 7.9, and is shown below in equations 7.22 and 7.23:

$$\exists e \text{ medial sulci}(e) \wedge \text{ventral sulci } (e) \tag{7.22}$$

$$\exists e \text{ lateral sulci}(e) \wedge \text{ventral sulci}(e) \tag{7.23}$$

We use e here instead of s because these formulae are applicable not only to unlabelled sulci objects (s), but also primary sulci objects (p), for

example, the Calcarine sulcus, which can be described by the predicates medial sulci and ventral sulci, according to our definitions.

Likewise, deductions can be made based on the axioms 7.9 to 7.21 involving the anatomical relations. In equation 7.9 we state that for all s and for all p, s is only anatomically anterior of p if and only if it is not posterior of p as well. Similarly, s is not posterior of p if and only if it is anatomically anterior of p. Therefore, the following formula is true:

$$\neg\exists s \forall p \text{ anatomical anterior of}(s, p) \wedge \text{anatomical posterior of}(s, p) \quad (7.24)$$

because there does not exist an object s which is both anatomically anterior of and anatomically posterior of p. However, we can deduce the following formula, which utilises two predicates which are not conditional on each other:

$$\exists s \forall p \text{ anatomical anterior of}(s, p) \wedge \text{anatomical inferior of}(s, p) \quad (7.25)$$

This formula holds true for s because there can exist an object s which can be both anatomically anterior of and anatomically inferior of p. Furthermore, we can deduce more complex relationships from the axioms 7.15 to 7.18 describing relation implications that:

$$\exists x \forall p \text{ anterior of}(x, p) \wedge \text{posterior of}(x, p) \quad (7.26)$$

$$\begin{aligned} &\exists x \ \forall p \text{ anterior of}(x, p) \\ &\wedge \text{ posterior of}(x, p) \\ &\wedge \text{ superior of}(x, p) \\ &\wedge \text{ inferior of}(x, p) \end{aligned} \quad (7.27)$$

We can describe more complex relationships between variables and constants, wherein the exact nature of the relationship is unknown or more sensitive to variability:

$$\begin{aligned} &\exists x \ \forall p \text{ anterior dominant of}(x, p) \\ \vee &\text{ overlapping anterior dominant of}(x, p) \\ \wedge &\text{ overlapping medial dominant of}(x, p) \\ &\wedge \text{ superior of}(x, p) \end{aligned} \quad (7.28)$$

In this subsection we provide the basis for how we use FOL to construct queries in NeuroLang. Next, we apply our predicates and axioms to construct sulcus-specific queries as translations of their neuroanatomical descriptions.

7.1.1 Translation of classical neuroanatomy in NeuroLang using FOL

We use the above axioms and domain-specific predicates described in 7.1 to construct a query to localise the Inferior Frontal Sulcus (IFS), a sulcus in the frontal lobe which exists in all hemispheres and is integral for the localisation of Broca's area, a functional territory essential for speech production (Keller et al., 2007; Papoutsi et al., 2009). The IFS is represented as an unknown variable x, with characteristics and relationships to the labelled primary sulci. A query is a combination of predicates of the object to make a formula which narrows down the search to the brain region where the IFS is expected.

We characterise the IFS by using the predicates over x which model the anatomical description of the sulcus. As we described in section 3.2, we know that the IFS is an unlabelled sulcus on the lateral surface, in the frontal lobe. The frontal lobe is bounded by the Central sulcus posteriorly, and the Lateral fissure inferiorly. We construct individual formulae which characterise the IFS using predicates for both characteristics and relative relationships found in Tables 7.1 and 7.2.

Source	Description for Inferior frontal sulcus
Destrieux et al., 2010	"The IFS is connected to the inferior part of the precentral sulcus and runs parallel to the superior segment of the circular sulcus of the insula."
Rademacher et al., 1992	"...the superior and inferior frontal sulci follow a course parallel to each other and to the interhemispheric plane. Posteriorly both meet the precentral sulcus at right angles."
Keller et al., 2007	"[The IFS] is identified as the first ventral horizontal frontal sulcus extending from the inferior precentral sulcus...lying immediately dorsal to the anterior ascending ramus of the Sylvian fissure."
Catani and Schotten, 2013	"The superior and inferior frontal sulci extend horizontally from the precentral sulcus..."

Table 7.3: Descriptions of the inferior frontal sulcus (IFS) in four exemplary neuroanatomical sources.

From the classical neuroanatomy descriptions of the IFS (Table 7.3), we assemble the formulae as translations of the IFS characterisations, using the built-in predicates.

Each of the formulae applied to the unlabelled objects will be *true* or *false*. We combine formulae together to make a more detailed description

of the outcome we want, by adding quantifiers and logical connectives. When applying all the formulae together, we expect at least one object in S to be represented by the quantified variable as the intersection of all the relations and characteristics that apply to the IFS. In this case, the variable x is a bound variable of the predicate 'Inferior frontal sulcus candidate':

$$\begin{aligned} &\forall x \text{Inferior frontal sulcus candidate}(x) \Leftarrow \\ &\text{anatomical anterior of}(x, \textit{Central sulcus}) \\ \wedge\ &\text{anatomical superior of}(x, \textit{Ant. horizont. ramus Lateral fissure}) \\ \wedge\ &\text{lateral sulci}(x) \\ \wedge\neg\ &\text{Primary sulci}(x) \end{aligned} \tag{7.29}$$

Sulci are typically highly variable in size, shape and segmentation. Due to this nature, there often exists more than one sulcus which matches the classical neuroanatomical description. It is possible that the many localised sulci can be various separate segments of the same target sulcus. As we present in Table 7.3, the IFS descriptions are often combined with its neighboring sulci since they share many characteristics or can be connected. In such cases, it could be desirable to accept the targeted sulcus as a multi-segmented sulcus and label each of the segments as the target sulcus. In most cases however, a single sulcus is the desired outcome. It would be advantageous for the query to omit unwanted sulci which may be nearby and fit the query's description but are not anatomically part of the target sulcus. A solution is to ensure unicity of the results of a query. We introduce an option of a secondary query, with the predicate 'Inferior frontal sulcus', for choosing a single sulcus from the results of the first query (7.29), if the first query returns more than one sulcus.

$$\begin{aligned} &\forall x \text{Inferior frontal sulcus}(x) \Leftarrow \\ &\text{Inferior frontal sulcus candidate}(x) \\ \wedge\forall y(\ &\text{Inferior frontal sulcus candidate}(y) \wedge x \neq y \\ \wedge\ &(\text{mean } x \text{ coordinates}(x) > \text{mean } x \text{ coordinates}(y))) \end{aligned} \tag{7.30}$$

The second query (7.30) searches for one sulcus from the results of the first query (7.29). It does this by firstly checking that there is indeed more than one unique result belonging to 'Inferior frontal sulcus candidate'. The first condition this variable (y) needs to satisfy is that it belongs to the results found previously (Inferior frontal sulcus candidate(y)). The second condition ensures that the results of the first query include more than one sulcus ($x \neq y$). Then, it compares each unique pair of results from 7.29 to find the sulcus with, in this case, the largest mean x coordinates. We compare the mean x coordinates of

each sulcus pair in the first query. The x-coordinates indicate how medial or lateral the voxel is. We ensure that the sulcus we want does not have any other sulcus with a greater absolute mean x-coordinates value (mean x coordinates(x) $>$ mean x coordinates(y)). This implies that we take the sulcus which is the most lateral, on average. Thus, the second query 7.30 with the predicate 'Inferior frontal sulcus' ensures a result of one sulcus, the sulcus which satisfies all the conditions of the first query, and ensures that the single most lateral sulcus of those results, if more than one, was chosen.

The conditions included in both the first and second queries are mutable. In the second query, the comparison of x, y or z mean coordinates can be altered to ensure the outcome of the most medial, lateral, superior, inferior, anterior or inferior sulcus, from their average coordinate values.

7.2 BUILT-IN PREDICATES IN NEUROLANG

Within the domain-specific language of NeuroLang, the relations are predicates to express relationships of a target sulcus to the primary sulcus. In the previous section 7.1 we defined the predicates we built into the backend of NeuroLang which characterise features of objects and relationships between objects. We outlined the axioms which govern the rules for how to define or group objects within the NeuroLang domain. In this section, we describe how we computed the relationships used as predicates.

7.2.1 Bounding boxes

Relativity was determined using cardinal directionality (CD). CD conveys the relative relationships of objects in space, assuming a fixed reference (Navarrete et al., 2013). We considered CD in NeuroLang as the relationships of sulcal objects to each other, using the anatomical terms of location as interpretations of the x, y, and z axes in imaging space. For example, 'anterior' refers to the y-axis, where y=0 typically runs through or near the Central sulcus around the center of the brain. The most anterior point of the brain has the maximum y-value, while the most posterior point of the brain has the minimum y-value. Taking each sulcus as an object in 3-dimensional space, the sulcus was treated as a cuboid, in which its dimensions were the range of its extreme coordinates in each axis. We conceived bounding boxes around each sulcus, and relative directions of sulci to each other by the minimum and maximum of their bounding boxes in 3 dimensions. Therefore each sulcus was represented as a 2D rectangle in each dimension. Relationships of relativity between sulci in

each axis, outlined in Table 7.2, were determined based on the values of the coordinates on an axis and the proportion of coordinates on an axis.

We adopt the strategy laid out by Navarrete et al., 2013, for the comparison of rectangles which bound the sulci in each dimension. Suppose the minimum and maximum voxel values of two rectangles S and P are S_{min} / P_{min} and S_{max} / P_{max}, respectively. The minimum and maximum bounds for the regions would be at the line of *axis*=min and *axis*=max, where *axis* is the x, y or z dimensions. The type of relativity between two objects on an axis are calculated by comparing the $S_{min/max}$ and $P_{min/max}$ of either the entire bounding box or of 1mm² voxel volumes (standard voxel size). Using interval algebra, we compared intervals of 1mm volumes between pairs of sulci along the same axis, either on the medial-lateral (x-axis), anterior-posterior (y-axis), or superior-inferior (z-axis) axes. Each sulcal interval was compared with a primary sulcus interval on the same axis. Each pair was designated a term of relativity, using anteriority as an example relation, as follows:

7.2.1.1 *Absolute relativity*

On a single axis, the conditions for absolute relativity between two sulci are that there is no overlap between their rectangles. We applied the minimum bounding rectangle method as described in Navarrete et al., 2013, where the smallest 2-dimensional rectangle which binds the entire object on one axis is used as a representation of the object in space on that axis. Absolute relativity between two sulci was by establishing that the rectangle of a reference region was entirely separate of the rectangle of a primary region. A reference sulcal rectangle S was 'anatomical anterior of' a primary sulcal rectangle P if the y-values fulfilled the conditions of equation 7.31:

$$P_{min} < P_{max} < S_{min} < S_{max} \tag{7.31}$$

7.2.1.2 *Partial relativity*

Partial relativity was determined by using the 1mm² sulcus voxels per axis instead of the minimum bounding rectangle. Using again anteriority as an example, if there exists at least one voxel which belongs to a reference sulcus S which satisfies equation 7.31 relative to a primary sulcus P, S is 'anterior of' P.

7.2.1.3 *Dominant relativity*

To determine dominant relativity, we compared individual voxels of a reference sulcus S to the bounding box of a primary sulcus P. Each voxel of S was determined to have a relationship to the minimum bounding

rectangle of P; a voxel could be anterior of P, posterior of P, or overlapping with P on the y-axis. An S voxel was 'overlapping' if it satisfied the following equation:

$$P_{min} < S_{min} < S_{max} < P_{max} \tag{7.32}$$

The mode relation of all the voxels relations of S to P was selected, and branded as the 'dominant' relationship of S to P.

Predicates were created from the relativities. Absolute and partial relativity were in the form of two-place predicates, such as in equation 7.1. Dominant relativity predicates were one-place predicates for each primary sulcus in each dimension. For example, for:

$$\exists x \text{ Central sulcus overlapping antero-posteriorly}(x) \tag{7.33}$$

The precentral or postcentral sulci can both satisfy this query. Overlapping or parallel sulci are common across the cortex, and we present our method to computationally represent these relationships.

7.2.2 Planes in Neurolang

The process for dominant relativity (subsection 7.2.1.3) was carried out for sulci to determine whether they belonged on the medial, lateral, or ventral planes. Sulci were compared to the deepest point of the Callosal sulcus (maximum absolute value of x of the Callosal) for the medial and lateral planes, and the most inferior point of the Callosal sulcus (minimum value of z) for the ventral plane. One-place predicates were created for each plane, as shown in Table 7.1.

In addition to using planes, medial/lateral relationships could be applied by the dominant relationship of a reference sulcus S to a primary sulcus P on the x-axis, as described in section 7.2.1.3.

7.3 NEUROLANG QUERIES

The queries used in the final analyses of NeuroLang were representations of their anatomical descriptions, but not direct translations. In order to match the spatial representations of primary sulci relationships to the descriptive representations, we designed the queries on the sulci of the Destrieux atlas, a current widely-accepted atlas used in the HCP dataset. Through an iterative process of trial-and-error, we made adjustments along the way to more accurately localise the target sulcus, while conserving

Sulcus name	Queries for Inferior frontal sulcus
Inferior frontal	$\forall x$ *Inferior frontal sulcus candidate*$(x) \Leftarrow$ *anatomical anterior of*$(x,$ **Central sulcus**$)$ $\wedge$ *anatomical superior of*$(x,$ **Ant. horizontal Lateral fissure**$)$ $\wedge$ *lateral sulci*(x) $\wedge\neg$ *Primary sulci*(x) $\forall x$ *Inferior frontal sulcus*$(x) \Leftarrow$ *Inferior frontal sulcus candidate*(x) $\wedge\forall y$ *(Inferior frontal sulcus candidate*$(y) \wedge x \neq y$ $\wedge$(mean x coordinates$(x) >$ mean x coordinates$(y)))$

Table 7.4: Queries for the Inferior frontal sulcus in NeuroLang, in first-order logic.

anatomical information. We utilised the hold-out method of testing the query on a different subset of our subjects with each iteration.

For example, the IFS is described as lying 'dorsal to the anterior ascending ramus of the Sylvian fissure' (Keller et al., 2007) (Table 7.3), but is more accurately represented in space when replacing the anterior ascending ramus with the anterior horizontal ramus (Figure 7.1), and was thus how the query was constructed (Table 7.4).

The cingulate sulcus is one of the most consistent features on the medial plane, but is often broken up in atlases to correspond to other features such as surrounding cytoarchitectonics or relationships to functional areas (Amiez, Wilson, and Procyk, 2018; Destrieux et al., 2010; Fornito et al., 2006; Paus et al., 1996; Vogt et al., 1995). Thus, its nomenclature and segmentation often exhibit discrepancies (Palomero-Gallagher et al., 2008). We gather four sources of cingulate definitions from classical neuroanatomy in Table 7.5. Our query for the cingulate sulcus reflects its concentric trajectory to the callosal sulcus (the sulcus surrounding the corpus callosum), on the anterior side, in Table 7.3. We depict its representation, in the left hemisphere as an example, in Figure 7.3, with the selection of the most posterior sulcus in the case of more than one candidate, in Figure 7.4.

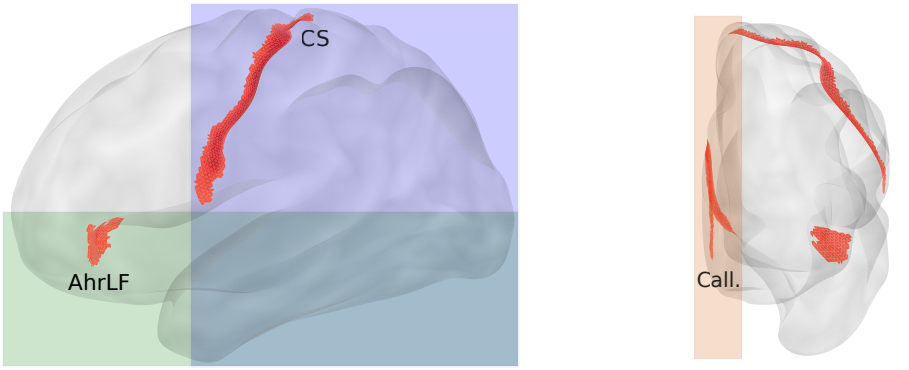

Figure 7.1: The inferior frontal sulcus as represented by its spatial relationships to the primary sulci: anatomically anterior of the Central sulcus (*CS*), anatomically superior of the Anterior horizontal ramus of the Lateral fissure (*AhrLF*), and on the lateral plane (lateral of the Callosal sulcus, *Call.*).

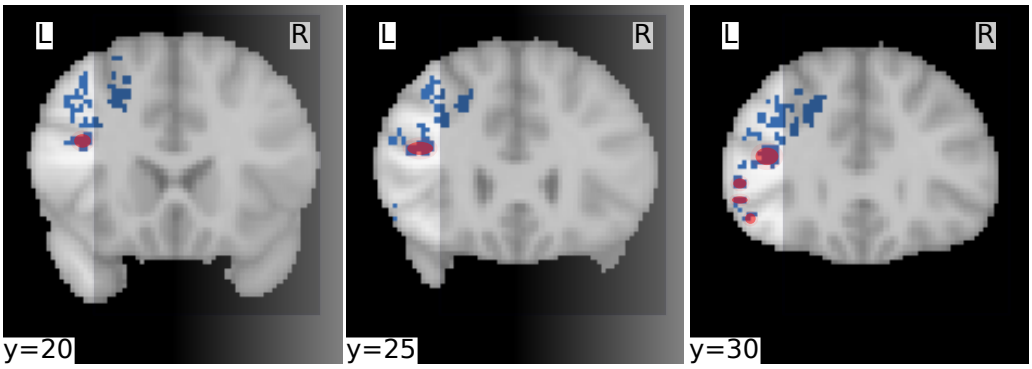

Figure 7.2: The results of the query searching for inferior frontal sulcus candidates. In the case of more than one result, the Inferior frontal sulcus query compares pairs of sulci, to choose the most lateral sulcus, the one with the largest average absolute x-value. The final result is highlighted in red.

Source	Description for Cingulate sulcus
Paus et al., 1996	"The cingulate sulcus courses around the corpus callosum and extends posteriorly into the parietal lobe as the marginal ramus."
Rademacher et al., 1992	"The cingulate sulcus follows a course parallel to the corpus callosum...anteriorly it arches over the genu of the corpus callosum."
Destrieux et al., 2010	"...the main part of [the cingulate] sulcus parallels the anterior and middle parts of the corpus callosum..."
Vogt et al., 1995	The cingulate sulcus can exist with or without segmentation or anastamoses, or as a single or parallel sulcus.

Table 7.5: Descriptions of the Cingulate sulcus in four exemplary neuroanatomical sources.

Sulcus name	Queries for Cingulate sulcus
Cingulate	$\forall x$ *Cingulate sulcus candidate*$(x) \Leftarrow$ *anterior of*$(x$, **Callosal sulcus**$)$ $\wedge$ *superior of*$(x$, **Callosal sulcus**$)$ $\wedge\neg$ *posteriorly dominant of*$(x$, **Callosal sulcus**$)$ $\wedge$ *medially dominant of*$(x$, **Central sulcus**$)$ $\wedge\neg$ *Found sulci*(x) $\wedge\neg$ *Primary sulci*(x) $\forall x$ *Cingulate sulcus*$(x) \Leftarrow$ *Cingulate sulcus candidate*(x) $\wedge\forall y$ *(Cingulate sulcus candidate*$(y) \wedge x \neq y$ $\wedge$(mean y coordinates$(x) <$ mean y coordinates$(y)))$

The Superior temporal sulcus is typically described as following a trajectory similar to the Lateral fissure just above it (Table 7.6).

We designed the query for the Superior temporal sulcus to include eliminating sulci *outside* the target positions in space (Table 7.3).

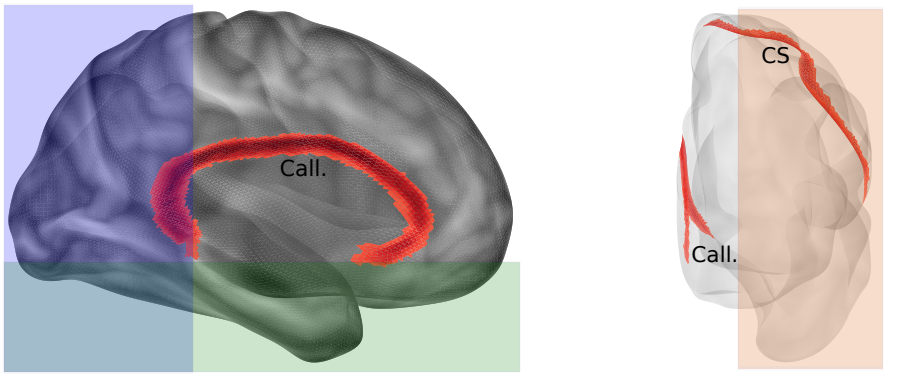

Figure 7.3: The cingulate sulcus as represented by its spatial relationships to the primary sulci: not posteriorly dominant of the Callosal sulcus (*Call.*), superior of the Callosal sulcus, and on the medial plane (medially dominant of the Central sulcus, *CS*).

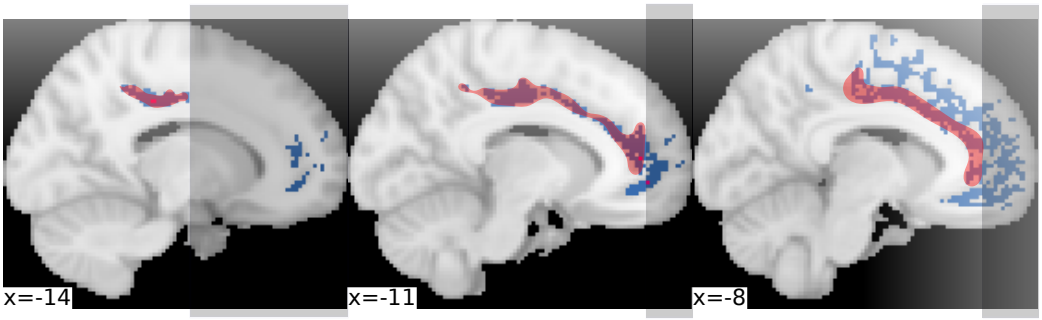

Figure 7.4: The results of the query searching for Cingulate sulcus candidates, in the left hemisphere. In the case of more than one result, the Cingulate sulcus query compares pairs of sulci, to choose the most anterior sulcus, the one with the smallest average y-value. The final result is highlighted in red.

Source	Description for Superior temporal sulcus
Rademacher et al., 1992	"The trunk of the superior temporal sulcus runs parallel to the sylvian fissure..."
Destrieux et al., 2010	"...the superior temporal sulcus, running parallel to the lateral sulcus, from the temporal pole to the inferior parietal lobule."
Ochiai et al., 2004	The superior temporal sulcus is divided into six sub-parts, spanning from the anterior temporal lobe to the intraparietal sulcus.
Ribas, 2010	"The superior temporal sulcus is always a very well defined and deep sulcus and often presents as a continuous sulcus because of its parallelism with the sylvian fissure."

Table 7.6: Descriptions of the Superior temporal sulcus in four exemplary neuroanatomical sources.

Sulcus name	Queries for Superior temporal sulcus
Superior temporal	$\forall$x *Superior temporal sulcus candidate*(x) $\Leftarrow$ *overlapping antero-posteriorly dominant of*(x, **Lateral fissure**) $\wedge$ *lateral sulci*(x) $\wedge\neg$ *Primary sulci*(x) $\wedge\neg$ *Found sulci*(x) $\forall$x *Superior temporal sulcus*(x) $\Leftarrow$ *Superior temporal sulcus candidate*(x) $\wedge\forall$y (Superior temporal sulcus(y) $\wedge$ $x \neq y$ $\wedge$ (mean x coordinates(x) $>$ mean x coordinates(y)))

The spatial representations of the query for the Superior temporal sulcus are shown in Figures 7.5 and 7.6.

Similarly, the Precentral sulcus is often described as an anterior imitation of the Central sulcus (Table 7.7).

As shown in Table 7.7, the precentral sulcus is often divided into segments. We therefore designed the query to omit irrelevant sulci rather than define the characteristics of the Precentral sulcus, which are rooted in its trajectory.

We depict the omissions of the queries for the Precentral sulcus in Figure 7.7. In Figure 7.8, we choose the most posterior candidate from the sagittal plane, as suggested by Germann et al., 2005.

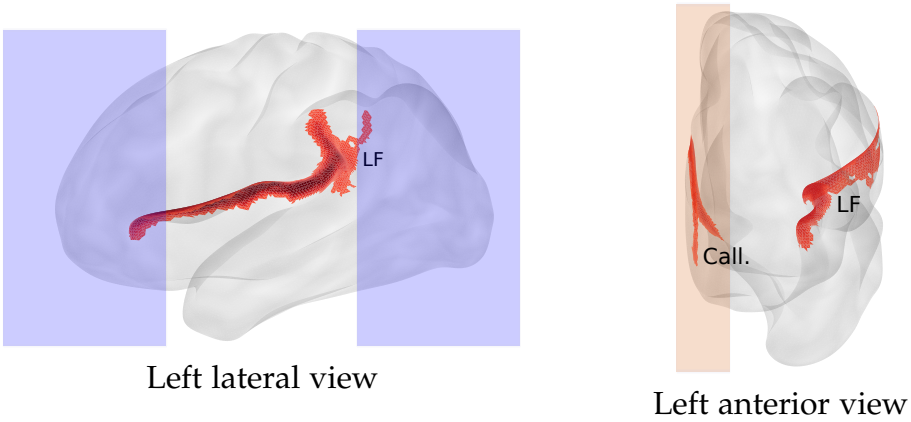

Left lateral view

Left anterior view

Figure 7.5: The Superior temporal sulcus as represented by its spatial relationships to the primary sulci: dominantly overlapping with the Lateral fissure (*LF*), on the anterior-posterior axis, and on the lateral plane (lateral to the Callosal sulcus (*Call.*).

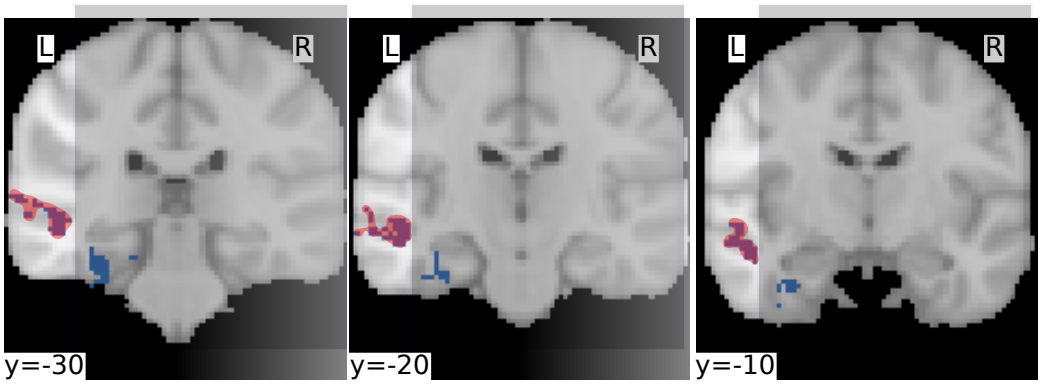

Figure 7.6: The results of the query searching for Superior temporal sulcus candidates, in the left hemisphere. In the case of more than one result, the Superior temporal sulcus query compares pairs of sulci, to choose the most lateral sulcus, the one with the largest absolute average x-value. The final result is highlighted in red.

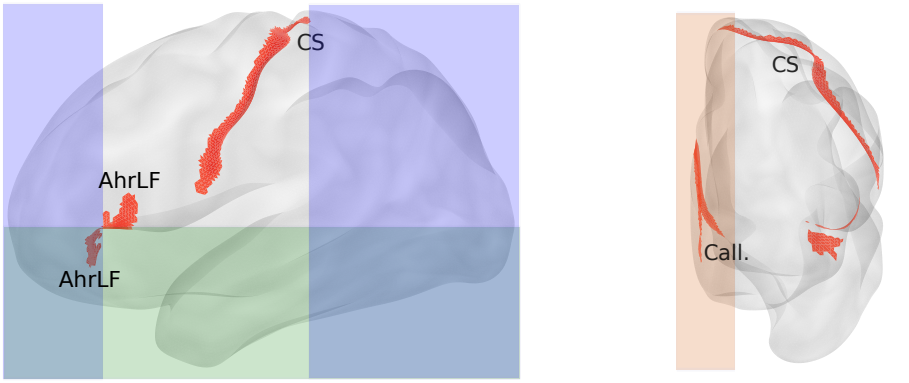

Left lateral view Left anterior view

Figure 7.7: The Precentral sulcus as represented by its spatial relationships to the primary sulci: posteriorly dominant of and anatomically superior of the Anterior horizontal lateral fissure (*AhrLF*), overlapping antero-posteriorly dominant of the Anterior vertical lateral fissure (*AvrLF*), not anatomically posterior of the Central sulcus (*CS*), overlapping medially dominant of the Central sulcus, and on the lateral plane (lateral of the Callosal sulcus (*Call.*).

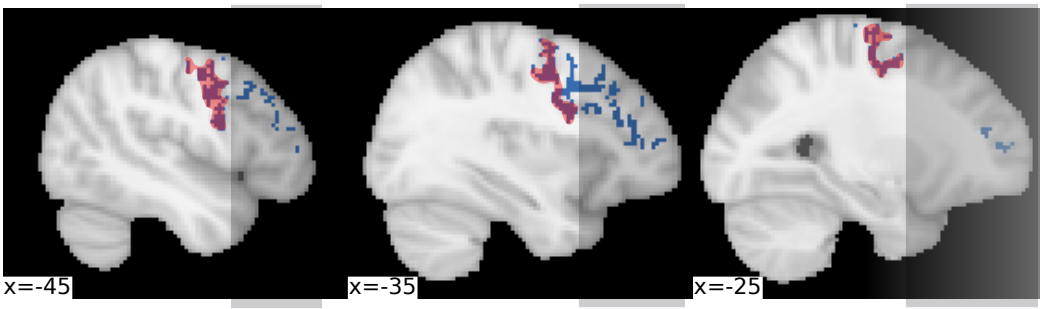

Figure 7.8: The results of the query searching for Precentral sulcus candidates, in the left hemisphere. In the case of more than one result, the Precentral sulcus query compares pairs of sulci, to choose the most posterior sulcus, the one with the smallest average y-value. The final result is highlighted in red.

Source	Description for Precentral sulcus
Destrieux et al., 2010	"The precentral sulcus anteriorly parallels the central sulcus and is divided into superior and inferior parts..."
Rademacher et al., 1992	"The precentral sulcus follows a dorsomedial to ventrolateral course that is rostral and roughly parallel to the central sulcus."
Catani and Schotten, 2013	"The precentral gyrus runs anterior and parallel to the central sulcus and is delimited anteriorly by the precentral sulcus."
Germann et al., 2005	"[The precentral sulcus] is oriented in a more or less dorsoventral direction and can be readily identified and followed in horizontal sections... [it] can be considered...as a sulcal complex consisting of a set of sulci."

Table 7.7: Descriptions of the Precentral sulcus in four exemplary neuroanatomical sources.

In total, we created 35 sulcus-specific queries in this way. The full list of sulcus-specific queries, written in FOL, and in the order in which they were used in NeuroLang to identify the sulci, can be found in Appendix A.2. NeuroLang's objective was to label a subset of sulci on each hemisphere, according to individual morphology. All queries were ran on all subjects, with each query searching for *if* there were at least one sulcus which satisfied the conditions of the query (SULCUS CANDIDATE), and if there were more than one, a second query to select the single most anterior, posterior, superior, inferior, medial or lateral SULCUS. The sulcus was labelled and excluded from subsequent searches.

Sulcus name	Queries for Precentral sulcus
Precentral	$\forall$x *Precentral sulcus candidate*(x) $\Leftarrow$ (*posteriorly dominant of*(x, **Ant. horizontal Lateral fissure**) $\vee$ *overlapping antero-posteriorly dominant of*(x, **Ant. vertical Lateral fissure**)) $\wedge\neg$ *anatomical posterior of*(x, **Central sulcus**) $\wedge$ *overlapping medially dominant of*(x, **Central sulcus**) $\wedge$ *anatomical superior of*(x, **Ant. horizontal Lateral fissure**) $\wedge$ *lateral sulci*(x) $\wedge\neg$ *Primary sulci*(x) $\forall$x *Precentral sulcus*(x) $\Leftarrow$ *Precentral sulcus candidate*(x) $\wedge\forall$y (*Precentral sulcus candidate*(y) $\wedge$ $x \neq y$ $\wedge$(mean y coordinates(x) $<$ mean y coordinates(y)))

Table 7.9: Queries for the Precentral sulcus in NeuroLang.

8 MANUAL SEGMENTATIONS

8.1 METHOD FOR MANUAL SEGMENTATIONS

As it stands, neuroimaging teeters at the crossroads of both classical neuroanatomy and computational neuroscience. The manual segmentation or labelling using methods derived from classical neuroanatomy have been coined as 'tedious anatomy' by Devlin and Poldrack, 2007. Such 'tedious anatomy' holds favour as a reliable source of 'ground truth' anatomy, but automated extraction and identification of sulci paves the way forward as neuroimaging analyses gain strength in numbers. Therefore, as a basis for our tool, we conducted our own 'tedious anatomy' on 10 subjects of the Human Connectome Project dataset. Our literature review in section 3.2 provides an overview of how classical neuroanatomy had been carried out and the classification of sulci, and we followed these characterisations of sulci. The subjects were 50% male, healthy, aged 22-31, right-handed. We carried out segmentations using the classical neuroanatomy method: beginning by orientating ourselves in the brain using the primary sulci as landmarks, we subsequently identified neighbouring sulci by their relationship to the primary sulci, and from those the remaining tertiary sulci which are typically shallower and more variable in their morphology. This work was done in collaboration with Nikos Makris at Harvard University.

Each hemisphere was manually segmented using the open source tool Blender (Community BO, 2018). The sulci were segmented according to their descriptions in section 3.2. We labelled a range of 38-41 sulci per hemisphere, with an average of 39. Each sulcus segmentation was confirmed by our expert neuroanatomist collaborator, Dr Nikos Makris. The morphology of the sulcal segmentation was discussed on the individual level, and on the population level we observed emerging patterns. This information was included in the consideration for sulcal ordering in the subsequent semi-hierarchical set for NeuroLang, depicted in Figure 3.2.

We accomplished three fundamental goals by manually segmenting 20 hemispheres:

- The establishment of 'ground truth' for which to compare and contrast our NeuroLang results with. This was of particular importance for the tertiary sulci which lack consistent template counterparts.

- Evidence-based analysis of sulcal 'stability' in addition to the literature-based. This measure of stability was incorporated into our sulcal organisations.
- The order in which we segmented sulci manually along with the semi-hierarchical organisation of our atlas governed the order in which the queries label sulci in our NeuroLang analyses.

8.2 SULCAL ATLAS AS A SOURCE FOR ANATOMICAL LABELLING

In this chapter we present work in collaboration with Kamalakar Dadi, Gael Varoquaux, Krzysztof J Gorgolewski, Demian Wassermann, Bertrand Thirion and Arthur Mensch. Kamalakar Dadi is the first author of this paper, and conducted the experiments with Arthur Mensch. I was involved in the anatomical naming of the atlas regions, and decided to give all regions purely anatomical names (e.g. 'posterior Inferior frontal gyrus') as opposed to named regions (e.g. 'Broca's area'), functional (e.g. 'primary motor cortex') or cytoarchitectonic (e.g. 'Brodmann area 44') labels. The labels by anatomical location are more common and widely-accepted.

The anatomical framework gathered as the basis for this work, described in full in section 3.2, was utilised and expanded upon to include gyri, subcortical structures and white matter tracts. Data-driven brain regions derived from functional signals at dimensions of 64, 128, 256, 512 and 1024.

At each dimension, the modes with regions were matched with brain regions in existing gold-standard atlases: the Harvard-Oxford atlas (Desikan et al., 2006), Destrieux atlas (Destrieux et al., 2010), the MIST atlas (Urchs et al., 2019), Johns Hopkins University (JHU) atlas (Hua et al., 2008), and the Dierdrichsen cerebellum atlas (Diedrichsen et al., 2009). We named each mode from the anatomical structure that it most overlapped with. When the overlap was weak, we looked up the structure in standard classic anatomy references (Catani and Schotten, 2013; Duvernoy, 1999; Ono, Kubik, and Abernathey, 1990; Rademacher et al., 1992; Schmahmann et al., 1999). An example of this process is shown in Figure 8.1.

Structural anatomical names were given to each parcel at each dimension, in a Dictionary of Functional Modes (DiFuMo) (Dadi et al., 2020). Each label within a dimension was unique and derived from the extensive anatomical research conducted as a basis for NeuroLang, with the sulci specifically being a manifestation of our sulcal atlas.

The extraction of brain regions by certain specifications is far from new; more recently, atlases have been able to benefit from multimodal imag-

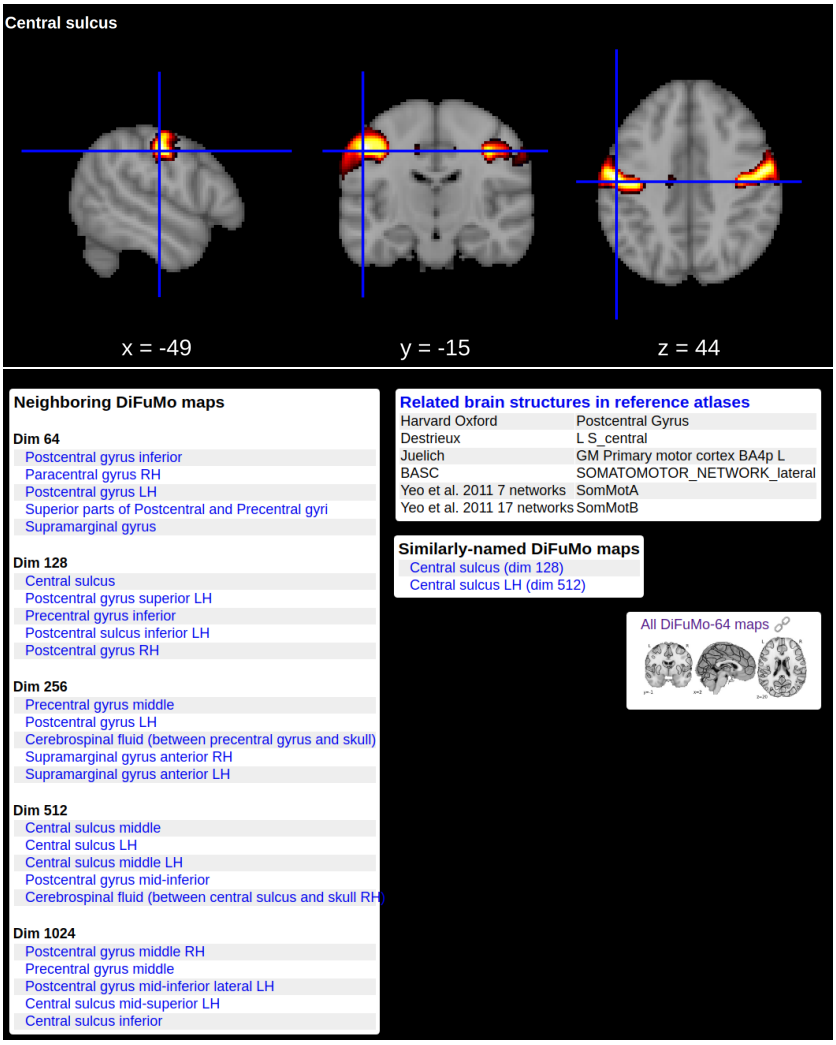

Figure 8.1: DiFuMo atlas region depicting the functional signal corresponding to the Central sulcus in both hemispheres, in 64 dimensions. Each functional region in DiFuMo was given the label of its largest overlap in 4 atlases. We checked the given label for accuracy and, in the case of disagreements, manually checked and labelled according to classical neuroanatomy sources. The DiFuMo region location is also compared with neighbouring regions within the same and other dimensions. For full details, please refer to Dadi et al., 2020. The DiFuMo atlas parcellations in the five dimensions can be found at https://parietal-inria.github.io/DiFuMo/.

ing (Desikan et al., 2006; Eickhoff et al., 2007; Glasser et al., 2016). DiFuMo, alternatively, captures brain activity and the defined regions according to this signal often correspond to classical anatomical delineations.

This work provides multidimensional atlases of functional modes which can be used to extract functional signals or investigate relationships of functional signals with connectivity. The standardisation of anatomical nomenclature facilitates multimodal study and establishes consistent interpretation of results across dimensions. The DiFuMo atlas parcellations in the five dimensions can be found at https://parietal-inria.github.io/DiFuMo/.

8.3 VALIDATION FOR NEUROLANG QUERIES

We established a dataset of ground truth sulci for which we can validate our query sulcus results with. Sensitivity of a query is determined by the proportion of correctly identified items. One way we validate sensitivity of a query is with its manual segmentation counterpart. This provides an indication of overlap in position on the cortex.

Sensitivity of each secondary query was determined by the ratio of overlap between each query result and the probability map for its manually segmented counterpart. With the notable exception of the cingulate sulcus, tertiary sulci were typically smaller, shallower, or less stable in their existence or morphology, and had no distinct Destrieux counterpart. For tertiary query results, we firstly examined the ratio of existence, that is, the proportion of subjects in which a sulcus was found from the query. Validation of tertiary sulci was confirmed by plotting all the query results probabilistically and then confirming the percentage overlap of each tertiary query result with the probability map of its ground truth counterpart. Figure 8.3 shows the proportion of each query result overlap to its ground truth counterpart. In addition to this and when applicable, we manually identified the sulcus from the probability map blindly, without the query name.

8.3.1 Sulcal stability of manual segmentations

Ten subjects of the HCP dataset which were not included in the NeuroLang dataset were manually segmented using the tool Blender, according to classical neuroanatomy guidelines. An average of 39 sulci were labelled in each hemisphere, including the primary sulci. Based on these 10 subjects, we generated probability maps of the location of each sulcus per hemisphere. The probability maps for each sulcus were considered as the

'ground truth' for validation of our query results. Please refer to Figure 8.2 below for some notable manual segmentation probability maps. These indicated the reliability and range of variability which various sulci exhibit. From the probability maps, we calculated the mean probability and the mass probability per sulcus. We evaluated sulcal location reliability by measuring the largest common sulcus surface area. Mass probability maps provided a quantification of ground truth sulcal stability (Figure 8.2). We took this into account when establishing our semi-hierarchical sulcal atlas (Figure 3.2). We discuss the use of our manual segmentations as a baseline for our analyses with NeuroLang in Chapter 9 which follows.

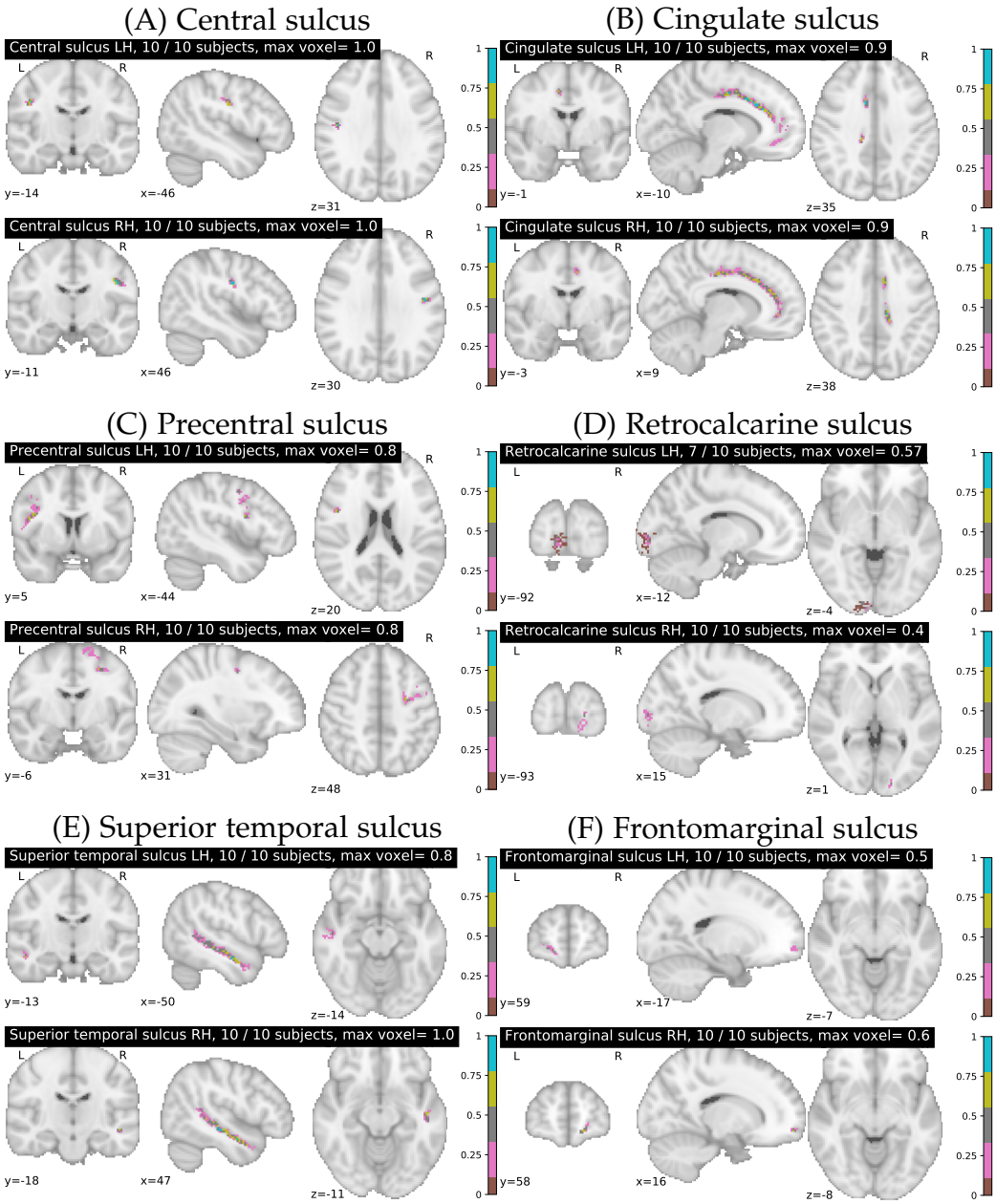

Figure 8.2: Probability maps for some notable manually segmented sulci in 10 subjects, in both hemispheres. The Central sulcus (A) is a primary sulcus and is considered amongst the most stable across the cortex, the precentral (C) and superior temporal (E) sulci are classified as secondary sulci, and the cingulate (B), retrocalcarine (D) and frontomarginal (F) sulci are categorised as tertiary sulci.

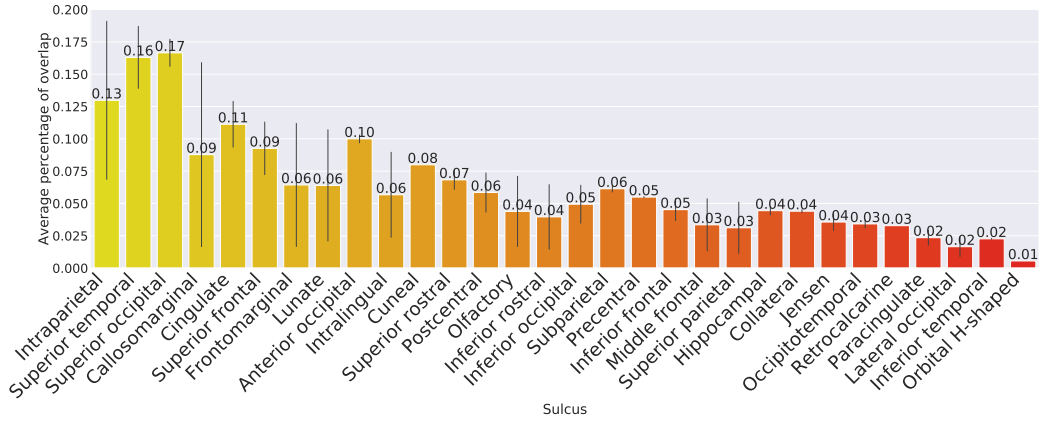

Figure 8.3: Average overlap of each query's result in 52 subjects to the average of their manual segmentation counterpart, in both hemispheres. Average overlap between the two provides an indication of stability in terms of the locations of the sulci from queries used in NeuroLang. The higher the average overlap, the higher the overlap in the location of a sulcus in the expected location, as determined by the manual segmentations. Error bars show confidence interval at 95%.

9 OUTCOMES OF NEUROLANG EXPERIMENTS

We delve into the details of the experiments and results obtained from our analyses using NeuroLang. We ran the same 35 queries for two analyses: on unlabelled and un-anatomically segmented sulci extracted by Mindboggle in 52 subjects of the HCP dataset (50% male, 22-35 years old, right-handed), and on the manually segmented sulci in a subset of 10 subjects of the HCP dataset. We investigate how the NeuroLang queries are able to identify the specific morphologies of sulci within individual subjects, and population-level trends of sulcal morphologies and stabilities. We quantify sulcal stability within our population to obtain a novel organisation of the cortex.

9.1 NEUROLANG ON MINDBOGGLE-EXTRACTED SULCI

To test our queries, we required a way to obtain unlabelled sulci from a subject, which are unsegmented and do not conform to an existing atlas. The open-source software Mindboggle (Klein et al., 2017) fitted our requirements as a method for procuring sulci with these specifications, or what they call 'folds'. Mindboggle, as we described in subsection 4.1.4, extracts folds based on the shape and depth measures of the cortex, features which are characteristic to sulci (subsection 3.1.1). The folds are variable in size and shape and do not always conform to neuroanatomical expectations of sulcal morphology. For this reason, Mindboggle allows for the extraction of 'sulci' from folds, which are segmented and labelled anatomically according to the Desikan-Killiany-Tourville labelling protocol (Klein and Tourville, 2012). For our purposes, we purposefully avoided the use of predetermined anatomical labelling, as we wanted to do the labelling ourselves with our queries. For this reason, we used the Mindboggle 'folds' instead of 'sulci'. This allowed us to get a sense of how well our queries can identify and label sulci without any prior anatomical segmentation. Thus, we aim to capture much of the individual particularities of sulcal morphology by using un-anatomically segmented sulci, and evaluate the specificity of the queries which were designed to localise them.

The process for extracting 'folds' in Mindboggle has default settings, using the subject's original T1 image. We used the default setting to extract the unlabelled folds per hemisphere, with the exception of the 'depth

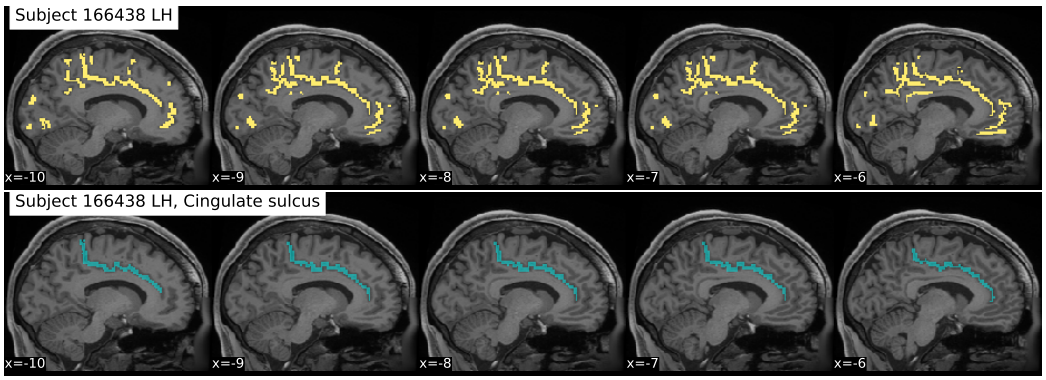

(A) Left hemisphere

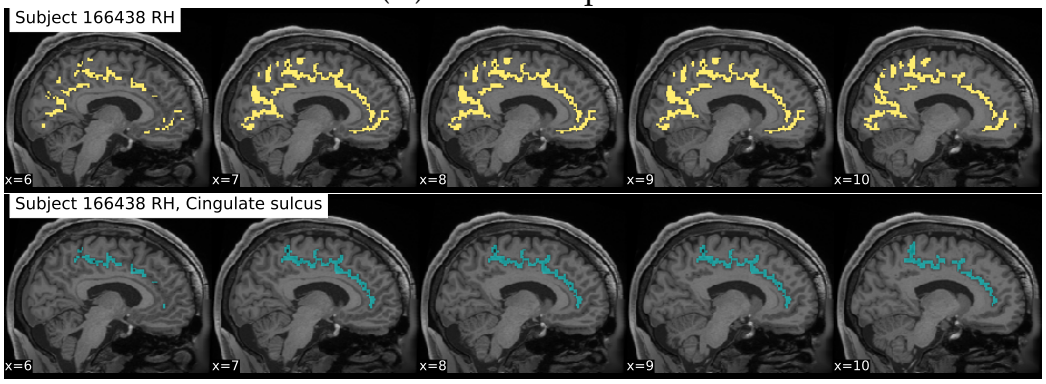

(B) Right hemisphere

Figure 9.1: How the cingulate sulcus query in NeuroLang extracts the cingulate sulcus from all the unlabelled sulci. Above, in yellow, we show all the folds extracted in one subject (166348 of the Human Connectome Project) on the medial plane by the software Mindboggle (Klein et al., 2017). Below, in blue, we present the results of the query for the cingulate sulcus in the same slices of the same subject, in subject space.

threshold' for the fold extraction, which we altered by increasing from 2 to 5.75, allowing for the extraction of deeper folds than the default. The other default settings in Mindboggle extract sulci with a minimum number of vertices of 10,000, and a minimum fold size of 50 (Klein et al., 2017). An average of 33 folds were extracted per hemisphere. The ideal output of each query was one fold (specificity), the desired one (sensitivity). A specificity of 0 was when a query found no sulcus. In the Human Connectome Project dataset pipeline, the subjects' original T1 MRI images are processed to ACPC space (Glasser et al., 2013). We ran our NeuroLang pipeline using the original HCP ACPC space, but then the query results were non-linearly converted to Montreal Neurological Institute (MNI) (standard) space. All results were analysed in MNI space.

Tertiary sulci have been difficult to assess on the population level due to their unreliability of their existence and morphology in each hemisphere. NeuroLang queries first determine the existence of a certain sulcus accord-

ing to its description, and statistical maps are based on the morphology of the sulcus on the population level, including the proportion of its existence within the population. This reflects studies carried out in the classical neuroanatomy method, wherein variable sulci such as the lunate sulcus have been investigated in a set of subjects, first determining the proportion of its existence within the population and then exploring trends in its location and morphology (Armstrong et al., 1991; Paus et al., 1996; Yücel et al., 2001).

We examine the subject-specific portrayal of sulci on the group level, in terms of trends of sulci across a population, and hemispheric and gender asymmetries. We obtained two sets of results: NeuroLang queries tested on the Mindboggle-extracted sulci (52 subjects), and the same NeuroLang queries tested on the manually segmented sulci (10 subjects). We compare and contrast the results of these two analyses, and scrutinize probability maps of sulcal location, variability and density. Sensitivity of the query was verified based on their overlap with their manual segmentation counterpart, shown in Figure 8.3. This is mostly a reflection of spread of the query results over the expected location. We verify the percentage of region overlap of NeuroLang sulci results with their ground truth counterparts.

9.1.1 Hemispheric and Gender symmetries

Independent sample t-tests were employed to determine gender- or hemispheric- asymmetries of the average query results of the analysis done on Mindboggle-extracted sulci using NeuroLang queries. We used independent samples t-tests to compare the mean probabilities of the queries in each hemisphere, and each gender. There was no significant difference in the average query proportions between hemispheres (two-sample t(51) = -0.36, p = 0.72) nor gender (two-sample t(d51) = 0.72, p = 0.48).

9.2 NEUROLANG ON MANUALLY SEGMENTED SULCI

In chapter 8, we described how we manually segmented each sulcus in 10 subjects of the HCP based on our extensive literature review of sulci presented in chapter 3.2. This dataset acted as our 'ground truth' and provided us with neuroanatomically accurate sulci in terms of their locations and shapes (Figure 8.2). For this reason, it was a good dataset to compare and contrast the results from the Mindboggle analysis with.

We ran the same 35 queries as for the Mindboggle analysis on our dataset of 10 manually segmented subjects. For this analysis, we were

not interested in evaluating the specificity of the queries themselves, but rather the sensitivity of the queries in terms of ground truth location of query result. We did not expect the queries to perfectly match with the ground truth sulci, as the queries were designed and tested using the Destrieux atlas, as we outlined in 7.3. We were interested in comparing and contrasting two outcomes from our two analyses, and using NeuroLang on manually segmented sulci provided a validation method for these two outcomes:

1. **Location of query result**: While sulci can exhibit much variability on the individual level, on the population level sulci are expected to be in a certain location. We validated accuracy of query localisation by checking Mindboggle query overlap with manual segmentation query overlap, shown in more detail in Figure 8.3.

2. **Stability of sulci**: An indication of sulcal stability is gathered from the similarity of a query result's probability mass distribution to the primary sulci probability mass distributions. This was done for the Mindboggle queries, and to validate their stabilities against 'ground truth', we did the same for the manual segmentation queries. We will discuss the results from these quantifications of stability in section 9.4, and how this provides a measure for cortical organisation in subsection 9.4.3.

9.3 SULCAL PATTERNS

NeuroLang queries identified sulci which were not altered to conform to a predetermined atlas. As shown in Figure 9.2, on the population level, the target sulci are in the location they are expected to be in from their anatomical descriptions in the literature. Their unmodified fold extraction reflect their natural morphologies before segmenting them to fit to a predetermined atlas. By using the unmodified sulci, we conserve as much individuality of the sulci per subject as possible. In this section we present evidence of how NeuroLang can accurately capture group-level sulcal patterns and individual morphology of sulci.

9.3.1 Sulcal patterns in the population

The nature of using spatial relativity to label sulci on the individual level allows for individualised sets of sulci. The result is a different set of existing sulci per hemisphere, a feature absent when using templates. On the population level, this allows for the investigation of trends of existence

and relationships to surrounding sulci for sulci which are often omitted from standard atlases.

This may be due to the specifications of the query or because we used the extracted 'folds' from Mindboggle instead of the 'sulci', meaning we identified and labelled the sulci of the cortex prior to their anatomical segmentation using a predetermined atlas (Klein et al., 2017). This means we identified and labelled atypically-shaped sulci, a common outcome of sulcal segmentation techniques (Auzias et al., 2015a; Klein et al., 2017).

In Figure 9.2, we provide evidence for queries which performed well on the population level in terms of neuroanatomical accuracy, such as the Cingulate sulcus (9.2B) or Superior temporal sulcus (9.2E), and queries which can still be improved, such as the Precentral sulcus (9.2C). We also give examples of tertiary sulci which exhibit reliability in their location and distribution of voxel overlaps, such as the Retrocalcarine (9.2D) and Frontomarginal sulci (9.2F). These are all evaluated in relation to the probability map 9.2A of the Destrieux atlas Central sulcus, a primary sulcus and considered to be one of the most stable and reliable sulci. We show how the NeuroLang queries work well to demonstrate population-level sulcal patterns.

9.3.2 Query results and discussion of individual NeuroLang sulcal queries

NeuroLang captures this variability of individual sulci on the subject level, a notoriously elusive task in automated labelling (Devlin and Poldrack, 2007). The Destrieux atlas includes 20 non-primary sulci alone, and 9 non-primary sulci grouped together with their surrounding gyri (Destrieux et al., 2010). NeuroLang has 35 sulcus queries. In this subsection we present evidence of how NeuroLang can accurately capture individual morphology of sulci, and how it can also present inaccuracies with sulci which are stable in their location but still highly variable, such as the precentral sulcus.

The software Mindboggle extracts 'folds' and then 'sulci'. The 'folds' are extracted based on depth values of each vertex and number of vertices per fold. The next step involves the merging or division of folds to conform to a predetermined template atlas. NeuroLang utilised the unanatomically segmented 'folds' to identify and label sulci per hemisphere. The identification of sulci using unlabelled folds provide a more genuine insight into the individual nature of each sulcus. The identified sulcus is represented with its individual morphological variability, including segmentations and branching, similar to sulcal morphology analyses carried out by anatomists (Duvernoy, 1999; Eichert et al., 2020; Falk, 1985; Ono,

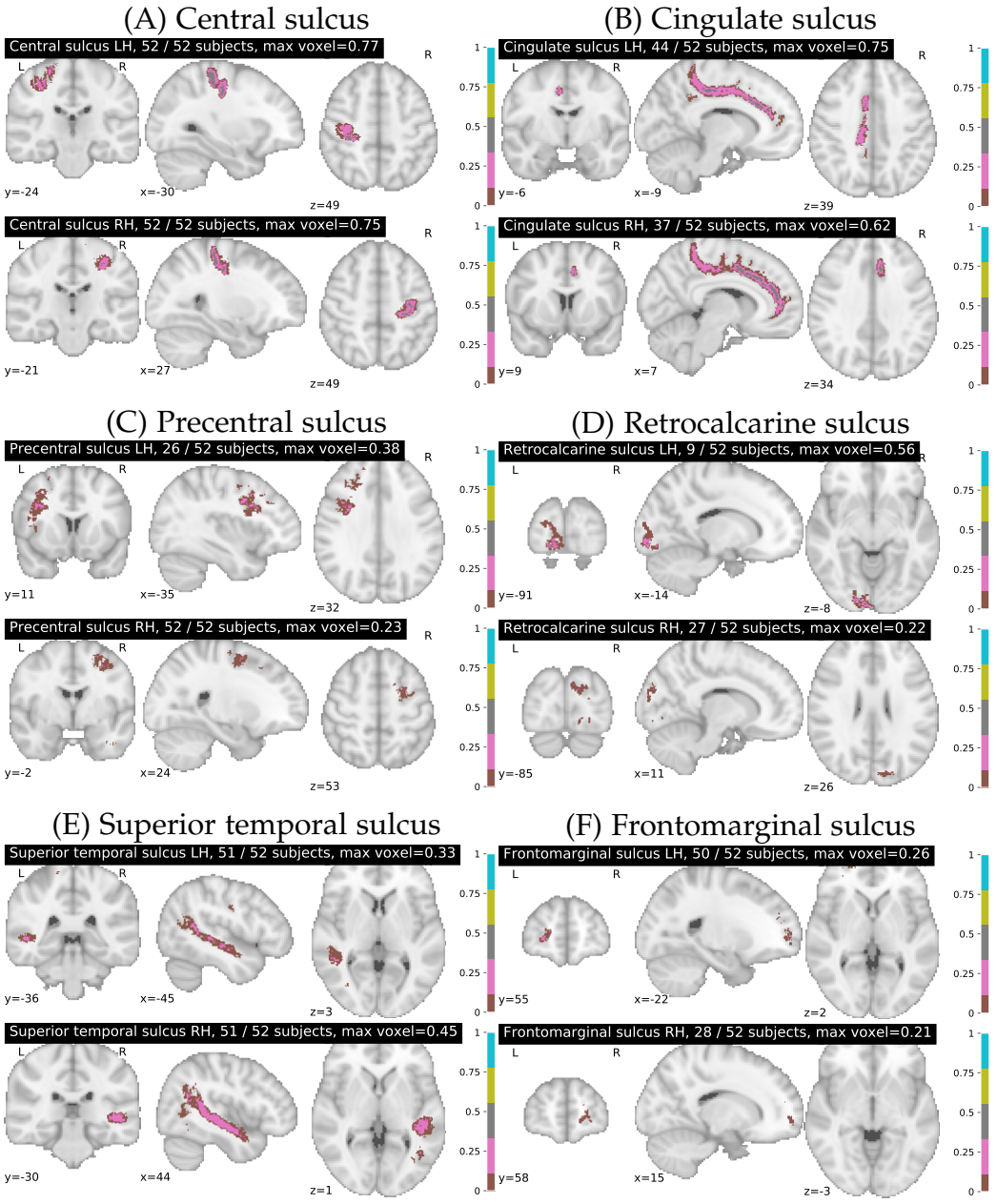

Figure 9.2: Probability maps for a primary sulcus and the query results of some notable sulci in 52 subjects, in both hemispheres. The Central sulcus (A) is a primary sulcus and was manually selected from the Destrieux atlas. It is shown here as a baseline of stability. The results of the query for the Cingulate (B), Precentral (C), Retrocalcarine (D), Superior temporal (E) and Frontomarginal (F) sulci are presented in both hemispheres, in the number of subjects in which results were found for each query. The results are shown in MNI standard space, thresholded to show the voxels with values above 0.1.

Kubik, and Abernathey, 1990; Paus et al., 1996; Sprung-Much and Petrides, 2020).

For 10 subjects, the individual maps of the query detecting the cingulate sulcus (Figure 9.3A), the precentral sulcus (Figure 9.3B) are shown below.

A common difficulty in mapping the segmentation and labelling of sulci is the ambiguity stemming from connected sulci. There are a few sulci which typically have this trait, notably the Precentral sulcus with other frontal lobe sulci. This can be effectively seen in Figure 9.3B, where we purposefully demonstrated examples of our Precentral query in cases where it accurately isolated the Precentral sulcus (e.g. subject 105923) and cases where the query labelled the Precentral sulcus along with the superior or middle frontal sulci (e.g. subjects 599671).

Other sulci also exhibit noteworthy variability, and here we discuss sulci in which the query performed well in terms of neuroanatomical accuracy, and some cases where the query did not reflect what we expected from the literature. Tertiary sulci have been difficult to assess on the population level due to their unreliability of their existence and morphology in each hemisphere. NeuroLang queries first determine the existence of a certain sulcus according to its description, and statistical maps are based on the morphology of the sulcus on the population level, including the proportion of its existence within the population. This reflects studies carried out in the classical neuroanatomy method, wherein variable sulci such as the lunate sulcus have been investigated in a set of subjects, first determining the proportion of its existence within the population and then exploring trends in its location and morphology (Armstrong et al., 1991; Paus et al., 1996; Yücel et al., 2001). We discuss some notable sulci, their pertinance in neuroscience, and our observations from our analyses.

CINGULATE SULCUS The cingulate sulcus is a prominent sulcus on the medial plane of the hemisphere, and one of the largest ones, following the Callosal sulcus' concentric trajectory. It forms the outer boundary of the limbic lobe, is a part of various surrounding functional areas and has several cytoarchitecturally distinct and functionally separate areas (Paus et al., 1996). It is for these reasons precisely that the cingulate sulcus is subdivided in the Destrieux atlas into 3 regions which are based on the cytoarchitectonic parcellations and functional divisions of the cingulate gyrus, the anterior cingulate gyrus with sulcus $(\mathrm{G\_and\_S\_cingul-Ant})$, the mid-anterior cingulate gyrus with sulcus $(\mathrm{G\_and\_S\_cingul-Mid-Ant})$ and the mid-posterior cingulate gyrus with sulcus $(\mathrm{G\_and\_S\_cingul-Mid-Post})$ (Destrieux et al., 2010). We show how NeuroLang has effectively located this sulcus in many subjects (Figure 9.2B) and single subjects (Figures 9.1, 9.3A). On the population level, the identification of the Cingulate sulcus acts as a marker between

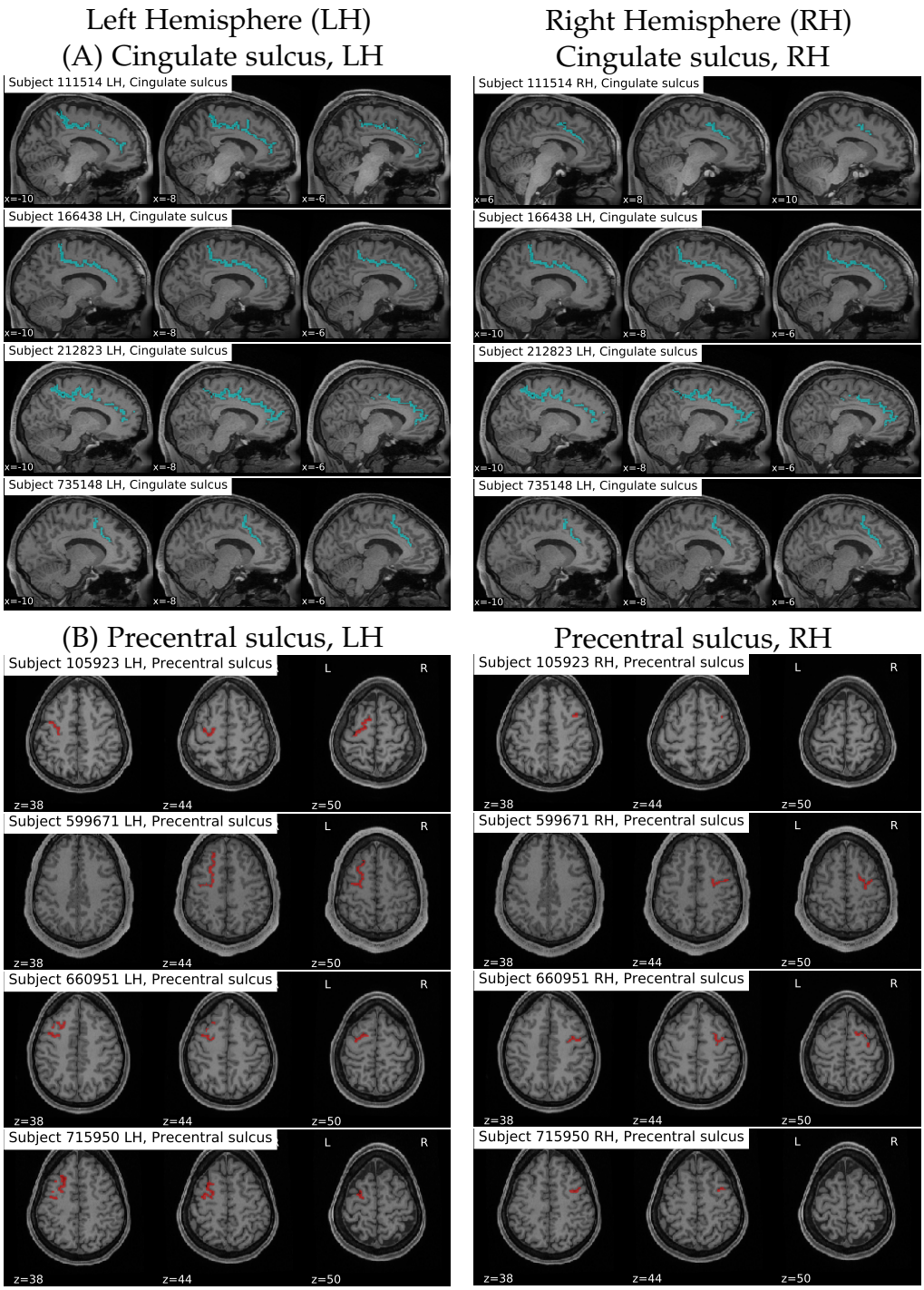

Figure 9.3: Individual maps for the Cingulate sulcus query results and the Precentral sulcus query results for 4 example subjects in both hemispheres, on the sagittal (A) and axial (B) planes. The images are shown in subject-space, to convey how NeuroLang preserves individual morphology when identifying and labelling sulci. This is especially apparent when identifying sulci known for their variability in segmentation, branching or neighboring connection such as the precentral sulcus (B).

the frontal lobe and the limbic lobe on the medial surface and can be used in conjunction with functional analyses to provide gross-level data on structure-function relationships of the cingulate cortex. On the individual level, the specific morphological length, shape, segmentation and branching of the cingulate can be analysed for subject-specific correlations of sulcal structure with function, cytoarchitectonics, cognitive associations or connectivity.

PARACINGULATE SULCUS The paracingulate sulcus is an inconsistent sulcus which, when present, is a continuous or segmented sulcus running along a parallel outer concentric trajectory to the cingulate sulcus. While the cingulate sulcus is present in 100% of hemispheres, the paracingulate sulcus is present less often, and its morphology is more varied. Several neuroanatomy studies have characterised it as present in about 70% of people in at least one hemisphere, with a leftward-asymmetry. It can present as continuous but more commonly is segmented into up to 4 segments. Yücel et al., 2001 developed a standard classification system for localising the paracingulate sulcus, based on length of the sulcal segments in the medial frontal cortex (Yücel et al., 2001). Its presence and morphology are believed to be linked to inter-individual variability in the cytoarchitectonic organisation and axonal tension of the medial frontal cortex region. This is thought to contribute to individual variabilities in cognitive performance such as language processes, or neurodevelopmental disorders such as schizophrenia or obsessive-compulsive disorder (Amiez, Wilson, and Procyk, 2018).

PRECENTRAL SULCUS While the precentral sulcus is a constant fixture on the frontal lobe, its morphology varies greatly in terms of its length, depth, segmentation, shape, branching and surrounding connections (Ono, Kubik, and Abernathey, 1990). It is not only a landmark in the frontal lobe used to delineate Brodmann areas 3,2,1, it is also a marker of the functional territory the primary motor cortex Rademacher et al., 1993. Its sulcal morphology is crucial to marking cytoarchitectonic boundaries, functional territories and regions of interest in connectivity. On the individual level, NeuroLang identifies the individual configuration of this sulcus, including the variability when it comes to connections with surrounding sulci (Figure 9.3B).

LUNATE SULCUS The lunate sulcus is often associated with primate anatomy (Allen, Bruss, and Damasio, 2006), and its existence and proportion in the population is debated (Armstrong et al., 1991). While in chimpanzee brains it is a prominent occipital lobe sulcus which delineates the primary visual cortex (Falk, 1985), in humans it can be attributed to

a variable descending sulcus in the posterior occipital lobe. Its existence and morphology are highly variable, helped by the fact that the occipital lobe sulci are generally less stable in their morphology than in other lobes. Allen, Bruss, and Damasio (2006) examined 110 brains and localised composite lunate structures in 32.7% of left and 26.4% of right hemispheres. We localised sulci which fit the composite lunate sulcus description in 81% of left and 19% of right hemispheres. While the probability maps of these variable sulci match the description of lunate sulci, we stress the fragmented and variable nature of occipital sulci and acknowledge that what we attribute as lunate sulci may be fragments of other occipital sulci (Iaria and Petrides, 2007).

CUNEAL SULCUS The cuneal sulcus is typically described as a short 'dimple' on the cuneus, following the trajectory of the calcarine sulcus just inferior to it. The inferior part of the cuneus makes up the primary visual cortex. The primary visual cortex is composed of Brodmann areas 17 along the calcarine cortex, and Brodmann area 18 surrounding it (Rademacher et al., 1993). The cuneal sulcus runs along the trajectory of the transition period between areas 17 and 18, suggesting a role as a marker between these territories. Further work investigating the relationship between the existence and morphology of the cuneal sulcus with the cytoarchitecture of Brodmann areas 17 and 18 is needed.

Tertiary sulci are relevant to anatomical landmarking, and are often used as corresponding markers of cytoarchitectonic boundaries. For example, the anterior parolfactory sulcus may be a boundary for, or a part of, Brodmann area 25, a region that may be implicated in depression (Hamani et al., 2011; Spasojević et al., 2011). They also make up distinguishing features on an individual level, and may be related to individual cognitive correlates. For example, the middle frontal sulcus is often variable in existence and morphology, and was made notable by its prominence in Einstein's brain (Falk, Lepore, and Noe, 2013). Paus et al., 1996 carried out extensive manual anatomy to determine morphology of the paracingulate sulcus, a sulcus with a potential role in speech production (Paus et al., 1996). These examples support the claim that the inconsistency of cortical sulci largely contributes to the inter-individual variability of cognitive, cytoarchitectonic and pathological correlates. Each hemisphere is composed of a subset of sulci which are always present, and a subset of sulci which are sometimes present. The applicability of our complementary method lies largely in its suitability for cortical features with large variability.

9.4 STABILITY OF SULCI

The ability for NeuroLang to provide subject-specific representations of sulci gives us the opportunity to observe population-level trends of cortical organisation of the sulci. By interpreting query performance, we infer reliability of sulcal existence, location and morphology from the group level probability maps and their contrasts with the primary sulci.

9.4.1 Subject-specific representations of sulci

Even sulci which are highly reliable in their location, such as the cingulate sulcus, exhibit high variability in elements of their morphology such as segmentation, branching and connections to surrounding sulci. NeuroLang allows for the morphological assessment of individual sulcal morphologies on the mass scale while staying faithful to true anatomy. As can be seen in Figures 9.3A and 9.3B, each sulcus manifests in a unique way, and can be correlated to unique patterns of gyrification and cytoarchitectonic regions. These, in turn, relate to specific functional correlates.

Figure 9.3B depicts the difficulties in segmenting the precentral sulcus, a sulcus which has typically between 0-5 segments (Ono, Kubik, and Abernathey, 1990; Rademacher et al., 1992), numerous branches of varying lengths, and often is anteriorly connected with the superior or inferior frontal sulci (Amunts et al., 2000; Germann et al., 2005; Ono, Kubik, and Abernathey, 1990). This can be clearly seen in the individual maps for the results of the precentral query.

Our results show that our measures of sulcal stabilities from our queries are not necessarily in agreement with their positions in the hierarchical organisation as described in the literature, and we present in Figure 3.1. In Figure 3.1, we define the secondary sulci as the lone sulcal regions in the Destrieux atlas, and infer that they demonstrate a larger degree of dependability on the cortex. Results on the population level show that many secondary sulci, such as the precentral sulcus (Figure 9.2C), displayed more variability, perhaps because they are often segmented more than once, and some tertiary sulci, such as the cingulate, retrocalcarine or frontomarginal sulci (Figure 9.2) had a large overlap across subjects in their location. Individual examination of sulcal patterns has the potential to complement efforts to uncover widespread yet detailed patterns of sulcal variability. We can harness the stability we observe from sulcal patterns to quantify different degrees of stability for an organisation of the cortex.

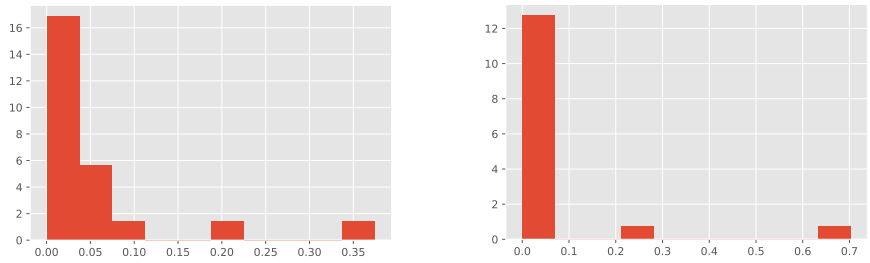

(A) Central sulcus, LH (B) Superior temporal sulcus, LH

Figure 9.4: Histograms to visualise the probability mass distributions of voxel overlap of the Central sulcus and Superior temporal sulcus in the left hemisphere, from 52 subjects. 20 bins were constructed for each histogram.

9.4.2 Quantification of stability

Primary sulci were obtained using the Destrieux atlas in all subjects. They had the highest maximum voxel overlap values, at 0.67, 0.6 (Parieto-occipital sulcus in the left and right hemispheres, respectively) to 0.83 (Calcarine sulcus, LH) and 0.79 (Callosal sulcus, RH), with an average of 0.75 (LH) and 0.73 (RH). The primary sulci have the most stable probability maps, with the highest maximum overlap values. Histograms of the probability mass functions for the voxel probabilities of each sulcus were created, separated into 20 equal ranges (histogram bins). The minimum Hellinger distance is a distribution divergence metric, which we use to estimate robustness (González-Castro, Alaiz-Rodríguez, and Alegre, 2013). We used the Hellinger distance (defined in equation 9.1) to compare the probability mass distributions used to construct each histogram, between two sulci. Probability mass distributions (*pmd*) for each query result gives us a probability measure of the possible values for an observation. We visualise it with histograms, which give us an indication of the spread of the data, or the probability that the sulcus is clustered nearby in all subjects. Examples of these histograms for the Central sulcus and the Superior temporal sulcus in the left hemisphere are shown in Figure 9.4.

The Hellinger distance is a quantification, between 0 and 1, of the similarity (closer to 0) or disparity (further from 0) between two probability distributions. It gauges the distance between two distributions (Oosterhoff and Zwet, 2012). The Hellinger distance is a useful metric when comparing imbalanced datasets (Aler, Valls, and Boström, 2020), such as the probability mass distributions per query sulcus, visualised in the histograms in Figure 9.4.

In our case, we use the Hellinger distance to quantify the distance between the voxel distributions of a query sulcus (represented by q) and the primary sulci (each represented by p). We use it to provide an indication

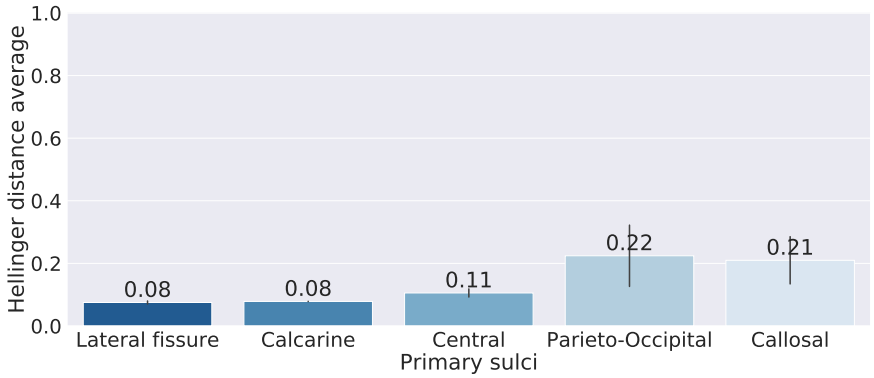

Figure 9.5: Hellinger distance average of each primary sulcus probability mass distribution (*pmd*) to the other 4 primary sulci *pmd*s, in both hemispheres. Hellinger distance provides a measure of distance between two *pmd*s, signifying how similar the distribution of overlap between the two is. A Hellinger distance value of 0 represents exact overlap between the two distributions, and 1 represents no overlap at all. Hellinger distance averages of the primary sulci to each other was determined as a baseline for sulcal stability. Error bars show the confidence interval of 95%.

of how much more varied the probability of a query sulcus map is, relative to the primary sulci. Supposing that q represents the *pmd* of the subject overlap across voxels for a query sulcus, and p represents the *pmd* of the subject overlap across voxels for a primary sulcus, we represent the Hellinger distance of q to one primary sulcus p as H. We present the Hellinger distance between two (*pmd*s), q and p, in equation 9.1.

$$H = \frac{\|(\sqrt{p} - \sqrt{q})\|}{\sqrt{2}} \tag{9.1}$$

Using equation 9.1, we quantified query sulcus stability by the average of each H of q to the five p, as put forth by Aler, Valls, and Boström, 2020. We did this for each q. We therefore use H to represent a measure of the distance between the distribution of voxel overlaps of a query to the distribution of voxel overlaps of a primary sulcus. The average of these 5 measurements per query sulcus is represented by $\overset{q}{H}$. To establish a baseline of a minimum distance between the most stable sulci, we determined the average of the Hellinger distances of each primary sulci to the other 4, shown in Figure 9.5. In the case of the Hellinger distances of the primary sulci to each other, p is one primary sulcus, and q another.

The Hellinger distance informs us of similarity of voxel overlap probability distributions across the probability maps of the sulci, without consideration to the location or morphology of the sulci. We consider $\overset{q}{H}$

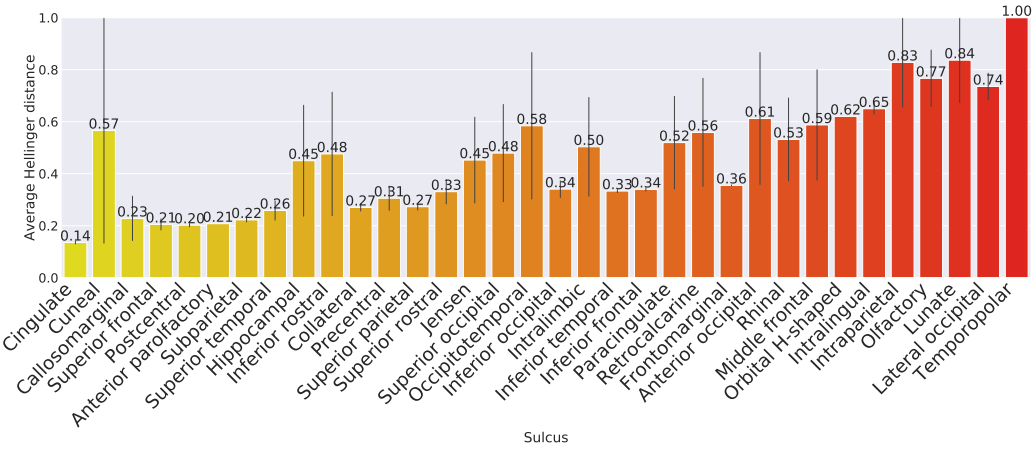

Figure 9.6: Hellinger distance average of each query sulcus probability mass distribution (*pmd*) to the primary sulci *pmd*. Hellinger distance provides a measure of distance between two *pmd*s, signifying how similar the distribution of voxel overlap between the two is. A Hellinger distance value of 0 represents exact overlap between the two distributions, and 1 represents no overlap at all. The sulci at the far left end of the bar plot represent the most stable sulci. Their low values signify that they their voxel overlap distributions were similar to those of the primary sulci, which are the most stable. Error bars show the confidence interval of 95%.

to be the average distance of the query result to the primary sulci. In Figure 9.6 we show the results of the $\bar{H}^{q}$ of each query sulcus, in order of minimum to maximum distance from the primary sulci.

9.4.3 Organisation of sulci from stability

The primary sulci have been established to have the greatest stability on the cortex, as we have shown from our literature review (section 3.2) and quantification of stability using Hellinger distances (Figure 9.5). For this reason, we take a measure of the primary sulci stability as a baseline for which we measure the stabilities of the other sulci against. To measure this differences in sulcal stability, we used the Hellinger distance, in the way we described in the previous section, to reveal the similarity of the patterns of voxel probability distribution between the average of each query's probability mass distribution to each primary sulci.

The primary sulci had the highest proportion of voxel overlap in the probability maps, meaning their location was the most consistent across subjects (Figures 9.2, 8.2). This was expected not only due to their anatomical traits but also the fact that we used the Destrieux atlas to extract the primary sulci to ensure that the queries used, which we based on relationships to the primary sulci, were as reliable as possible. The

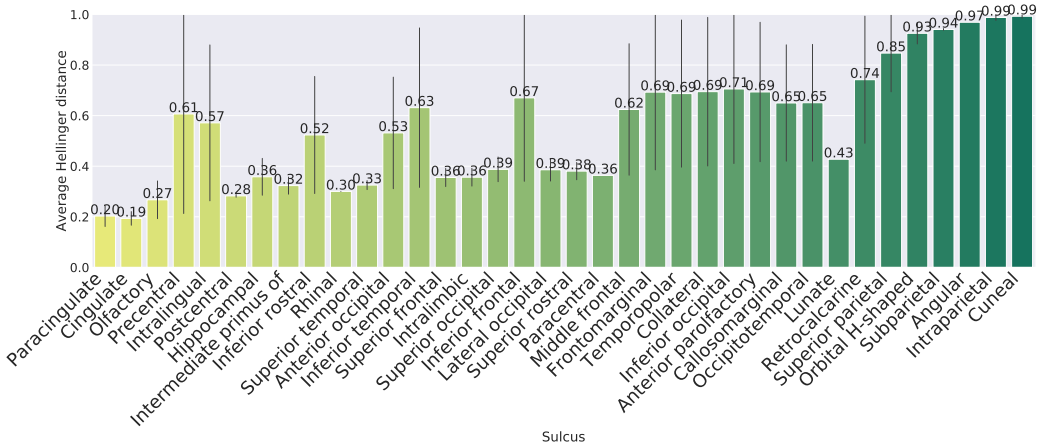

Figure 9.7: Hellinger distance average of each query result probability mass distribution (*pmd*) of the manually segmented sulci to the average *pmd*s of the primary sulci, in both hemispheres. Hellinger distance provides a measure of distance between two *pmd*s, signifying how similar the distribution of voxel overlap between the two is. A Hellinger distance value of 0 represents exact overlap between the two distributions, and 1 represents no overlap at all. The sulci at the far left end of the bar plot represent the most stable sulci. Their low values signify that they their voxel overlap distributions were similar to those of the primary sulci, which are the most stable. Error bars show the confidence interval of 95%.

computation of each sulcus' probability map similarity to the primary sulci provides an indication of the stability of each sulcus' locations. The sulci which were not identified in the majority of subjects also exhibited dissimilarity from their $\overset{q}{H}$ ($\geqslant$0.50), reflecting instability in their probability of location on the cortex.

We can see from Figure 9.6 that the cingulate sulcus had the smallest $\overset{q}{H}$ value. A similar pattern was found when the queries were run on the manual segmentations (Figure 9.7), which were larger in length or shape, and typically had more branching and connections to surrounding sulci, as in subject-specific neuroanatomy. We can see this reflected in the results from the analysis using the manually segmented sulci: in Figure 9.7, we see how the query results for the cingulate and paracingulate sulci using the manual segmentations had the closest average similarity ($\overset{q}{H}$) to the primary sulci, at 0.20 and 0.19, respectively. Next smallest in Figure 9.6 is the cuneal sulcus, with the closest average similarity ($\overset{q}{H}$) to the primary sulci, presumably due to the likelihood of the cuneal sulcus being mistakenly labelled as either the parieto-occipital or the calcarine sulci (Myslobodsky et al., 1991). The next few most similar sulci were other secondary sulci which are typically associated with stability, including the

olfactory (0.27), postcentral (0.28) and precentral (0.51), with the least stable being the variable cuneal sulcus (0.99). While there is indeed some overlap with the most 'stable' sulci from the Mindboggle analysis (Figure 9.6), such as the cingulate (0.14), postcentral (0.2) and precentral (0.31), there is much disagreement as well, with the Mindboggle analysis showing greater stability in tertiary sulci. The cuneal sulcus, for example, measures 0.57 but with great variability. We can gather that the manual segmentations were a more true-to-true-form sulcal representation and therefore more in line with what we expected in terms of organisation of stability across secondary and tertiary sulci. Given the congruence in sulcal stability from the Mindboggle and manual segmentation analyses, we infer from this that the cingulate sulcus had the highest proportion of voxel overlap across subjects, suggesting the highest stability after the primary sulci.

In both the Mindboggle sulci and the manual segmentation sulci analyses, we see $\overset{q}{H}$ values of 0.1-0.4 in sulci which were localised in over half the subjects in each hemisphere. The low $\overset{q}{H}$ values express a similarity in average *pmd* of the query sulcus to the primary sulci *pmd*s. This reflects a stability in their probabilities of locations, tending to exist in a condensed location, thus with a higher overlap of voxels in the area across subjects.

Another indication of sulcal stability came from determining the ratio of overlap between each query result and the probability map of its ground truth counterpart from the manual segmentations. Comparing with the current atlas included in the Human Connectome Project pipeline, the Destrieux atlas contains 20 standalone sulci regions which we could compare to (Appendix A.1), and our manual segmentations included thorough tertiary sulcal labelling of up to 42 sulci. We showed that, for the queries that identified a sulcus in over half the subjects, one major sulcus per lobe had the highest stability; the superior temporal, superior occipital, frontomarginal, cingulate and intralingual sulci had the greatest overlap with their manual segmentation counterparts. This suggests that while factors such as depth or segmentation of the sulcus may vary, relativity of sulcal location within each lobe remains stable.

In Figure 3.2, we defined the secondary sulci as the lone sulcal regions in the Destrieux atlas, and infer that they demonstrate a larger degree of dependability on the cortex. Our results show that the stability of sulci are not necessarily in agreement with their positions in the hierarchical organisation as described in the literature, as presented in Figure 3.2. Results on the population level show that many secondary sulci, such as the precentral sulcus (Figure 9.2), displayed more variability, perhaps because it is often discontinuous (Germann et al., 2005; Ono, Kubik, and Abernathey, 1990), and some tertiary sulci, such as the cingulate, retrocalcarine

or frontomarginal sulci (Figure 9.2) had a large overlap across subjects in their location.

9.4.3.1 *Lobular stabilities*

Taking into account the different comparisons of query outcomes to the stability of the primary sulci, we can adapt or customise our hierarchical organisation by our quantification of sulcal stabilities. In Figure 9.8 we implement our data-driven measures of stability from Figure 9.6 onto our schematic of cortical organisation of sulci. Yellow is the closest similarity of a query sulcus' probability mass distribution to the primary sulci, red is the furthest. From left to right, the sulci are organised by lobular position: frontal, temporal, occipital and parietal lobes, as in Figure 3.2 in section 3.3. By presenting the data in this schematic we can see whole-brain level trends of sulcal stability. We support the lobe-level stability by considering the $\overset{q}{H}$ of each query sulcus from Figure 9.6. We consider the sulci with an $\overset{q}{H}$ value of $\leqslant 0.50$ to be the more stable sulci. We note how, while the stability seems to be spread across lobes, the frontal lobe contains the most stable sulci, with 9/13 sulci (69%) with an $\overset{q}{H}$ of 0.32 and a standard deviation of 0.11. This is consistent with the literature, which describes the frontal lobe sulci consistently across sources (subsection 3.2.2). The parietal lobe is next, with 5/8 sulci (63%) with $\overset{q}{H} \leqslant 0.50$, with an average of 0.27 ± 0.09, then the temporal lobe with 4/7 (57%), average of 0.33 ± 0.08. Lastly, the occipital lobe with 2/8 sulci (25%), with an average $\overset{q}{H}$ of 0.41 ± 0.07. Again, this is in line with what we know of the occipital lobe, with its notoriously inconsistent sulci on the lateral plane (subsection 3.2.5) (Iaria and Petrides, 2007).

We show that the cingulate sulcus, though one of the largest non-primary sulci, has the greatest stability in its existence, location and shape. As discussed in the introduction, sulci have been typically categorised by factors such as existence across subjects and morphological patterns; we propose to add the factor of our quantification of sulcal stability, and to migrate the cingulate sulcus from tertiary sulcus to the first secondary sulcus to be identified in future analyses.

On the population level, we present a data-driven method for quantifying unreliable sulci using their classical anatomy translations. We establish a evidence-based hierarchical order from which we can further develop tools for sulcal identification. We have discussed how brain mapping tools are heavily reliant on cortical landmarks, which have varying degrees of stability (chapter 4). In this section we have established a data-driven method for concluding sulcal stability within a given population. This can

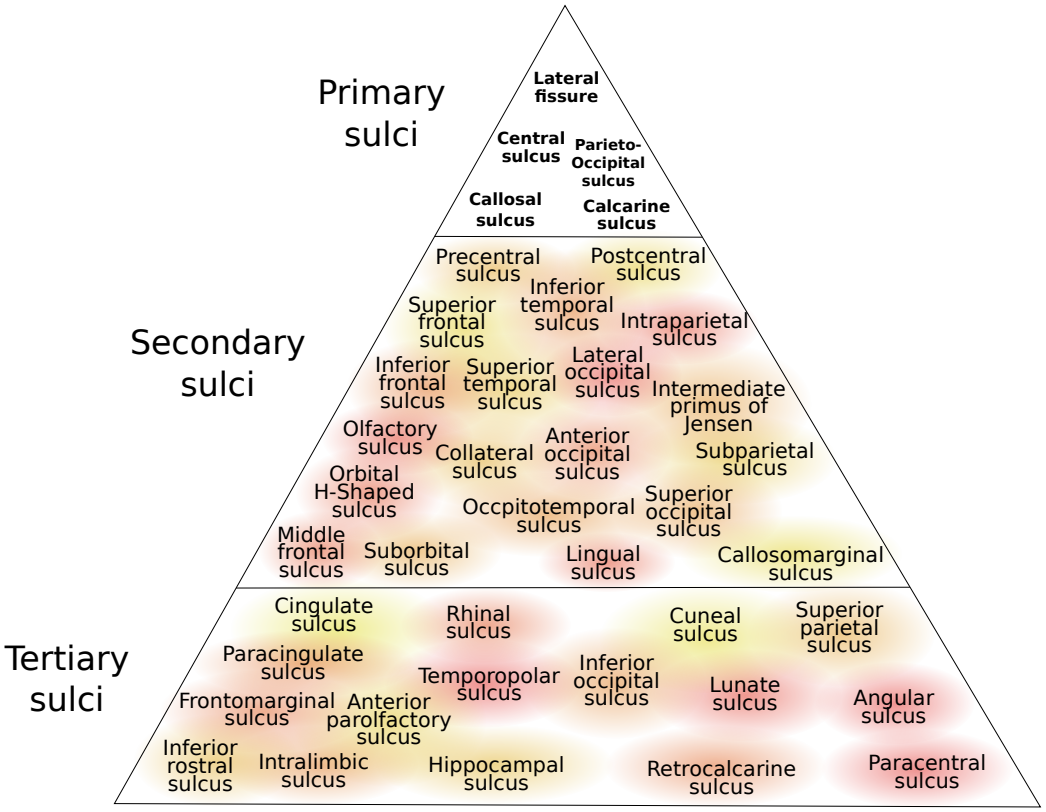

Figure 9.8: Schematic representing data-driven quantification of sulcal stability. Stability was derived from the average of a query's Hellinger distances to each primary sulcus, in both hemispheres, as depicted in Figure 9.6.

be used generally, to understand general organisation of the cortex, or specifically for template placement within a given population.

9.5 CONCLUSION

We have described how we use sulcus-specific queries to navigate, identify and label sulci. We have shown their outcomes, evaluated their performances, and quantified their results for a determination of sulcal stability within our population.

By investigating our results, we noticed how the manually segmented sulci had large variability in branching, but remained highly consistent in location. However, the sample size for the manual segmentations (n=10) was considerably smaller than the sample size for the analysis on the Mindboggle-extracted sulci (n=52). The consistency in location was most pronounced in the tertiary sulci, such as the retrocalcarine or frontomarginal sulci (Figures 8.2D, 8.2F). Retrocalcarine or frontomarginal sulci, as extracted by Mindboggle and identified by NeuroLang, were found in less subjects with greater variability, while their locations remained fairly consistent yet less so than the manual segmentations (Figures 9.2D, 9.2F). However, the frontomarginal sulcus had relatively high overlap with its ground truth counterpart while the retrocalcarine sulcus did not. Regardless of the congruence between the NeuroLang result and manual segmentations in location of the retrocalcarine sulcus, overlap remained low, as a result of the high precision of the manual segmentations, and inconsistencies in shape. The precision of the manual segmentations is depicted by their compactness in the probability maps (Figure 8.2). The queries are designed to designate a range of area in which the target sulcus is expected, if existent. We note that the query-localised sulci displayed a larger spread of area than the manually segmented sulci. In section 9.4.3, we present a novel schematic of cortical organisation of sulci from data-driven quantification of sulcal stability.

Patterns of sulcal stability, shape and depth are constant investigations relevant to neuroimaging, where reliable cortical features are one of the foundations of brain mapping. In this chapter we presented work on one way of quantifying sulcal stability in a population of 52 subjects. Our work complements other efforts to investigate differences in other sulcal features such as sulcal shape (Perrot, Rivière, and Mangin, 2008) or geometry of sulci (Cykowski et al., 2008; Kaltenmark et al., 2020; Leroy et al., 2015).

Part III

IMPLICATIONS OF SULCAL MAPPING USING QUERIES

10 CONTRIBUTION TO SULCAL MAPPING

While classical neuroanatomy has progressed slowly and incrementally, the explosion of information awarded us in the past 50 years has allowed for the immediate visual exploration of theoretical knowledge amassed over the centuries (Evans et al., 2012; Yarkoni et al., 2011). As a result of this, it was favourable to procure methods of standardisation for neuroimaging which would allow for the efficient and effective probing of the brain on a large scale. While it is widely acknowledged that each brain presents unique anatomical features, there is also widespread agreement on cortical landmarks and features shared among all healthy brains. Data-driven and atlas-driven approaches drive forth the progress of neuroimaging, but oftentimes detailed anatomical accuracy across individuals is sacrificed (Behnke et al., 2003). Atlas-driven approaches, while efficient, rely on surface registration methods which are not adaptable to all brain types and ages (Auzias et al., 2015b), and by necessity focus on the majority overlap of cortical regions among brain populations, ignoring individual variability.

This thesis presents our work on the development and implementation of our novel brain mapping tool, NeuroLang. Our framework is founded upon the characterisations of sulci in classical neuroanatomy, and the formalisms defined by first-order logic. Our work undertook the task of bridging the gap between these two domains.

Our sulcal atlas reviewed a breadth of work on sulcal anatomy spanning the last century. We standardised the naming process, proposed a semi-hierarchical organisation of the cortex according to lobe position and relativity to cortical landmarks, and applied the atlas to a dictionary of data-driven brain regions defined by functional signals. Additionally, we utilised our atlas definitions to create a 10-subject dataset of manual segmentations with ground truth neuroanatomy.

We summarised the theory of first-order logic and its applicability for cortical knowledge representation. We considered interval algebra as a means for translating relative relationships of pairs of sulci. We combined the elements of computational infrastructure to the base of classical neuroanatomy knowledge and developed 35 sulcus-specific queries for NeuroLang. Its implementation led to the examination of group-level trends and individual sulcal sets and morphological investigations. We proposed a method for interpreting data-driven quantifications of sulcal stability, and a novel organisation of the cortex according to this metric.

In this part, we focus on the significance of sulcal representations, from our method and otherwise. We assess the implications of our method within the field of sulcal mapping. We consider group-level and individual effects and specifically examine certain sulci of interest of varying stability. We then regard the relationships of sulcal query results to their surrounding cytoarchitectonic regions.

11 SIGNIFICANCE OF SULCAL REPRESENTATIONS

11.1 CORTICAL FOLDING PATTERNS

The cortex begins to form during the first few weeks of gestation. Progress of cortical formation can be marked by the folding patterns of the first sulci to appear, typically the ones which evolve to be the most prominent on the surface (Chi, Dooling, and Gilles, 1977; Yun et al., 2019). Amongst these are what come to be known as the primary sulci, or interlobular sulci. They tend to be deeper and more stable in their location, depth, shape and development (Mangin et al., 2004a; Yun et al., 2019).

As humans evolved intelligence, the brain expanded. Harari, 2011 hypothesises how this delicate balance could be maintained, given that the head still needed to be small enough to both fit through a birthing canal and hold up on two legs. He theorised that Homo sapiens thus had to make a few sacrifices; babies are born prematurely relative to other mammal species, while the head is small enough, and the human spine bears the brunt of the trauma of holding up our large and heavy heads to maintain bipedalism (Harari, 2011).

Expanding theories on cortical evolution suggest how the brain folds in on itself to increase its surface area, to accommodate the expansion of the cortices and keep the skull at a reasonable circumference (Harari, 2011; Xu et al., 2010). It's believed that the folded cortex allows for more densely packed neurons and thus, exponentially more connectivity potentials. Van Essen (1997) theorised how the patterns of folding reflect the tension of the underlying subcortical and corticocortical projections (Van Essen, 1997). Patterns of sulcal formation are dependent on both genetic and environmental influences. The primary sulci, formed during gestation, are more heavily influenced by genetic factors (Chi, Dooling, and Gilles, 1977; Ono, Kubik, and Abernathey, 1990).

The variability of sulcal patterns and cortical folding patterns is intertwined. Similarly to sulcal stability, variability of Brodmann areas also varies across regions and subjects (Amunts, Schleicher, and Zilles, 2007; Fischl et al., 2008). Some have looked into this relationship between macroanatomical and microanatomical features of the cortex. In particular, Fischl et al., 2008 investigated whether stability of Brodmann areas contributes to a cortical hierarchy, similar to how we categorise our sulcal

hierarchy, as well as how cortical folding patterns relate to predictability of cytoarchitectonic areas.

The analysis of folding patterns in relation to Brodmann areas depicts compelling patterns of alignment which suggests a relationship in the cortical hierarchies (Fischl et al., 2008; Rademacher et al., 1993). Fischl et al., 2008 showed how primary functional areas, such as the primary visual cortex (Brodmann area 17), showed that a high predictability in cortical folding patterns was mirrored in the high predictability of the Brodmann area morphology. The accuracy in predictability declined as they moved to predicting folding patterns in secondary and integrative functional areas. This contributes to the idea that there is a global cortical hierarchy which is interdependent on sulcal morphology. The later the stage of sulcal development, the more the sulcus is dependent on a variety of factors, and the more variable is the sulcus' existence and morphology, and thus its relationship to other cortical, functional and connectivity correlates.

In addition to the genetic and non-genetic components driving the formation of folds, there is evidence to suggest that mechanical morphogenesis also plays a major role in the maturation of folds, as we alluded to in section 3.1. Constrained by volume, Heuer and Toro, 2019 propose that the brain folds the way that it does because it is energetically favourable to do so within the constrained space (Heuer and Toro, 2019). The arrangement they form in – a blueprint observed across populations – can be attributed to a number of developmental causes; some suggest the tension of axonal development (Van Essen, 1997). The pattern of sulcal development provides a framework for the identification of sulcal location and properties (Mangin et al., 2004a)

The gradient of variability exuding from regions of origin is a concept explored by Margulies et al., 2016. By investigating patterns of cortical landmarks, they devised a system of cortical organisation based on principal gradients. While they focused on the nodes of the default-mode network, we adopt the concept to focus on the primary sulci as cortical nodes, with gradients of instability emanating from them.

11.2 SULCI AND CYTOARCHITECTONICS

11.2.1 Sulci as region delineators

Certain characteristics of sulci have been suggested which we investigate in this work, notably the relationships of certain sulci as region delineators, particularly for cytoarchitectonic regions. Variability of sulcal morphology

and cytoarchitectonics have long been linked, as sulci have been used as a way to characterise a cytoarchitectonic region.

NeuroLang queries were constructed upon relationships of the sulci as 3D volumes instead of as points on a 2D folded sheet. Some sulci are particularly useful for identifying primary function areas on a large scale, such as the primary motor and primary somatosensory areas (bounded by the precentral, central and postcentral sulci) (Coulon et al., 2011; Germann et al., 2005). Other sulci, while highly variable, are used in identifying functional areas which are themselves variable and dependent on multiple individual factors. Structural and functional regions which are implicated in inter-individual characteristics such as personality (e.g. cingulate gyrus) (Amiez, Wilson, and Procyk, 2018), psychiatric disorders (e.g. Brodmann area 25) (Spasojević et al., 2011), or comparative anatomy (e.g. lunate sulcus) (Armstrong et al., 1991) can be associated with individual variability of the existence and morphology of their surrounding sulci. As the relationship between sulcal and cytoarchitectonic patterns becomes more clear, the call for individualised brain mapping becomes more relevant.

11.2.2 Sulci for cytoarchitectonic mapping

Korbinian Brodmann was among the first to recognise how primary functional areas occurred near or around primary sulci, in 1909 (Brodmann, 2007; Fischl et al., 2008). The organisation of the 'mosaic' of cytoarchitectonic regions of the cortex and the organisation of the cortical folding patterns share developmental trajectories and may be functionally linked (Fischl et al., 2008).

Cytoarchitectonic regions and their borders are structurally and functionally relevant (Amunts, Schleicher, and Zilles, 2007). Relationships between cytoarchitectonic regions and sulci as their borders is the subject of much investigation and has led to the growth of the field of probabilistic atlases for cytoarchitectonics (Amunts, Schleicher, and Zilles, 2007; Amunts et al., 2020; Bludau et al., 2014; Eickhoff et al., 2005a; Eickhoff et al., 2005b; Zilles and Amunts, 2010; Zilles et al., 1997).

Nevertheless, a cytoarchitectonic region is not necessarily inextricably linked to a sulcus. There are various regions which have no direct relationship to the existence or morphology of a sulcus. Additionally, it is unknown whether a cytoarchitectonic region, if indeed typically linked with a sulcal location, is necessarily *dependent* on that sulcus, or vice versa. While primary functional areas are linked to primary sulci, it is not necessarily the case for other cytoarchitectonic regions. As functional areas become more integrated, their positions on the cortex are relatively further away from primary sulci. The sulci, in turn, exhibit larger variability.

Current templates smooth over much of the sulcal variability in order to make template atlases more applicable and compatible with other cognitive correlates. But what if the preservation of individual sulcal morphology actually benefits the investigations into cytoarchitectonic patterns? If we assume the cortex to possess a putative hierarchy, dependent on the primary sulci, our proposition of a complementary system of brain mapping which preserves individual sulcal variability may aid in overall cortical mapping, as in a system where brain characterisations can be layered upon one another, such as sulci, cytoarchitectonic regions, functional activation, and connectivity patterns, to create a whole-brain perception from a subject's image. Furthermore, our method for quantifying sulcal stability may also aid in the characterisation of cytoarchitectonic regions and their relationships to surrounding sulci.

12 IMPLICATIONS OF NEUROLANG

The main objective of this tool is to identify and label sulci according to individual morphology. The primary use of NeuroLang is targeted as brain mapping on the population level which captures individual variability.

Additionally, NeuroLang can be used as a data-driven approach for sulcal morphology analyses and a way for quantifying sulcal stability within a given population. Manual segmentation of individual sulci on a large scale is tedious work, time-consuming, and requires expert neuroanatomical skill. NeuroLang queries are mutable and allow for varying characterisations of sulci, without the need for tedious anatomy.

Extensive work has been done to create data-driven approaches to demonstrate relationships of brain regions, for example by sulci (Destrieux et al., 2010; Rivière et al., 2009), white matter (Wassermann et al., 2016), cytoarchitectonics (Amunts et al., 2020), or myelin content (Glasser and Essen, 2011). For mapping sulci, typically, considerable anatomical knowledge of the cortex is a prerequisite, and painstaking effort of manual delineation is involved (Eichert et al., 2020; Ono, Kubik, and Abernathey, 1990; Paus et al., 1996; Rivière et al., 2009; Sprung-Much and Petrides, 2020; Yücel et al., 2001). An application for the individual analysis of cortices is to use NeuroLang to localise and identify specific sulci and compare their morphologies in large populations. Each NeuroLang query is mutable and therefore flexible to accommodate diverse descriptions of sulci according to the focus of the analysis. For example, Eichert et al. (2020) and Sprung-Much and Petrides (2020) examined the morphological variability of the subcentral and anterior rami of the lateral fissure, respectively. Extensive background knowledge and training was required to manually chart the anatomy of these sulci, followed by spatial probability maps and relationships to cognitive correlates.

Within the NeuroLang domain, queries can be altered, added or removed, according to the parameters of the experimental setup. With the option of identifying a single segment or multi-segmented sulci, NeuroLang is a viable option for large-scale sulcal analyses.

Part IV

CONCLUSION

13 CONCLUSION

This work focuses on bridging the gap between classical neuroanatomy and brain mapping. What we refer to as 'classical neuroanatomy' throughout this work refers to the centuries of understanding conducted by anatomists globally and often independently. We piece together various branches of cortical anatomy to understand relationships within and between different structures and regions, and associations between structure and function, structure and cortical organisation, and structure and individual correlates.

There is, nonetheless, much room for improvement and extension of our work. We will go over some of the limitations of the work we have presented, as well as possible future directions.

13.1 LIMITATIONS

We have presented the merits of using NeuroLang to chart and label sulci in a population. However, our method is far from perfect. Secondary sulci were confirmed by matching with the maximum overlap with a manually segmented corresponding sulcus. This was done to give an indication of consistency of location in the two analyses, but the overlap was nevertheless considerably low, suggesting a higher specificity but lower sensitivity. Our method therefore delivers more cohesive results on the subject level instead of on the population level for sensitivity of secondary sulci. Further work needs to be carried out to examine existence and patterns of morphology of variable sulci across individuals, as well as relationships between individual sulcal patterns and cytoarchitectonic areas, and sulcal organisation across the cortex in large samples.

13.2 FURTHER WORK

LARGER-SCALE ANALYSES NeuroLang has the potential for large-scale subject-specific representations, and we would like to put this into effect. Testing NeuroLang on a larger dataset would be the next step, and re-examining the population-level trends and organisation of sulcal stabilities.

STAR CALCULUS FOR SULCUS TRAJECTORY In this work we presented various methods for mapping sulci, but did not delve into the details of those not used in the final analyses. For example, we developed a method for representing 'trajectory' of a sulcus, or its orientation. The intention was to translate the characterisation of sulci as 'longitudinal orientation' or 'antero-inferior trajectory'. We used Star calculus, as reviewed by Dylla et al., 2017, to group each sulcus into one of four trajectory groups. As a simplification of sulcal orientations, it worked, but did not aid the queries in the localisation process, therefore this method was omitted from the final analyses. The use of Star calculus as the quantification of sulcal trajectory is an idea we strive to improve and incorporate into NeuroLang in the future.

INCORPORATING GYRI The characterisations of sulci and gyri on the cortex have always been coupled. Given their close associations, a next step in NeuroLang could be the labelling of gyri. Since sulci act as borders for gyri in many cases, the concave space in between them could be more easily identified as an expected gyrus. Thus NeuroLang could label the entire neocortex. Furthermore, we'd like to continue to develop the syntax of NeuroLang to be nearer to English.

INCORPORATING CYTOARCHITECTONICS Further down the line, we would like to incorporate other anatomical features of the cortex with sulcal mapping, chiefly, cytoarchitectonics. With the advent of probabilistic cytoarchitectonic maps, we would like to unite the efforts of cytoarchitectonic mapping with subject-specific and region-specific examination of sulcal-cytoarchitectonic relationships. Structurally, this could provide insight on connectivity of a region, individual folding patterns, or human developmental folding patterns. We thus have the potential to utilise this tool in the field of comparative anatomy. Disputed or complex sulci such as the lunate sulcus have the potential for large-scale segmentation with NeuroLang in humans at the moment, with the possibility of expanding the tool to be used for primates as well. This could be particularly useful for group-level examination of statistics of existence of this controversial sulcus in a large population.

Functionally, we would also like to investigate sulcal existence and morphology with cognitive correlates, with the potential to be used on not only healthy brains but also in pathology of the brain.

13.3 DATA SHARING

Our manual segmentation dataset is a rich dataset of ground truth neuroanatomy of sulci. Ground truth of sulci is a common element of sulcal mapping analysis, both for training and validation, as we have shown in our own work. We have shared our data with other members of the team and external teams for sulcal confirmation during training analyses for extraction and identification of sulci. We advocate for open science and availability of our manual segmentation dataset.

13.4 FINAL NOTE

We present the tool NeuroLang for mapping sulci on a large scale while retaining the morphology of sulcal individuality. One of our objectives is the individual identification of tertiary, less stable sulci which are often omitted in template-based atlases. A concept which NeuroLang preserves is the semi-hierarchical order in which classical neuroanatomists manually map the brain. Our work emphasises the difficulty in reliable identification of these less stable sulci and the need for further development of more accurate methods utilising individual cortical geometry. Our tool complements existing template-based methods for identification and labelling of the cortex. NeuroLang labels a subset of potential sulci on an unlabelled brain using spatial relations. An ample opportunity for the use of this tool is the mass identification and morphological assessment of lesser-analysed sulci, including those which are typically omitted from widely-used atlases due to their large inter-individual variability. By implementing our data-driven approach to sulcal mapping, we quantified stability of cortical features and propose a method for measuring population-level sulcal stabilities.

We demonstrate the value in individualistic sulcal identification. Sulcal morphology holds relationships to cytoarchitectonic region variability and correlates with regions of cognitive functions. On the population level, much of this variability is smoothed over. While this is beneficial for grasping overarching trends in major cortical regions, we emphasise the effort for a deeper focus on individuality in cortical morphology and its links to population anatomy, cytoarchitectonics and cognition. We thus hope that NeuroLang will be a useful addition to the field of brain mapping, one which helps bridge classical neuroanatomy and computational neuroimaging.

REFERENCES

REFERENCES

Abiteboul, S, R Hull, and V Vianu (1995). *Foundations of databases*. URL: http://www.sigmod.org/publications/dblp/db/books/dbtext/abiteboul95.html.

Aler, Ricardo, José M. Valls, and Henrik Boström (July 2020). "Study of Hellinger Distance as a splitting metric for Random Forests in balanced and imbalanced classification datasets." In: *Expert Systems with Applications* 149, p. 113264. ISSN: 09574174. DOI: 10.1016/j.eswa.2020.113264.

Allen, James F (1983). *Maintaining Knowledge about Temporal Intervals*. Tech. rep.

Allen, John S., Joel Bruss, and Hanna Damasio (Aug. 2006). "Looking for the lunate sulcus: A magnetic resonance imaging study in modern humans." In: *Anatomical Record - Part A Discoveries in Molecular, Cellular, and Evolutionary Biology* 288.8, pp. 867–876. ISSN: 0003276X. DOI: 10.1002/ar.a.20362.

Amiez, Céline, Charles R.E. Wilson, and Emmanuel Procyk (Dec. 2018). "Variations of cingulate sulcal organization and link with cognitive performance." In: *Scientific Reports* 8.1, p. 13988. ISSN: 20452322. DOI: 10.1038/s41598-018-32088-9. URL: www.nature.com/scientificreports/.

Amunts, K., A. Schleicher, and K. Zilles (Oct. 2007). *Cytoarchitecture of the cerebral cortex-More than localization*. DOI: 10.1016/j.neuroimage.2007.02.037.

Amunts, Katrin, Lutz Jäncke, Hartmut Mohlberg, Helmuth Steinmetz, and Karl Zilles (Mar. 2000). "Interhemispheric asymmetry of the human motor cortex related to handedness and gender." In: *Neuropsychologia* 38.3, pp. 304–312. ISSN: 00283932. DOI: 10.1016/S0028-3932(99)00075-5.

Amunts, Katrin, Hartmut Mohlberg, Sebastian Bludau, and Karl Zilles (Aug. 2020). "Julich-Brain: A 3D probabilistic atlas of the human brain's cytoarchitecture." In: *Science (New York, N.Y.)* 4588.July, pp. 1–10. ISSN: 1095-9203. DOI: 10.1126/science.abb4588. URL: http://www.ncbi.nlm.nih.gov/pubmed/32732281.

Amunts, Katrin, Axel Schleicher, Uli Bürgel, Hartmut Mohlberg, Harry B.M. Uylings, and Karl Zilles (Sept. 1999). "Broca's region revisited: Cytoarchitecture and intersubject variability." In: *Journal of Comparative Neurology* 412.2, pp. 319–341. ISSN: 00219967. DOI: 10.1002/(SICI)1096-9861(19990920)412:2<319::AID-CNE10>3.0.CO;2-7. URL: https:

//onlinelibrary.wiley.com/doi/full/10.1002/%28SICI%291096-9861%2819990920%29412%3A2%3C319%3A%3AAID-CNE10%3E3.0.CO%3B2-7https://onlinelibrary.wiley.com/doi/abs/10.1002/%28SICI%291096-9861%2819990920%29412%3A2%3C319%3A%3AAID-CNE10%3E3.0.CO%3B2-7https://onlinelibrary.wiley.com/doi/10.1002/(SICI)1096-9861(19990920)412:2<319::AID-CNE10>3.0.CO;2-7.

Amunts, Katrin, Peter H. Weiss, Hartmut Mohlberg, Peter Pieperhoff, Simon Eickhoff, Jennifer M. Gurd, John C. Marshall, Nadim J. Shah, Gereon R. Fink, and Karl Zilles (May 2004). "Analysis of neural mechanisms underlying verbal fluency in cytoarchitectonically defined stereotaxic space - The roles of Brodmann areas 44 and 45." In: *NeuroImage* 22.1, pp. 42–56. ISSN: 10538119. DOI: 10.1016/j.neuroimage.2003.12.031.

Armstrong, Este, Karl Zilles, Maria Curtis, and Axel Schleicher (Apr. 1991). "Cortical folding, the lunate sulcus and the evolution of the human brain." In: *Journal of Human Evolution* 20.4, pp. 341–348. ISSN: 00472484. DOI: 10.1016/0047-2484(91)90014-M.

Auzias, G., L. Brun, C. Deruelle, and O. Coulon (May 2015a). "Deep sulcal landmarks: Algorithmic and conceptual improvements in the definition and extraction of sulcal pits." In: *NeuroImage* 111, pp. 12–25. ISSN: 10959572. DOI: 10.1016/j.neuroimage.2015.02.008. URL: http://dx.doi.org/10.1016/j.neuroimage.2015.02.008.

Auzias, G., F. De Guio, A. Pepe, F. Rousseau, J.-F. Mangin, N. Girard, J. Lefevre, and O. Coulon (Apr. 2015b). "Model-driven parameterization of fetal cortical surfaces." In: *2015 IEEE 12th International Symposium on Biomedical Imaging (ISBI)*. Vol. 2015-July. IEEE, pp. 1260–1263. ISBN: 978-1-4799-2374-8. DOI: 10.1109/ISBI.2015.7164103. URL: http://ieeexplore.ieee.org/document/7164103/.

Auzias, G., J. Lefevre, A. Le Troter, C. Fischer, M. Perrot, J. Regis, and O. Coulon (2013). "Model-driven harmonic parameterization of the cortical surface: HIP-HOP." In: *IEEE Transactions on Medical Imaging* 32.5, pp. 873–887. ISSN: 02780062. DOI: 10.1109/TMI.2013.2241651.

Auzias, Guillaume, Olivier Coulon, and Andrea Brovelli (Apr. 2016). "MarsAtlas: A cortical parcellation atlas for functional mapping." In: *Human Brain Mapping* 37.4, pp. 1573–1592. ISSN: 10970193. DOI: 10.1002/hbm.23121. URL: https://pubmed.ncbi.nlm.nih.gov/26813563/.

Bailey, P and G von Bonin Urbana (1951). *The Isocortex of Man.*

Behnke, Kirsten J, Maryam E Rettmann, Dzung L Pham, Dinggang Shen, Susan M Resnick, Christos Davatzikos, and Jerry L Prince (2003). *Automatic classification of sulcal regions of the human brain cortex using pattern recognition*. Tech. rep. URL: http://iacl.ece.jhu.edu.

Bellec, Pierre, Pedro Rosa-Neto, Oliver C. Lyttelton, Habib Benali, and Alan C. Evans (July 2010). "Multi-level bootstrap analysis of stable clusters in resting-state fMRI." In: *NeuroImage* 51.3, pp. 1126–1139. ISSN:

10538119. DOI: 10.1016/j.neuroimage.2010.02.082. URL: https://pubmed.ncbi.nlm.nih.gov/20226257/.

Bludau, S., S. B. Eickhoff, H. Mohlberg, S. Caspers, A. R. Laird, P. T. Fox, A. Schleicher, K. Zilles, and K. Amunts (June 2014). "Cytoarchitecture, probability maps and functions of the human frontal pole." In: *NeuroImage* 93, pp. 260–275. ISSN: 10959572. DOI: 10.1016/j.neuroimage.2013.05.052.

Brodmann, K (2007). *Brodmann's: Localisation in the cerebral cortex*. URL: https://books.google.fr/books?hl=en&lr=&id=l1QsF0UdufgC&oi=fnd&pg=PR2&dq=Brodmann+Localisation+in+the+Cerebral&ots=_KClNVTA-k&sig=JQiBMB1U2w5XBf3cvaiaa5Xdcfw.

Catani, Marco and Michel Thiebaut de Schotten (Jan. 2013). *Atlas of Human Brain Connections*. Oxford University Press. DOI: 10.1093/med/9780199541164.001.0001.

Caviness, Verne S., James Meyer, Nikos Makris, and David N. Kennedy (1996). "MRI-based topographic parcellation of human neocortex: An anatomically specified method with estimate of reliability." In: *Journal of Cognitive Neuroscience* 8.6, pp. 566–587. ISSN: 0898929X. DOI: 10.1162/jocn.1996.8.6.566. URL: https://pubmed.ncbi.nlm.nih.gov/23961985/.

Chau, Anthony Minh Tien, Fiona Stewart, and Cristian Gragnaniello (2014). "Sulcal and gyral anatomy of the basal occipital–temporal lobe." In: *Surgical and Radiologic Anatomy* 36.10, pp. 959–965. ISSN: 12798517. DOI: 10.1007/s00276-014-1294-6. URL: https://pubmed.ncbi.nlm.nih.gov/24744138/.

Chi, Je G., Elizabeth C. Dooling, and Floyd H. Gilles (1977). "Gyral development of the human brain." In: *Annals of Neurology* 1.1, pp. 86–93. ISSN: 15318249. DOI: 10.1002/ana.410010109. URL: https://pubmed.ncbi.nlm.nih.gov/560818/.

Chomsky, N (2002). *Syntactic Structures*. Berlin: Mouton de Gruyter.

Cohen-Adad, J. (June 2014). *What can we learn from T2* maps of the cortex?* DOI: 10.1016/j.neuroimage.2013.01.023.

Community BO (2018). "Blender - a 3D modelling and rendering package." In: *Stichting Blender Foundation, Amsterdam* Available at: http://www.blender.org.

Coulon, Olivier, Fabrizio Pizzagalli, Grégory Operto, Guillaume Auzias, Chantal Delon-Martin, and Michel Dojat (2011). "Two new stable anatomical landmarks on the Central Sulcus: Definition, automatic detection, and their relationship with primary motor functions of the hand." In: *Proceedings of the Annual International Conference of the IEEE Engineering in Medicine and Biology Society, EMBS*, pp. 7795–7798. ISBN: 9781424441211. DOI: 10.1109/IEMBS.2011.6091921.

Cykowski, Matthew D., Olivier Coulon, Peter V. Kochunov, Katrin Amunts, Jack L. Lancaster, Angela R. Laird, David C. Glahn, and Peter T. Fox

(Sept. 2008). "The central sulcus: An observer-independent characterization of sulcal landmarks and depth asymmetry." In: *Cerebral Cortex* 18.9, pp. 1999–2009. ISSN: 10473211. DOI: 10.1093/cercor/bhm224. URL: https://pubmed.ncbi.nlm.nih.gov/18071195/.

Dadi, Kamalaker, Gaël Varoquaux, Antonia Machlouzarides-Shalit, Krzysztof J. Gorgolewski, Demian Wassermann, Bertrand Thirion, and Arthur Mensch (Nov. 2020). "Fine-grain atlases of functional modes for fMRI analysis." In: *NeuroImage* 221, p. 117126. ISSN: 10959572. DOI: 10.1016/j.neuroimage.2020.117126.

Dameron, Olivier, Mark A. Musen, and Bernard Gibaud (Mar. 2007). "Using semantic dependencies for consistency management of an ontology of brain-cortex anatomy." In: *Artificial Intelligence in Medicine* 39.3, pp. 217–225. ISSN: 09333657. DOI: 10.1016/j.artmed.2006.09.004.

Davison, Andrew P., Michael L. Hines, and Eilif Muller (2009). *Trends in programming languages for neuroscience simulations*. DOI: 10.3389/neuro.01.036.2009.

Desikan, Rahul S. et al. (July 2006). "An automated labeling system for subdividing the human cerebral cortex on MRI scans into gyral based regions of interest." In: *NeuroImage* 31.3, pp. 968–980. ISSN: 10538119. DOI: 10.1016/j.neuroimage.2006.01.021.

Destrieux, Christophe, Bruce Fischl, Anders Dale, and Eric Halgren (Oct. 2010). "Automatic parcellation of human cortical gyri and sulci using standard anatomical nomenclature." In: *NeuroImage* 53.1, pp. 1–15. ISSN: 10538119. DOI: 10.1016/j.neuroimage.2010.06.010.

Devlin, Joseph T. and Russell A. Poldrack (Oct. 2007). *In praise of tedious anatomy*. DOI: 10.1016/j.neuroimage.2006.09.055.

Diedrichsen, Jörn (Oct. 2006). "A spatially unbiased atlas template of the human cerebellum." In: *NeuroImage* 33.1, pp. 127–138. ISSN: 10538119. DOI: 10.1016/j.neuroimage.2006.05.056. URL: https://pubmed.ncbi.nlm.nih.gov/16904911/.

Diedrichsen, Jörn, Joshua H. Balsters, Jonathan Flavell, Emma Cussans, and Narender Ramnani (May 2009). "A probabilistic MR atlas of the human cerebellum." In: *NeuroImage* 46.1, pp. 39–46. ISSN: 10538119. DOI: 10.1016/j.neuroimage.2009.01.045.

Dockès, Jérôme, Russell A. Poldrack, Romain Primet, Hande Gözükan, Tal Yarkoni, Fabian Suchanek, Bertrand Thirion, and Gaël Varoquaux (Mar. 2020). "Neuroquery, comprehensive meta-analysis of human brain mapping." In: *eLife* 9. ISSN: 2050084X. DOI: 10.7554/eLife.53385.

Duvernoy, HM (1999). *The human brain: surface, three-dimensional sectional anatomy with MRI, and blood supply*. 2. 2nd ed. NY: Springer.

– (2005). *The human hippocampus: functional anatomy, vascularization and serial sections with MRI*. URL: https://books.google.fr/books?hl=en&

lr=&id=5GkpPjk5z1IC&oi=fnd&pg=PP9&dq=duvernoy+2005&ots=ubhx_WSBRc&sig=U0SJpJRLLVji4H-_USHhKKy6xpc.

Duvernoy, Henri M. (1988). *The Human Hippocampus*. J.F. Bergmann-Verlag. DOI: 10.1007/978-3-642-54195-7.

Dylla, Frank, Jae Hee Lee, Till Mossakowski, Thomas Schneider, André Van Delden, Jasper Van De Ven, and Diedrich Wolter (Apr. 2017). "A survey of qualitative spatial and temporal calculi: Algebraic and computational properties." In: *ACM Computing Surveys* 50.1, pp. 1–39. ISSN: 15577341. DOI: 10.1145/3038927. URL: https://dl.acm.org/doi/10.1145/3038927.

Eichert, Nicole, Kate Watkins, Rogier Mars, and Michael Petrides (Mar. 2020). "Morphological and functional variability in central and subcentral motor cortex of the human brain." In: *bioRxiv*, p. 2020.03.17.995035. DOI: 10.1101/2020.03.17.995035. URL: https://doi.org/10.1101/2020.03.17.995035.

Eickhoff, Simon B., Tomas Paus, Svenja Caspers, Marie Helene Grosbras, Alan C. Evans, Karl Zilles, and Katrin Amunts (July 2007). "Assignment of functional activations to probabilistic cytoarchitectonic areas revisited." In: *NeuroImage* 36.3, pp. 511–521. ISSN: 10538119. DOI: 10.1016/j.neuroimage.2007.03.060.

Eickhoff, Simon B., Klaas E. Stephan, Hartmut Mohlberg, Christian Grefkes, Gereon R. Fink, Katrin Amunts, and Karl Zilles (May 2005a). "A new SPM toolbox for combining probabilistic cytoarchitectonic maps and functional imaging data." In: *NeuroImage* 25.4, pp. 1325–1335. ISSN: 10538119. DOI: 10.1016/j.neuroimage.2004.12.034.

Eickhoff, Simon B., B. T.Thomas Yeo, and Sarah Genon (Nov. 2018). *Imaging-based parcellations of the human brain*. DOI: 10.1038/s41583-018-0071-7. URL: https://www.nature.com/articles/s41583-018-0071-7.

Eickhoff, Simon, Nathan B. Walters, Axel Schleicher, Jillian Kril, Gary F. Egan, Karl Zilles, John D.G. Watson, and Katrin Amunts (Mar. 2005b). "High-resolution MRI reflects myeloarchitecture and cytoarchitecture of human cerebral cortex." In: *Human Brain Mapping* 24.3, pp. 206–215. ISSN: 1065-9471. DOI: 10.1002/hbm.20082. URL: http://doi.wiley.com/10.1002/hbm.20082.

Elliot Smith, Cf (1902). *On the Morphology of the Brain in the Mammalia*. Tech. rep., p. 386.

Evans, A. C., D. L. Collins, S. R. Mills, E. D. Brown, R. L. Kelly, and T. M. Peters (1994). "3D statistical neuroanatomical models from 305 MRI volumes." In: *IEEE Nuclear Science Symposium & Medical Imaging Conference*. pt 3. Publ by IEEE, pp. 1813–1817. ISBN: 0780314875. DOI: 10.1109/nssmic.1993.373602.

Evans, Alan C., Andrew L. Janke, D. Louis Collins, and Sylvain Baillet (Aug. 2012). *Brain templates and atlases*. DOI: 10.1016/j.neuroimage.2012.01.024. URL: https://pubmed.ncbi.nlm.nih.gov/22248580/.

Falk, Dean (1985). "Apples, oranges, and the lunate sulcus." In: *American Journal of Physical Anthropology* 67.4, pp. 313–315. ISSN: 10968644. DOI: 10.1002/ajpa.1330670403. URL: https://pubmed.ncbi.nlm.nih.gov/4061586/.

Falk, Dean, Frederick E. Lepore, and Adrianne Noe (2013). "The cerebral cortex of Albert Einstein: A description and preliminary analysis of unpublished photographs." In: *Brain* 136.4, pp. 1304–1327. ISSN: 14602156. DOI: 10.1093/brain/aws295.

Fischl, Bruce (Aug. 2012). *FreeSurfer*. DOI: 10.1016/j.neuroimage.2012.01.021.

Fischl, Bruce, Arthur Liu, and Anders M. Dale (Jan. 2001). "Automated manifold surgery: Constructing geometrically accurate and topologically correct models of the human cerebral cortex." In: *IEEE Transactions on Medical Imaging* 20.1, pp. 70–80. ISSN: 02780062. DOI: 10.1109/42.906426. URL: https://pubmed.ncbi.nlm.nih.gov/11293693/.

Fischl, Bruce, Niranjini Rajendran, Evelina Busa, Jean Augustinack, Oliver Hinds, B. T.Thomas Yeo, Hartmut Mohlberg, Katrin Amunts, and Karl Zilles (Aug. 2008). "Cortical folding patterns and predicting cytoarchitecture." In: *Cerebral Cortex* 18.8, pp. 1973–1980. ISSN: 10473211. DOI: 10.1093/cercor/bhm225. URL: https://academic.oup.com/cercor/article/18/8/1973/287246.

Fischl, Bruce, Martin I. Sereno, and Anders M. Dale (1999). "Cortical surface-based analysis: II. Inflation, flattening, and a surface-based coordinate system." In: *NeuroImage* 9.2, pp. 195–207. ISSN: 10538119. DOI: 10.1006/nimg.1998.0396. URL: https://pubmed.ncbi.nlm.nih.gov/9931269/.

Fischl, Bruce, Martin I. Sereno, Roger B.H. Tootell, and Anders M. Dale (Jan. 1999). "High-resolution intersubject averaging and a coordinate system for the cortical surface." In: *Human Brain Mapping* 8.4, pp. 272–284. ISSN: 10659471. DOI: 10.1002/(SICI)1097-0193(1999)8:4<272::AID-HBM10>3.0.CO;2-4. URL: https://onlinelibrary.wiley.com/doi/full/10.1002/%28SICI%291097-0193%281999%298%3A4%3C272%3A%3AAID-HBM10%3E3.0.CO%3B2-4https://onlinelibrary.wiley.com/doi/abs/10.1002/%28SICI%291097-0193%281999%298%3A4%3C272%3A%3AAID-HBM10%3E3.0.CO%3B2-4https://onlinelibrary.wiley.com/doi/10.1002/(SICI)1097-0193(1999)8:4<272::AID-HBM10>3.0.CO;2-4.

Fischl, Bruce et al. (Jan. 2004). "Automatically Parcellating the Human Cerebral Cortex." In: *Cerebral Cortex* 14.1, pp. 11–22. ISSN: 10473211. DOI: 10.1093/cercor/bhg087. URL: https://academic.oup.com/cercor/article/14/1/11/433466.

Fornito, Alex, Sarah Whittle, Stephen J. Wood, Dennis Velakoulis, Christos Pantelis, and Murat Yücel (Nov. 2006). "The influence of sulcal variability on morphometry of the human anterior cingulate and paracingulate cortex." In: *NeuroImage* 33.3, pp. 843–854. ISSN: 10538119. DOI: 10.1016/j.neuroimage.2006.06.061. URL: https://pubmed.ncbi.nlm.nih.gov/16996751/.

Germann, Jürgen, Steve Robbins, Ulrike Halsband, and Michael Petrides (Dec. 2005). "Precentral sulcal complex of the human brain: Morphology and statistical probability maps." In: *The Journal of Comparative Neurology* 493.3, pp. 334–356. ISSN: 0021-9967. DOI: 10.1002/cne.20820. URL: http://doi.wiley.com/10.1002/cne.20820.

Glasser, Matthew F. and David C. van Essen (Aug. 2011). "Mapping human cortical areas in vivo based on myelin content as revealed by T1- and T2-weighted MRI." In: *Journal of Neuroscience* 31.32, pp. 11597–11616. ISSN: 02706474. DOI: 10.1523/JNEUROSCI.2180-11.2011. URL: http://insight-journal.org/midas/collection/view/190..

Glasser, Matthew F. et al. (Oct. 2013). "The minimal preprocessing pipelines for the Human Connectome Project." In: *NeuroImage* 80, pp. 105–124. ISSN: 10538119. DOI: 10.1016/j.neuroimage.2013.04.127.

Glasser, Matthew F. et al. (Aug. 2016). "A multi-modal parcellation of human cerebral cortex." In: *Nature* 536.7615, pp. 171–178. ISSN: 14764687. DOI: 10.1038/nature18933. URL: http://balsa.wustl.edu/WN56..

González-Castro, Víctor, Rocío Alaiz-Rodríguez, and Enrique Alegre (Jan. 2013). "Class distribution estimation based on the Hellinger distance." In: *Information Sciences* 218, pp. 146–164. ISSN: 00200255. DOI: 10.1016/j.ins.2012.05.028.

González García, Cristian, Edward Rolando Núñez-Valdez, Pablo Moreno-Ger, Rubén González Crespo, B. Cristina Pelayo G-Bustelo, and Juan Manuel Cueva Lovelle (Aug. 2019). "Agile development of multiplatform educational video games using a Domain-Specific Language." In: *Universal Access in the Information Society* 18.3, pp. 599–614. ISSN: 16155297. DOI: 10.1007/s10209-019-00681-y. URL: https://link.springer.com/article/10.1007/s10209-019-00681-y.

Hamani, Clement, Helen Mayberg, Scellig Stone, Adrian Laxton, Suzanne Haber, and Andres M. Lozano (Feb. 2011). *The subcallosal cingulate gyrus in the context of major depression*. DOI: 10.1016/j.biopsych.2010.09.034.

Harari, Yuval Noah (2011). *Sapiens-A Brief History of Humankind*. Tech. rep. URL: http://hallowesbrown.net/Sapiens%E2%80%93a_brief_history_of_humankind.pdf.

Heuer, K., Omer Faruk Gulban, Pierre Louis Bazin, Anastasia Osoianu, Romain Valabregue, Mathieu Santin, Marc Herbin, and Roberto Toro (Sept. 2019). "Evolution of neocortical folding: A phylogenetic comparative

analysis of MRI from 34 primate species." In: *Cortex* 118, pp. 275–291. ISSN: 19738102. DOI: 10.1016/j.cortex.2019.04.011.

Heuer, Katja and Roberto Toro (Dec. 2019). *Role of mechanical morphogenesis in the development and evolution of the neocortex*. DOI: 10.1016/j.plrev.2019.01.012.

Hua, Kegang, Jiangyang Zhang, Setsu Wakana, Hangyi Jiang, Xin Li, Daniel S. Reich, Peter A. Calabresi, James J. Pekar, Peter C.M. van Zijl, and Susumu Mori (Jan. 2008). "Tract probability maps in stereotaxic spaces: Analyses of white matter anatomy and tract-specific quantification." In: *NeuroImage* 39.1, pp. 336–347. ISSN: 10538119. DOI: 10.1016/j.neuroimage.2007.07.053. URL: https://pubmed.ncbi.nlm.nih.gov/17931890/.

Iaria, Giuseppe and Michael Petrides (Mar. 2007). "Occipital sulci of the human brain: Variability and probability maps." In: *The Journal of Comparative Neurology* 501.2, pp. 243–259. ISSN: 00219967. DOI: 10.1002/cne.21254. URL: http://doi.wiley.com/10.1002/cne.21254.

Im, Kiho, Hang Joon Jo, Jean Franois Mangin, Alan C. Evans, Sun I. Kim, and Jong Min Lee (Mar. 2010). "Spatial distribution of deep sulcal landmarks and hemispherical asymmetry on the cortical surface." In: *Cerebral Cortex* 20.3, pp. 602–611. ISSN: 10473211. DOI: 10.1093/cercor/bhp127. URL: https://pubmed.ncbi.nlm.nih.gov/19561060/.

Jurafsky, Daniel and James H Martin (2019). *Speech and Language Processing An Introduction to Natural Language Processing, Computational Linguistics, and Speech Recognition Third Edition draft*. Tech. rep.

Kaltenmark, Irène, Christine Deruelle, Lucile Brun, Julien Lefèvre, Olivier Coulon, and Guillaume Auzias (Dec. 2020). "Group-level cortical surface parcellation with sulcal pits labeling." In: *Medical Image Analysis* 66, p. 101749. ISSN: 13618415. DOI: 10.1016/j.media.2020.101749. URL: https://linkinghub.elsevier.com/retrieve/pii/S1361841520301134.

Keller, Simon Sean, John Robin Highley, Marta Garcia-Finana, Vanessa Sluming, Roozbeh Rezaie, and Neil Roberts (Aug. 2007). "Sulcal variability, stereological measurement and asymmetry of Broca's area on MR images." In: *Journal of Anatomy* 0.0, 070901070703001–??? ISSN: 0021-8782. DOI: 10.1111/j.1469-7580.2007.00793.x. URL: http://doi.wiley.com/10.1111/j.1469-7580.2007.00793.x.

Kennedy, D. N., N. Lange, N. Makris, J. Bates, J. Meyer, and V. S. Caviness (1998). "Gyri of the human neocortex: An MRI-based analysis of volume and variance." In: *Cerebral Cortex* 8.4, pp. 372–384. ISSN: 10473211. DOI: 10.1093/cercor/8.4.372. URL: https://pubmed.ncbi.nlm.nih.gov/9651132/.

Klein, Arno and Jason Tourville (Dec. 2012). "101 Labeled Brain Images and a Consistent Human Cortical Labeling Protocol." In: *Frontiers in*

Neuroscience 6.DEC, p. 171. ISSN: 1662-4548. DOI: 10.3389/fnins.2012.00171. URL: http://journal.frontiersin.org/article/10.3389/fnins.2012.00171/abstract.

Klein, Arno et al. (Feb. 2017). "Mindboggling morphometry of human brains." In: *PLOS Computational Biology* 13.2. Ed. by Dina Schneidman, e1005350. ISSN: 1553-7358. DOI: 10.1371/journal.pcbi.1005350. URL: https://dx.plos.org/10.1371/journal.pcbi.1005350.

Kujovic, Milenko, Karl Zilles, Aleksandar Malikovic, Axel Schleicher, Hartmut Mohlberg, Claudia Rottschy, Simon B. Eickhoff, and Katrin Amunts (Jan. 2013). "Cytoarchitectonic mapping of the human dorsal extrastriate cortex." In: *Brain Structure and Function* 218.1, pp. 157–172. ISSN: 18632653. DOI: 10.1007/s00429-012-0390-9. URL: https://link.springer.com/article/10.1007/s00429-012-0390-9.

Leroy, François et al. (Jan. 2015). "New human-specific brain landmark: The depth asymmetry of superior temporal sulcus." In: *Proceedings of the National Academy of Sciences of the United States of America* 112.4, pp. 1208–1213. ISSN: 10916490. DOI: 10.1073/pnas.1412389112. URL: www.pnas.org/cgi/doi/10.1073/pnas.1412389112.

Lohmann, Gabriele, D. Yves Von Cramon, and Alan C.F. Colchester (2008). "Deep sulcal landmarks provide an organizing framework for human cortical folding." In: *Cerebral Cortex* 18.6, pp. 1415–1420. ISSN: 14602199. DOI: 10.1093/cercor/bhm174. URL: https://pubmed.ncbi.nlm.nih.gov/17921455/.

Louboutin, Mathias, Michael Lange, Fabio Luporini, Navjot Kukreja, Philipp A. Witte, Felix J. Herrmann, Paulius Velesko, and Gerard J. Gorman (Mar. 2019). "Devito (v3.1.0): an embedded domain-specific language for finite differences and geophysical exploration." In: *Geoscientific Model Development* 12.3, pp. 1165–1187. ISSN: 1991-9603. DOI: 10.5194/gmd-12-1165-2019. URL: https://gmd.copernicus.org/articles/12/1165/2019/.

Mangin, J. F., D. Rivière, A. Cachia, E. Duchesnay, Y. Cointepas, D. Papadopoulos-Orfanos, P. Scifo, T. Ochiai, F. Brunelle, and J. Régis (Jan. 2004a). "A framework to study the cortical folding patterns." In: *NeuroImage*. Vol. 23. SUPPL. 1. Academic Press, S129–S138. DOI: 10.1016/j.neuroimage.2004.07.019.

Mangin, J.-F, D Rivière, O Coulon, C Poupon, A Cachia, Y Cointepas, J.-B Poline, D Le Bihan, J Régis, and D Papadopoulos-Orfanos (2004b). "Coordinate-based versus structural approaches to brain image analysis." In: *Artificial Intelligence in Medicine* 30, pp. 177–197. DOI: 10.1016/S0933-3657(03)00064-2.

Mangin, Jean François, Eric Jouvent, and Arnaud Cachia (Aug. 2010). *In-vivo measurement of cortical morphology: Means and meanings*. DOI: 10.

1097/WCO.0b013e32833a0afc. URL: https://pubmed.ncbi.nlm.nih.gov/20489617/.

Margulies, Daniel S., Justin L. Vincent, Clare Kelly, Gabriele Lohmann, Lucina Q. Uddin, Bharat B. Biswal, Arno Villringer, F. Xavier Castellanos, Michael P. Milham, and Michael Petrides (Nov. 2009). "Precuneus shares intrinsic functional architecture in humans and monkeys." In: *Proceedings of the National Academy of Sciences of the United States of America* 106.47, pp. 20069–20074. ISSN: 00278424. DOI: 10.1073/pnas.0905314106. URL: www.pnas.org/cgi/content/full/.

Margulies, Daniel S. et al. (Nov. 2016). "Situating the default-mode network along a principal gradient of macroscale cortical organization." In: *Proceedings of the National Academy of Sciences of the United States of America* 113.44, pp. 12574–12579. ISSN: 10916490. DOI: 10.1073/pnas.1608282113. URL: https://www.pnas.org/content/113/44/12574https://www.pnas.org/content/113/44/12574.abstract.

Martin, RF and DM Bowden (2000). "Primate brain maps." In:

Myslobodsky, M. S., J. Glicksohn, R. Coppola, and D. R. Weinberger (Jan. 1991). "Occipital lobe morphology in normal individuals assessed by magnetic resonance imaging (MRI)." In: *Vision Research* 31.10, pp. 1677–1685. ISSN: 00426989. DOI: 10.1016/0042-6989(91)90019-2.

Navarrete, Isabel, Antonio Morales, Guido Sciavicco, and M. Antonia Cardenas-Viedma (Jan. 2013). "Spatial reasoning with rectangular cardinal relations: The convex tractable subalgebra." In: *Annals of Mathematics and Artificial Intelligence* 67.1, pp. 31–70. ISSN: 10122443. DOI: 10.1007/s10472-012-9327-5. URL: https://link.springer.com/article/10.1007/s10472-012-9327-5.

Nowinski, Wieslaw L. (July 2020). *Evolution of Human Brain Atlases in Terms of Content, Applications, Functionality, and Availability*. DOI: 10.1007/s12021-020-09481-9. URL: https://doi.org/10.1007/s12021-020-09481-9.

Ochiai, Taku, Stephan Grimault, Didier Scavarda, Giorgi Roch, Tomokatsu Hori, Denis Rivière, Jean François Mangin, and Jean Régis (June 2004). "Sulcal pattern and morphology of the superior temporal sulcus." In: *NeuroImage* 22.2, pp. 706–719. ISSN: 10538119. DOI: 10.1016/j.neuroimage.2004.01.023.

Ono, M, S Kubik, and CD Abernathey (1990). "Atlas of the cerebral sulci." In:

Oosterhoff, J. and W. R. van Zwet (2012). "A Note on Contiguity and Hellinger Distance." In: *Selected Works of Willem van Zwet*. Springer New York, pp. 63–72. DOI: 10.1007/978-1-4614-1314-1{_}6. URL: https://link.springer.com/chapter/10.1007/978-1-4614-1314-1_6.

Palomero-Gallagher, Nicola, Hartmut Mohlberg, Karl Zilles, and Brent Vogt (June 2008). "Cytology and receptor architecture of human anterior

cingulate cortex." In: *Journal of Comparative Neurology* 508.6, pp. 906–926. ISSN: 00219967. DOI: 10.1002/cne.21684. URL: https://onlinelibrary.wiley.com/doi/full/10.1002/cne.21684https://onlinelibrary.wiley.com/doi/abs/10.1002/cne.21684https://onlinelibrary.wiley.com/doi/10.1002/cne.21684.

Pandya, Deepak, Benjamin Seltzer, Michael Petrides, and Patsy Benny Cipolloni (Aug. 2015). *Cerebral Cortex: Architecture, Connections, and the Dual Origin Concept*. Oxford University Press. DOI: 10.1093/med/9780195385151.001.0001.

Papoutsi, Marina, Jacco A. De Zwart, J. Martijn Jansma, Martin J. Pickering, James A. Bednar, and Barry Horwitz (Sept. 2009). "From phonemes to articulatory codes: An fMRI study of the role of broca's area in speech production." In: *Cerebral Cortex* 19.9, pp. 2156–2165. ISSN: 10473211. DOI: 10.1093/cercor/bhn239. URL: https://academic.oup.com/cercor/article/19/9/2156/282849.

Paus, Tomáš, Naim Otaky, Zografos Caramanos, David Macdonald, Alex Zijdenbos, Dina D'Avirro, Daniel Gutmans, Colin Holmes, Francesco Tomaiuolo, and Alan C. Evans (1996). "In vivo morphometry of the intrasulcal gray matter in the human cingulate, paracingulate, and superior-rostral sulci: Hemispheric asymmetries, gender differences and probability maps." In: *Journal of Comparative Neurology* 376.4, pp. 664–673. ISSN: 00219967. DOI: 10.1002/(SICI)1096-9861(19961223)376:4<664::AID-CNE12>3.0.CO;2-M. URL: https://pubmed.ncbi.nlm.nih.gov/8978477/.

Perrot, Matthieu, Denis Rivière, and Jean François Mangin (2008). "Identifying cortical sulci from localization, shape and local organization." In: *2008 5th IEEE International Symposium on Biomedical Imaging: From Nano to Macro, Proceedings, ISBI*, pp. 420–423. ISBN: 9781424420032. DOI: 10.1109/ISBI.2008.4541022.

Pizzagalli, Fabrizio et al. (Oct. 2019). "The reliability and heritability of cortical folds and their genetic correlations across hemispheres." In: *bioRxiv*, p. 795591. DOI: 10.1101/795591. URL: https://doi.org/10.1101/795591.

Poldrack, Russell A., Chris I. Baker, Joke Durnez, Krzysztof J. Gorgolewski, Paul M. Matthews, Marcus R. Munafò, Thomas E. Nichols, Jean Baptiste Poline, Edward Vul, and Tal Yarkoni (Feb. 2017). "Scanning the horizon: Towards transparent and reproducible neuroimaging research." In: *Nature Reviews Neuroscience* 18.2, pp. 115–126. ISSN: 14710048. DOI: 10.1038/nrn.2016.167. URL: https://pubmed.ncbi.nlm.nih.gov/28053326/.

Rademacher, J., A. M. Galaburda, D. N. Kennedy, P. A. Filipek, and V. S. Caviness (1992). "Human cerebral cortex: Localization, parcellation, and morphometry with magnetic resonance imaging." In: *Journal of Cognitive*

Neuroscience 4.4, pp. 352–374. ISSN: 0898929X. DOI: 10.1162/jocn.1992.4.4.352. URL: https://pubmed.ncbi.nlm.nih.gov/23968129/.

Rademacher, J., J. Rademacher, V. S. Caviness, H. Steinmetz, and A. M. Galaburda (July 1993). "Topographical variation of the human primary cortices: implications for neuroimaging, brain mapping, and neurobiology." In: *Cerebral Cortex* 3.4, pp. 313–329. ISSN: 14602199. DOI: 10.1093/cercor/3.4.313. URL: https://academic.oup.com/cercor/article/3/4/313/356342.

Rauber, André, Du Bois, and Rodrigo Geraldo Ribeiro (2019). *HMusic: A domain specific language for music programming and live coding*. Tech. rep.

Ribas, Guilherme Carvalhal (Feb. 2010). "The cerebral sulci and gyri." In: *Neurosurgical Focus* 28.2, E2. ISSN: 10920684. DOI: 10.3171/2009.11.FOCUS09245. URL: https://thejns.org/focus/view/journals/neurosurg-focus/28/2/article-pE2.xml.

Rilling, James K. (Jan. 2014). *Comparative primate neuroimaging: Insights into human brain evolution*. DOI: 10.1016/j.tics.2013.09.013.

Rivière, D, D Geffroy, I Denghien, N Souedet, and Y Cointepas (July 2009). "BrainVISA: an extensible software environment for sharing multimodal neuroimaging data and processing tools." In: *NeuroImage* 47, S163. ISSN: 10538119. DOI: 10.1016/s1053-8119(09)71720-3.

Roland, P. E. and K. Zilles (Jan. 1994). "Brain atlases - a new research tool." In: *Trends in Neurosciences* 17.11, pp. 458–467. ISSN: 01662236. DOI: 10.1016/0166-2236(94)90131-7.

Rosse, Cornelius, José L. Mejino, Bharath R. Modayur, Rex Jakobovits, Kevin P. Hinshaw, and James F. Brinkley (Jan. 1998). *Motivation and organizational principles for anatomical knowledge representation: The digital anatomist symbolic knowledge base*. DOI: 10.1136/jamia.1998.0050017. URL: https://academic.oup.com/jamia/article-lookup/doi/10.1136/jamia.1998.0050017.

Schaefer, Alexander, Ru Kong, Evan M Gordon, Timothy O Laumann, Xi-Nian Zuo, Avram J Holmes, Simon B Eickhoff, and B T Thomas Yeo (Sept. 2018). "Local-Global Parcellation of the Human Cerebral Cortex from Intrinsic Functional Connectivity MRI." In: *Cerebral Cortex* 28.9, pp. 3095–3114. ISSN: 1047-3211. DOI: 10.1093/cercor/bhx179. URL: https://pubmed.ncbi.nlm.nih.gov/28981612/.

Schmahmann, Jeremy D., Julien Doyon, David McDonald, Colin Holmes, Karyne Lavoie, Amy Hurwitz, Noor Kabani, Arthur Toga, Alan Evans, and Michael Petrides (Sept. 1999). "Three-dimensional MRI atlas of the human cerebellum in proportional stereotaxic space." In: *NeuroImage* 10.3 I, pp. 233–260. ISSN: 10538119. DOI: 10.1006/nimg.1999.0459.

Shams, Zahra, David G. Norris, and José P. Marques (July 2019). "A comparison of in vivo MRI based cortical myelin mapping using T1w/T2w

and R1 mapping at 3T." In: *PLoS ONE* 14.7. ISSN: 19326203. DOI: 10.1371/journal.pone.0218089.

Smullyan, Raymond M. (1968). *First-Order Logic*. Springer Berlin Heidelberg. DOI: 10.1007/978-3-642-86718-7.

Spasojević, Goran D., Slobodan Malobabić, Dušan Šuščević, Lazar Stijak, Valentina Nikolić, and Igor Gojković (May 2011). "Morphological variability of the subcallosal area of man." In: *Surgical and Radiologic Anatomy* 33.4, pp. 313–318. ISSN: 09301038. DOI: 10.1007/s00276-010-0689-2.

Sprung-Much, Trisanna and Michael Petrides (Mar. 2020). "Morphology and Spatial Probability Maps of the Horizontal Ascending Ramus of the Lateral Fissure." In: *Cerebral Cortex* 30.3, pp. 1586–1602. ISSN: 14602199. DOI: 10.1093/cercor/bhz189. URL: https://academic.oup.com/cercor/article/30/3/1586/5610054.

Talairach, J, G Szikla, P Tournoux, A Prosalentis, M Bordas-Ferrier, L Covello, M Iacob, and E Mempel (1967). *Atlas d'anatomie stereotaxique du telencephale.* Paris: Masson.

Talairach, J and P Tournoux (1988). *Co-planar stereotaxic atlas of the human brain.* New York: Thieme.

Thomas Yeo, B. T. et al. (Sept. 2011). "The organization of the human cerebral cortex estimated by intrinsic functional connectivity." In: *Journal of Neurophysiology* 106.3, pp. 1125–1165. ISSN: 00223077. DOI: 10.1152/jn.00338.2011. URL: www.jn.org.

Tian, Hao, Rajshekhar Sunderraman, Robert Calin-Jageman, Hong Yang, Ying Zhu, and Paul S. Katz (2006). "NeuroQL: A domain-specific query language for neuroscience data." In: *Lecture Notes in Computer Science (including subseries Lecture Notes in Artificial Intelligence and Lecture Notes in Bioinformatics)*. Vol. 4254 LNCS. Springer Verlag, pp. 613–624. ISBN: 3540467882. DOI: 10.1007/11896548{_}46. URL: https://link.springer.com/chapter/10.1007/11896548_46.

Toi, A., W. S. Lister, and K. W. Fong (Dec. 2004). "How early are fetal cerebral sulci visible at prenatal ultrasound and what is the normal pattern of early fetal sulcal development?" In: *Ultrasound in Obstetrics and Gynecology* 24.7, pp. 706–715. ISSN: 09607692. DOI: 10.1002/uog.1802. URL: https://pubmed.ncbi.nlm.nih.gov/15586358/.

Toro, Roberto and Yves Burnod (Nov. 2003). "Geometric atlas: Modeling the cortex as an organized surface." In: *NeuroImage* 20.3, pp. 1468–1484. ISSN: 10538119. DOI: 10.1016/j.neuroimage.2003.07.008.

Toro, Roberto, Peter T. Fox, and Tomáš Paus (Nov. 2008). "Functional coactivation map of the human brain." In: *Cerebral Cortex* 18.11, pp. 2553–2559. ISSN: 10473211. DOI: 10.1093/cercor/bhn014. URL: https://academic.oup.com/cercor/article/18/11/2553/291317.

Tzourio-Mazoyer, N., B. Landeau, D. Papathanassiou, F. Crivello, O. Etard, N. Delcroix, B. Mazoyer, and M. Joliot (Jan. 2002). "Automated anatom-

ical labeling of activations in SPM using a macroscopic anatomical parcellation of the MNI MRI single-subject brain." In: *NeuroImage* 15.1, pp. 273–289. ISSN: 10538119. DOI: 10.1006/nimg.2001.0978.

Urchs, Sebastian, Jonathan Armoza, Clara Moreau, Yassine Benhajali, Jolène St-Aubin, Pierre Orban, and Pierre Bellec (Mar. 2019). "MIST: A multi-resolution parcellation of functional brain networks." In: *MNI Open Research* 1, p. 3. DOI: 10.12688/mniopenres.12767.2. URL: https://doi.org/10.12688/mniopenres.12767.1.

Van Essen, D C and H A Drury (1997). *Structural and Functional Analyses of Human Cerebral Cortex Using a Surface-Based Atlas*. Tech. rep. URL: http://v1.wustl.edu/caret.html..

Van Essen, David C. (Jan. 1997). *A tension-based theory of morphogenesis and compact wiring in the central nervous system*. DOI: 10.1038/385313a0. URL: https://pubmed.ncbi.nlm.nih.gov/9002514/.

Van Harmelen, F and Porter Lifschitz V (2008). *Handbook of Knowledge Representation*. Elsevier.

Vogt, Brent A., Esther A. Nimchinsky, Leslie J. Vogt, and Patrick R. Hof (1995). "Human cingulate cortex: Surface features, flat maps, and cytoarchitecture." In: *Journal of Comparative Neurology* 359.3, pp. 490–506. ISSN: 10969861. DOI: 10.1002/cne.903590310. URL: https://pubmed.ncbi.nlm.nih.gov/7499543/.

Wassermann, Demian, Nikos Makris, Yogesh Rathi, Martha Shenton, Ron Kikinis, Marek Kubicki, and Carl Fredrik Westin (2013). "On describing human white matter anatomy: The white matter query language." In: *Lecture Notes in Computer Science (including subseries Lecture Notes in Artificial Intelligence and Lecture Notes in Bioinformatics)*. Vol. 8149 LNCS. PART 1. Springer, Berlin, Heidelberg, pp. 647–654. ISBN: 9783642408106. DOI: 10.1007/978-3-642-40811-3{_}81. URL: http://demianw.github.com/tract_querier.

– (Dec. 2016). "The white matter query language: a novel approach for describing human white matter anatomy." In: *Brain Structure and Function* 221.9, pp. 4705–4721. ISSN: 18632661. DOI: 10.1007/s00429-015-1179-4. URL: https://pubmed.ncbi.nlm.nih.gov/26754839/.

Weinberg, Richard (1905). *Die Gehirnform der Polen. Eine rassenanatomische Untersuchung. Eingeführt durch eine kurze Darstellung des Körperbaues dieses Volksstammes on JSTOR*. URL: https://www.jstor.org/stable/25745612.

Xu, Gang, Andrew K. Knutsen, Krikor Dikranian, Christopher D. Kroenke, Philip V. Bayly, and Larry A. Taber (July 2010). "Axons pull on the brain, but tension does not drive cortical folding." In: *Journal of Biomechanical Engineering* 132.7. ISSN: 01480731. DOI: 10.1115/1.4001683. URL: http://asmedigitalcollection.asme.org/biomechanical/article-pdf/132/7/071013/5772109/071013_1.pdf.

Yarkoni, Tal, Russell A. Poldrack, Thomas E. Nichols, David C. Van Essen, and Tor D. Wager (Aug. 2011). "Large-scale automated synthesis of human functional neuroimaging data." In: *Nature Methods* 8.8, pp. 665–670. ISSN: 15487091. DOI: 10.1038/nmeth.1635. URL: https://www.nature.com/articles/nmeth.1635.

Yücel, Murat, Geoffrey W. Stuart, Paul Maruff, Dennis Velakoulis, Simon F. Crowe, Greg Savage, and Christos Pantelis (2001). "Hemispheric and gender-related differences in the gross morphology of the anterior cingulate/paracingulate cortex in normal volunteers: An MRI morphometric study." In: *Cerebral Cortex* 11.1, pp. 17–25. ISSN: 10473211. DOI: 10.1093/cercor/11.1.17. URL: https://pubmed.ncbi.nlm.nih.gov/11113032/.

Yun, Hyuk Jin, Ai Wern Chung, Lana Vasung, Edward Yang, Tomo Tarui, Caitlin K. Rollins, Cynthia M. Ortinau, P. Ellen Grant, and Kiho Im (Mar. 2019). "Automatic labeling of cortical sulci for the human fetal brain based on spatio-temporal information of gyrification." In: *NeuroImage* 188, pp. 473–482. ISSN: 10959572. DOI: 10.1016/j.neuroimage.2018.12.023.

Zilles, Karl and Katrin Amunts (Feb. 2010). *Centenary of Brodmann's map conception and fate*. DOI: 10.1038/nrn2776. URL: www.nature.com/reviews/neuro.

Zilles, Karl, Este Armstrong, Axel Schleicher, and Hans Joachim Kretschmann (Nov. 1988). "The human pattern of gyrification in the cerebral cortex." In: *Anatomy and Embryology* 179.2, pp. 173–179. ISSN: 03402061. DOI: 10.1007/BF00304699. URL: https://pubmed.ncbi.nlm.nih.gov/3232854/.

Zilles, Karl et al. (1997). "Quantitative analysis of sulci in the human cerebral cortex: Development, regional heterogeneity, gender difference, asymmetry, intersubject variability and cortical architecture." In: *Human Brain Mapping*. Vol. 5. 4. Hum Brain Mapp, pp. 218–221. DOI: 10.1002/(SICI)1097-0193(1997)5:4<218::AID-HBM2>3.0.CO;2-6. URL: https://pubmed.ncbi.nlm.nih.gov/20408218/.

APPENDICES

A | SULCI IN NEUROLANG

A.1 SULCI WITH THEIR DESTRIEUX COUNTERPARTS

Sulcus name	Destrieux name
Inferior temporal sulcus	`S_temporal_inf`
Olfactory sulcus	`S_orbital_med-olfact`
Precentral sulcus	`S_precentral-sup-part` or `S_precentral-inf-part`
Superior temporal sulcus	`S_temporal_sup`
Postcentral sulcus	`S_postcentral`
Orbital H-shaped sulcus	`S_orbital-H_Shaped`
Occipitotemporal sulcus	`S_oc-temp_lat`
Intermediate primus of Jensen	`S_interm_prim-Jensen`
Inferior frontal sulcus	`S_front_inf`
Intraparietal sulcus	`S_intrapariet_and_P_trans`
Anterior occipital sulcus	`S_occipital_ant`
Subparietal sulcus	`S_subparietal`
Superior frontal sulcus	`S_front_sup`
Callosomarginal sulcus	`S_cingul-Marginalis`
Superior occipital sulcus	`S_oc_sup_and_transversal`
Collateral sulcus	`S_collat_transv_ant` or `S_collat_transv_post`
Intralingual sulcus	`S_oc-temp_med_and_Lingual`
Lateral occipital sulcus	`S_oc_middle_and_Lunatus`
Middle frontal sulcus	`S_front_middle`
Superior rostral sulcus	`S_suborbital`
Cingulate sulcus	
Paracingulate sulcus	
Inferior occipital	
Anterior parolfactory	
Lunate sulcus	
Cuneal sulcus	
Frontomarginal sulcus	
Hippocampal sulcus	
Superior parietal sulcus	
Rhinal sulcus	
Temporopolar sulcus	
Retrocalcarine sulcus	
Paracentral sulcus	
Angular sulcus	
Inferior rostral sulcus	
Intralimbic sulcus	

A.2 SULCI EXAMPLES WITH THEIR QUERIES IN FIRST-ORDER LOGIC

In response to feedback from the jury, we provide below the queries used for all 35 sulci in our NeuroLang analyses, in order, using first-order logic.

Sulcus name	Query
Inferior temporal	$\forall x$ *Inferior temporal sulcus candidate*$(x) \Leftarrow$ *overlapping antero-posteriorly of*$(x,$ **Lateral fissure**$)$ $\wedge$ *anatomical inferior of*$(x,$ **Ant. horiz. Lateral fissure**$)$ $\wedge$ *lateral sulci*(x) $\wedge\neg$ *Primary sulci*(x) $\forall x$ *Inferior temporal sulcus*$(x) \Leftarrow$ *Inferior temporal sulcus candidate*(x) $\wedge\forall y$ *(Inferior temporal sulcus candidate*$(y) \wedge x \neq y$ $\wedge$(mean x coordinates$(x) >$ mean x coordinates$(y)))$
Superior frontal	$\forall x$ *Superior frontal candidate*$(x) \Leftarrow$ (*posterior dominant of*$(x,$ **Ant. horiz. Lateral fissure**$)$ $\vee$ *overlapping antero-posteriorly of*$(x,$ **Ant. vertical Lateral fissure**$))$ $\wedge\neg$ *posteriorly dominant of*$(x,$ **Central sulcus**$)$ $\wedge$ *anatomical anterior of*$(x,$ **Lateral fissure**$)$ $\wedge$ *overlapping medially of*$(x,$ **Central sulcus**$)$ $\wedge$ *anatomical anterior of*$(x,$ **Central sulcus**$)$ $\wedge\neg$ *anatomical anterior of*$(x,$ **Ant. horiz. Lateral fissure**$)$ $\wedge$ *lateral sulci*(x) $\wedge\neg$ *Primary sulci*(x) $\forall x$ *Superior frontal sulcus*$(x) \Leftarrow$ *Superior frontal sulcus candidate*(x) $\wedge\forall y$ *(Superior frontal sulcus candidate*$(y) \wedge x \neq y$ $\wedge$(mean z coordinates$(x) >$ mean z coordinates$(y)))$

Precentral	$\forall$x *Precentral sulcus candidate*(x) $\Leftarrow$ (*posteriorly dominant of*(x, **Ant. horizontal Lateral fissure**) $\vee$ *overlapping antero-posteriorly dominant of*(x, **Ant. vertical ramus of Lateral fissure**)) $\wedge$ *anatomical anterior of*(x, **Lateral fissure**) $\wedge$ *anatomical anterior of*(x, **Central sulcus**) $\wedge$ *overlapping medially dominant of*(x, **Central sulcus**) $\wedge\neg$ *anatomical anterior of*(x, **Ant. horizontal Lateral fissure**) $\wedge$ *lateral sulci*(x) $\wedge\neg$ *Primary sulci*(x) $\forall$x *Precentral sulcus*(x) $\Leftarrow$ Precentral sulcus candidate(x) $\wedge\forall$y Precentral sulcus candidate(y) $\wedge\, x \neq y$ $\wedge$(mean y coordinates(x) $<$ mean y coordinates(y))
Occipitotemporal	$\forall$x *Occipitotemporal sulcus candidate*(x) $\Leftarrow$ (*anatomical inferior of*(x, **Parieto-occipital sulcus**) $\wedge$ *anatomical anterior of*(x, **Parieto-occipital sulcus**) $\wedge$ *lateral dominant of*(x, **Parieto-occipital sulcus**) $\wedge$ *posterior dominant of*(x, **Ant. vertical Lateral fissure**) $\wedge\neg$ *Primary sulci*(x) $\wedge\neg$ *Found sulci*(x) $\forall$x *Occipitotemporal sulcus*(x) $\Leftarrow$ Occipitotemporal sulcus candidate(x) $\wedge\forall$y Occipitotemporal sulcus candidate(y) $\wedge\, x \neq y$ $\wedge$(mean x coordinates(x) $>$ mean x coordinates(y))

Superior temporal	$\forall$x *Superior temporal sulcus candidate*(x) $\Leftarrow$ (*overlapping antero-postiorly dominant of*(x, **Lateral fissure**) $\wedge$ *lateral sulci*(x) $\wedge\neg$ *Primary sulci*(x) $\wedge\neg$ *Found sulci*(x) $\forall$x *Superior temporal sulcus*(x) $\Leftarrow$ Superior temporal sulcus candidate(x) $\wedge\forall$y Superior temporal sulcus candidate(y) $\wedge\, x \neq y$ $\wedge$(mean x coordinates(x) $>$ mean x coordinates(y))
Superior parietal	$\forall$x *Superior parietal sulcus candidate*(x) $\Leftarrow$ (*anatomical superior of*(x, **Calcarine sulcus**) $\wedge$ *overlapping medially dominant of*(x, **Parieto-occipital sulcus**) $\wedge$ *anatomical posterior of*(x, **Central sulcus**) $\wedge\neg$ *Primary sulci*(x) $\wedge\neg$ *Found sulci*(x) $\forall$x *Superior parietal sulcus*(x) $\Leftarrow$ Superior parietal sulcus candidate(x) $\wedge\forall$y Superior parietal sulcus candidate(y) $\wedge\, x \neq y$ $\wedge$(mean x coordinates(x) $<$ mean x coordinates(y))

Intermediate primus of Jensen	$\forall$x *Intermediate primus of Jensen candidate*(x) $\Leftarrow$ *posterior dominant of*(x, **Central sulcus**) $\wedge$ *anatomical superior of*(x, **Calcarine sulcus**) $\wedge$ *anterior dominant of*(x, **Parieto-occipital sulcus**) $\wedge\neg$ *medial dominant of*(x, **Lateral fissure**) $\wedge\neg$ *Primary sulci*(x) $\wedge\neg$ *Found sulci*(x) $\forall$x *Intermediate primus of Jensen*(x) $\Leftarrow$ *Intermediate primus of Jensen candidate*(x) $\wedge\forall$y (*Intermediate primus of Jensen candidate*(y) $\wedge$ $x \neq y$ $\wedge$(mean x coordinates(x) $>$ mean x coordinates(y)))
Superior rostral	$\forall$x *Superior rostral sulcus candidate*(x) $\Leftarrow$ *medial dominant of*(x, **Central sulcus**) $\wedge$ *anatomical anterior of*(x, **Central sulcus**) $\wedge$ *anatomical inferior of*(x, **Central sulcus**) $\wedge\neg$ *Primary sulci*(x) $\wedge\neg$ *Found sulci*(x) $\forall$x *Superior rostral sulcus*(x) $\Leftarrow$ *Superior rostral sulcus candidate*(x) $\wedge\forall$y (*Superior rostral sulcus candidate*(y) $\wedge$ $x \neq y$ $\wedge$(mean x coordinates(x) $<$ mean x coordinates(y)))

Subparietal	$\forall$x *Subparietal candidate*(x) $\Leftarrow$ *anatomical posterior of*(x, **Central sulcus**) $\wedge$ *superior dominant of*(x, **Lateral fissure**) $\wedge$ *anterior dominant of*(x, **Parieto-occipital sulcus**) $\wedge$ *lateral sulci*(x) $\wedge\neg$ *Primary sulci*(x) $\wedge\neg$ *Found sulci*(x) $\forall$x *Subparietal sulcus*(x) $\Leftarrow$ *Subparietal sulcus candidate*(x) $\wedge\forall$y *(Subparietal sulcus candidate*(y) $\wedge$ $x \neq y$ $\wedge$(mean x coordinates(x) $<$ mean x coordinates(y)))
Lateral occipital	$\forall$x *Lateral occipital sulcus candidate*(x) $\Leftarrow$ *anatomical posterior of*(x, **Lateral fissure**) $\wedge$ *anatomical inferior of*(x, **Lateral fissure**) $\wedge\neg$ *Primary sulci*(x) $\wedge\neg$ *Found sulci*(x) $\forall$x *Lateral occipital sulcus*(x) $\Leftarrow$ *Lateral occipital sulcus candidate*(x) $\wedge\forall$y *(Lateral occipital sulcus candidate*(y) $\wedge$ $x \neq y$ $\wedge$(mean x coordinates(x) $>$ mean x coordinates(y)))

Frontomarginal	$\forall$x *Frontomarginal candidate*(x) $\Leftarrow$ *anatomical anterior of*(x, **Central sulcus**) $\wedge$ *anatomical superior of*(x, **Ant. horiz. Lateral fissure**) $\wedge\neg$ *anatomical inferior of*(x, **Ant. vertical Lateral fissure**) $\wedge$ *lateral sulci*(x) $\wedge\neg$ *Primary sulci*(x) $\wedge\neg$ *Found sulci*(x) $\forall$x *Frontomarginal sulcus*(x) $\Leftarrow$ *Frontomarginal sulcus candidate*(x) $\wedge\forall$y (*Frontomarginal sulcus candidate*(y) $\wedge$ $x \neq y$ $\wedge$(mean z coordinates(x) $<$ mean z coordinates(y)))
Anterior occipital	$\forall$x *Anterior occipital sulcus candidate*(x) $\Leftarrow$ *anatomical inferior of*(x, **Parieto-occipita sulcus**) $\wedge$ *anatomical posterior of*(x, **Callosal sulcus**) $\wedge\neg$ *posterior dominant of*(x, **Parieto-occipital sulcus**) $\wedge\neg$ *Primary sulci*(x) $\wedge\neg$ *Found sulci*(x) $\forall$x *Anterior occipital sulcus*(x) $\Leftarrow$ *Anterior occipital sulcus candidate*(x) $\wedge\forall$y (*Anterior occipital sulcus candidate*(y) $\wedge$ $x \neq y$ $\wedge$(mean z coordinates(x) $<$ mean z coordinates(y)))

Postcentral	$\forall$x *Postcentral candidate*(x) $\Leftarrow$ *anatomical superior of*(x, **Calcarine sulcus**) $\wedge$ *overlapping supero-inferiorly dominant of*(x, **Central sulcus**) $\wedge$ *anterior dominant of*(x, **Parieto-occipital sulcus**) $\wedge\neg$ *anterior dominant of*(x, **Central sulcus**) $\wedge\neg$ *anatomical inferior of*(x, **Lateral fissure**) $\wedge$ *lateral sulci*(x) $\wedge\neg$ *Primary sulci*(x) $\wedge\neg$ *Found sulci*(x) $\forall$x *Postcentral sulcus*(x) $\Leftarrow$ *Postcentral sulcus candidate*(x) $\wedge\forall$y *(Postcentral sulcus candidate*(y) $\wedge$ $x \neq y$ $\wedge$(mean y coordinates(x) $<$ mean y coordinates(y)))
Collateral	$\forall$x *Collateral sulcus candidate*(x) $\Leftarrow$ *anatomical inferior of*(x, **Lateral fissure**) $\wedge$ *anatomical posterior of*(x, **Central sulcus**) $\wedge$ *lateral dominant of*(x, **Calcarine sulcus**) $\wedge\neg$ *Primary sulci*(x) $\wedge\neg$ *Found sulci*(x) $\forall$x *Collateral sulcus*(x) $\Leftarrow$ *Collateral sulcus candidate*(x) $\wedge\forall$y *(Collateral sulcus candidate*(y) $\wedge$ $x \neq y$ $\wedge$(mean x coordinates(x) $>$ mean x coordinates(y)))

Callosomarginal	$\forall$x *Callosomarginal candidate*(x) $\Leftarrow$ *anatomical superior of*(x, **Callosal sulcus**) $\wedge$ *medially dominant of*(x, **Central sulcus**) $\wedge$ *posterior dominant of*(x, **Central sulcus**) $\wedge\neg$ *Primary sulci*(x) $\wedge\neg$ *Found sulci*(x) $\forall$x *Callosomarginal sulcus*(x) $\Leftarrow$ *Callosomarginal sulcus candidate*(x) $\wedge\forall$y *(Callosomarginal sulcus candidate*(y) $\wedge$ $x \neq y$ $\wedge$(mean z coordinates(x) $>$ mean z coordinates(y)))
Inferior frontal	$\forall$x *Inferior frontal sulcus candidate*(x) $\Leftarrow$ *anatomical anterior of*(x, **Central sulcus**) $\wedge$ *anatomical superior of*(x, **Ant. horizontal Lateral fissure**) $\wedge$ *lateral sulci*(x) $\wedge\neg$ *Primary sulci*(x) $\wedge\neg$ *Found sulci*(x) $\forall$x *Inferior frontal sulcus*(x) $\Leftarrow$ *Inferior frontal sulcus candidate*(x) $\wedge\forall$y *(Inferior frontal sulcus candidate*(y) $\wedge$ $x \neq y$ $\wedge$(mean x coordinates(x) $>$ mean x coordinates(y)))

Olfactory	$\forall$x *Olfactory candidate*(x) $\Leftarrow$ *anatomical anterior of*(x, **Ant. vertical Lateral fissure**) $\wedge$ *anatomical inferior of*(x, **Ant. horiz. Lateral fissure**) $\wedge$ *medial dominant of*(x, **Lateral fissure**) $\wedge\neg$ *Primary sulci*(x) $\wedge\neg$ *Found sulci*(x) $\forall$x *Olfactory sulcus*(x) $\Leftarrow$ *Olfactory sulcus candidate*(x) $\wedge\forall$y (*Olfactory sulcus candidate*(y) $\wedge$ $x \neq y$ $\wedge$(mean y coordinates(x) $>$ mean y coordinates(y)))
Orbital H-shaped	$\forall$x *Orbital H-shaped sulcus candidate*(x) $\Leftarrow$ *anatomical anterior of*(x, **Ant. horiz. Lateral fissure**) $\wedge$ *anatomical inferior of*(x, **Calcarine sulcus**) $\wedge$ *medial dominant of*(x, **Lateral fissure**) $\wedge\neg$ *Primary sulci*(x) $\wedge\neg$ *Found sulci*(x) $\forall$x *Orbital H-shaped sulcus*(x) $\Leftarrow$ *Orbital H-shaped sulcus candidate*(x) $\wedge\forall$y (*Orbital H-shaped sulcus candidate*(y) $\wedge$ $x \neq y$ $\wedge$(mean z coordinates(x) $<$ mean z coordinates(y)))

Intraparietal	$\forall x$ *Intraparietal candidate*$(x) \Leftarrow$ *anatomical posterior of*$(x,$ **Central sulcus**$)$ $\wedge$ *anatomical superior of*$(x,$ **Lateral fissure**$)$ $\wedge$ *anatomical anterior of*$(x,$ **Parieto-occipital sulcus**$)$ $\wedge\neg$ *Primary sulci*(x) $\wedge\neg$ *Found sulci*(x) $\forall x$ *Intraparietal sulcus*$(x) \Leftarrow$ *Intraparietal sulcus candidate*(x) $\wedge\forall y$ *(Intraparietal sulcus candidate*$(y) \wedge x \neq y$ $\wedge$(mean x coordinates$(x) >$ mean x coordinates$(y)))$
Intralingual	$\forall x$ *Intralingual sulcus candidate*$(x) \Leftarrow$ *anatomical inferior of*$(x,$ **Parieto-occipital sulcus**$)$ $\wedge$ *anatomical posterior of*$(x,$ **Callosal sulcus**$)$ $\wedge$ *medial dominant of*$(x,$ **Lateral fissure**$)$ $\wedge\neg$ *Primary sulci*(x) $\wedge\neg$ *Found sulci*(x) $\forall x$ *Intralingual sulcus*$(x) \Leftarrow$ *Intralingual sulcus candidate*(x) $\wedge\forall y$ *(Intralingual sulcus candidate*$(y) \wedge x \neq y$ $\wedge$(mean z coordinates$(x) <$ mean z coordinates$(y)))$

Cingulate	$\forall$x *Cingulate sulcus candidate*(x) $\Leftarrow$ *anterior of*(x, **Callosal sulcus**) $\wedge$ *superior of*(x, **Callosal sulcus**) $\wedge\neg$ *posteriorly dominant of*(x, **Callosal sulcus**) $\wedge$ *medially dominant of*(x, **Central sulcus**) $\wedge\neg$ *Primary sulci*(x) $\wedge\neg$ *Found sulci*(x) $\forall$x *Cingulate sulcus*(x) $\Leftarrow$ *Cingulate sulcus candidate*(x) $\wedge\forall$y (*Cingulate sulcus candidate*(y) $\wedge$ $x \neq y$ $\wedge$(mean y coordinates(x) $<$ mean y coordinates(y)))
Paracingulate	$\forall$x *Paracingulate sulcus candidate*(x) $\Leftarrow$ *anterior of*(x, **Callosal sulcus**) $\wedge$ *superior of*(x, **Callosal sulcus**) $\wedge$ *medial dominant of*(x, **Central sulcus**) $\wedge\neg$ *posterior dominant of*(x, **Central sulcus**) $\wedge\neg$ *Primary sulci*(x) $\wedge\neg$ *Found sulci*(x) $\forall$x *Paracingulate sulcus*(x) $\Leftarrow$ *Paracingulate sulcus candidate*(x) $\wedge\forall$y (*Paracingulate sulcus candidate*(y) $\wedge$ $x \neq y$ $\wedge$(mean y coordinates(x) $>$ mean y coordinates(y)))

Inferior occipital	$\forall$x *Inferior occipital sulcus candidate*(x) $\Leftarrow$ *anatomical inferior of*(x, **Parieto-occipital sulcus**) $\wedge$ *anatomical posterior of*(x, **Lateral fissure**) $\wedge\neg$ *anatomical anterior of*(x, **Parieto-occipital sulcus**) $\wedge$ *medially dominant of*(x, **Central sulcus**) $\wedge$ *lateral sulci*(x) $\wedge\neg$ *Found sulci*(x) $\wedge\neg$ *Primary sulci*(x) $\forall$x *Inferior occipital sulcus*(x) $\Leftarrow$ *Inferior occipital sulcus candidate*(x) $\wedge\forall$y *(Inferior occipital sulcus candidate*(y) $\wedge$ $x \neq y$ $\wedge$(mean z coordinates(x) $<$ mean z coordinates(y)))
Inferior rostral	$\forall$x *Inferior rostral sulcus candidate*(x) $\Leftarrow$ *anatomical anterior of*(x, **Lateral fissure**) $\wedge$ *inferior of*(x, **Callosal sulcus**) $\wedge$ *inferior dominant of*(x, **Callosal sulcus**) $\wedge$ *medial dominant of*(x, **Central sulcus**) $\wedge\neg$ *Primary sulci*(x) $\wedge\neg$ *Found sulci*(x) $\forall$x *Inferior rostral sulcus*(x) $\Leftarrow$ *Inferior rostral sulcus candidate*(x) $\wedge\forall$y *(Inferior rostral sulcus candidate*(y) $\wedge$ $x \neq y$ $\wedge$(mean z coordinates(x) $<$ mean z coordinates(y)))

Retrocalcarine	$\forall$x *Retrocalcarine sulcus candidate*(x) $\Leftarrow$ *anatomical posterior of*(x, **Parieto-occipital sulcus**) $\wedge$ *anatomical inferior dominant of*(x, **Parieto-occipital sulcus**) $\wedge$ *overlapping medially dominant of*(x, **Calcarine sulcus**) $\wedge\neg$ *Primary sulci*(x) $\wedge\neg$ *Found sulci*(x) $\forall$x *Retrocalcarine sulcus*(x) $\Leftarrow$ *Retrocalcarine sulcus candidate*(x) $\wedge\forall$y *(Retrocalcarine sulcus candidate*(y) $\wedge$ $x \neq y$ $\wedge$(mean y coordinates(x) $<$ mean y coordinates(y)))
Lunate	$\forall$x *Lunate sulcus candidate*(x) $\Leftarrow$ *anatomical posterior of*(x, **Calcarine sulcus**) $\wedge$ *overlapping medially dominant of*(x, **Calcarine sulcus**) $\wedge\neg$ *anatomical superior of*(x, **Callosal sulcus**) $\wedge\neg$ *anatomical inferior of*(x, **Calcarine sulcus**) $\wedge\neg$ *Primary sulci*(x) $\wedge\neg$ *Found sulci*(x) $\forall$x *Lunate sulcus*(x) $\Leftarrow$ *Lunate sulcus candidate*(x) $\wedge\forall$y *(Lunate sulcus candidate*(y) $\wedge$ $x \neq y$ $\wedge$(mean y coordinates(x) $<$ mean y coordinates(y)))

Middle frontal	$\forall$x *Middle frontal sulcus candidate*(x) $\Leftarrow$ *anatomical anterior of*(x, **Ant. horiz. Lateral fissure**) $\wedge\neg$ *Primary sulci*(x) $\wedge\neg$ *Found sulci*(x) $\forall$x *Middle frontal sulcus*(x) $\Leftarrow$ *Middle frontal sulcus candidate*(x) $\wedge\forall$y *(Middle frontal sulcus candidate*(y) $\wedge\, x \neq y$ $\wedge$(mean y coordinates(x) $>$ mean y coordinates(y)))
Hippocampal	$\forall$x *Hippocampal sulcus candidate*(x) $\Leftarrow$ *anatomical posterior of*(x, **Ant. vertical Lateral fissure**) $\wedge$ (*lateral dominant of*(x, **Callosal sulcus**) $\vee$ *overlapping antero-posteriorly dominant of*(x, **Callosal sulcus**)) $\wedge$ *anatomical inferior of*(x, **Lateral fissure** $\wedge\neg$ *lateral dominant of*(x, **Lateral fissure**) $\wedge\neg$ *Primary sulci*(x) $\wedge\neg$ *Found sulci*(x) $\forall$x *Hippocampal sulcus*(x) $\Leftarrow$ *Hippocampal sulcus candidate*(x) $\wedge\forall$y *(Hippocampal sulcus candidate*(y) $\wedge\, x \neq y$ $\wedge$(mean x coordinates(x) $<$ mean x coordinates(y)))

Superior occipital	$\forall$x *Superior occipital sulcus candidate*(x) $\Leftarrow$ *anatomical superior of*(x, **Callosal sulcus**) $\wedge$ *posterior dominant of*(x, **Central sulcus**) $\wedge\neg$ *Primary sulci*(x) $\wedge\neg$ *Found sulci*(x) $\forall$x *Superior occipital sulcus*(x) $\Leftarrow$ *Superior occipital sulcus candidate*(x) $\wedge\forall$y *(Superior occipital sulcus candidate*(y) $\wedge\, x \neq y$ $\wedge$(mean y coordinates(x) $>$ mean y coordinates(y)))
Rhinal	$\forall$x *Rhinal sulcus candidate*(x) $\Leftarrow$ *anatomical inferior of*(x, **Ant. horiz. Lateral fissure**) $\wedge$ *medial dominant of*(x, **Lateral fissure**) $\wedge\neg$ *Primary sulci*(x) $\wedge\neg$ *Found sulci*(x) $\forall$x *Rhinal sulcus*(x) $\Leftarrow$ *Rhinal sulcus candidate*(x) $\wedge\forall$y *(Rhinal sulcus candidate*(y) $\wedge\, x \neq y$ $\wedge$(mean y coordinates(x) $>$ mean y coordinates(y)))

Temporopolar	$\forall$x *Temporopolar sulcus candidate*(x) $\Leftarrow$ *anatomical inferior of*(x, **Calcarine sulcus**) $\wedge$ *anatomical posterior of*(x, **Ant. horiz. Lateral fissure**) $\wedge\neg$ *anatomical anterior of*(x, **Ant. vertical Lateral fissure**) $\wedge\neg$ *Primary sulci*(x) $\wedge\neg$ *Found sulci*(x) $\forall$x *Temporopolar sulcus*(x) $\Leftarrow$ *Temporopolar sulcus candidate*(x) $\wedge\forall$y *(Temporopolar sulcus candidate*(y) $\wedge\, x \neq y$ $\wedge$(mean z coordinates(x) $<$ mean z coordinates(y)))
Cuneal	$\forall$x *Cuneal sulcus candidate*(x) $\Leftarrow$ (*posterior dominant of*(x, **Parieto-occipital sulcus**) $\vee$ *overlapping antero-posteriorly dominant of*(x, **Parieto-occipital sulcus**)) $\wedge\neg$ *anatomical inferior of*(x, **Parieto-occipital sulcus**) $\wedge\neg$ *anatomical anterior of*(x, **Parieto-occipital sulcus**) $\wedge\neg$ *lateral dominant of*(x, **Parieto-occipital sulcus**) $\wedge\neg$ *anatomical posterior of*(x, **Calcarine sulcus**) $\wedge\neg$ *Primary sulci*(x) $\wedge\neg$ *Found sulci*(x) $\forall$x *Cuneal sulcus*(x) $\Leftarrow$ *Cuneal sulcus candidate*(x) $\wedge\forall$y *(Cuneal sulcus candidate*(y) $\wedge\, x \neq y$ $\wedge$(mean x coordinates(x) $<$ mean x coordinates(y)))

Paracentral	$\forall$x *Paracentral sulcus candidate*(x) $\Leftarrow$ *anatomical superior of*(x, **Parieto-occipital sulcus**) $\wedge$ *medial dominant of*(x, **Central sulcus**) $\wedge\neg$ *Primary sulci*(x) $\wedge\neg$ *Found sulci*(x) $\forall$x *Paracentral sulcus*(x) $\Leftarrow$ *Paracentral sulcus candidate*(x) $\wedge\forall$y (*Paracentral sulcus candidate*(y) $\wedge$ $x \neq y$ $\wedge$(mean x coordinates(x) $<$ mean x coordinates(y)))
Angular	$\forall$x *Angular sulcus candidate*(x) $\Leftarrow$ (*anatomical posterior of*(x, **Central sulcus**) $\wedge$ *anterior dominant of*(x, **Parieto-occipital sulcus**) $\wedge$ *lateral dominant of*(x, **Central sulcus**) $\wedge\neg$ *anatomical inferior of*(x, **Parieto-occipital sulcus**) $\wedge\neg$ *Primary sulci*(x) $\wedge\neg$ *Found sulci*(x) $\forall$x *Angular sulcus*(x) $\Leftarrow$ *Angular sulcus candidate*(x) $\wedge\forall$y (*Angular sulcus candidate*(y) $\wedge$ $x \neq y$ $\wedge$(mean x coordinates(x) $>$ mean x coordinates(y)))
Intralimbic	$\forall$x *Intralimbic sulcus candidate*(x) $\Leftarrow$ *anatomical anterior of*(x, **Parieto-occipital sulcus**) $\wedge$ *medial dominant of*(x, **Callosal sulcus**) $\wedge$ *superior dominant of*(x, **Callosal sulcus**) $\wedge\neg$ *Primary sulci*(x) $\wedge\neg$ *Found sulci*(x) $\forall$x *Intralimbic sulcus*(x) $\Leftarrow$ *Intralimbic sulcus candidate*(x) $\wedge\forall$y (*Intralimbic sulcus candidate*(y) $\wedge$ $x \neq y$ $\wedge$(mean x coordinates(x) $<$ mean x coordinates(y)))

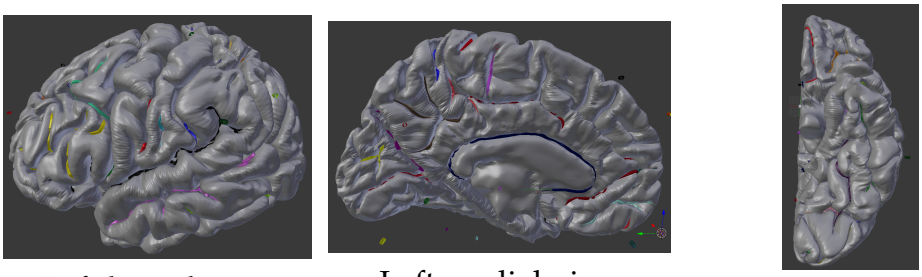

Left lateral view | Left medial view | Left ventral view

Figure A.1: Manual segmentations of one left hemisphere of a Human Connectome Project dataset subject. Segmentations were done on the pial surface, labelling the fundus of each sulcus.

A.3 MANUAL SEGMENTATIONS IN BLENDER

The pial surface of each subject's T1 image was converted to a mesh in the polygon file format which was used in the tool Blender. Each sulcus was segmented starting from the end points where it folded inwards, and followed along the fundus of the sulcus until reaching the end of the sulcus where convexity ended. An example in the left hemisphere is presented in Figure A.1. Segmentations were performed using subject space. The sulci per hemisphere were then extracted with their labels in the wavefront object file format.

In each hemisphere, 5 primary sulci were labelled first. Next, the prominent secondary sulci in each lobe, which varied from 16 to 20. Finally, any remaining sulci were identified based on the definitions in our literature review, and confirmed with Dr Nikos Makris.

The extracted manual segmentations for each subject were added into the NeuroLang domain as symbols, with the sulcus name as the symbol name, and the coordinates of the sulcal label as the symbol values. The values could be in arrays of either Cartesian coordinates (e.g. [-10.02, 20.00, 3.58]) or mesh node coordinates (e.g. [28 40 15]).

This supplementary information was provided in response to feedback from the jury.

CONTRIBUTIONS

- Machlouzarides-Shalit, A, Gallardo, G, Wassermann, D. (2018) 'Sulcal neuroanatomy and relative relationships using spatial gradients', *Organisation of Human Brain Mapping*. https://hal.archives-ouvertes.fr/hal-02957840.
- Machlouzarides-Shalit, A, Makris, N, Iovene, V, Wassermann, D. (2019) 'A novel sulcal hierarchy based on manually labelled sulci', *Organisation of Human Brain Mapping*. https://hal.archives-ouvertes.fr/hal-02347268.
- Dadi, Kamalaker, Gaël Varoquaux, Antonia Machlouzarides-Shalit, Krzysztof J. Gorgolewski, Demian Wassermann, Bertrand Thirion, and Arthur Mensch (2020). "Fine-grain atlases of functional modes for fMRI analysis." *NeuroImage*, 221, p. 117126. issn: 10959572. doi:10.1016/j.neuroimage.2020.117126., https://hal.archives-ouvertes.fr/hal-02904869.
- Machlouzarides-Shalit, A, Zanitti, G, Makris, N, Iovene, V, Favelier, G, Lemaitre, G, Wassermann, D. (2020) 'NeuroLang: representing neuroanatomy with sulcus-specific queries', *Organisation of Human Brain Mapping*. https://hal.archives-ouvertes.fr/hal-02879734.
- Machlouzarides-Shalit, A, Zanitti, G, Makris, N, Iovene, V, Zdanovitch, N, Wassermann, D. (2020), 'NeuroLang: representing neuroanatomy with sulcus-specific queries', *in prep*.

université PARIS-SACLAY

ÉCOLE DOCTORALE
Sciences et technologies de l'information et de la communication (STIC)

Titre: Développement de représentations neuroanatomiques individuelles via un langage de Domaine-Spécifique

Mots clés: Sulci, NeuroLang, Cartographie du cerveau, langage de domaine-specifique, requete

Résumé: Dans le domaine de la cartographie cérébrale, nous avons identifié le besoin d'un outil fondé sur la connaissance détaillée des sulci. Dans cette thèse, nous développons un nouvel outil de cartographie cérébrale appelé NeuroLang, qui s'appuie sur la géométrie spatiale du cerveau.
Nous avons abordé cette question avec deux approches: premièrement, nous avons fermement fondé notre théorie sur la neuroanatomie classique. Deuxièmement, nous avons conçu et implémenté des méthodes pour les requêtes spécifiques au sulcus dans le langage spécifique au domaine, NeuroLang. Nous avons testé notre méthode sur 52 sujets et évalué les performances de NeuroLang pour des cartographie du cortex spécifiques à la population et au sujet. Ensuite, nous proposons une nouvelle organisation hiérarchique basée sur les données de la stabilité sulcal appuyée sur ces données.
Pour conclure, nous avons résumé l'implication de notre méthode dans le domaine actuel, ainsi que notre contribution globale au domaine de la cartographie cérébrale.

Title: Development of subject-specific representations of neuroanatomy via a domain-specific language

Keywords: Sulci, NeuroLang, Brain mapping, Domain-specific language, Query

Abstract: Within the field of brain mapping, we identified the need for a tool which is grounded in the detailed knowledge of individual variability of sulci. In this thesis, we develop a new brain mapping tool called NeuroLang, which utilises the spatial geometry of the brain.
We approached this challenge with two perspectives: firstly, we grounded our theory firmly in classical neuroanatomy. Secondly, we designed and implemented methods for sulcus-specific queries in the domain-specific language, NeuroLang. We tested our method on 52 subjects and evaluated the performance of NeuroLang for population and subject-specific representations of neuroanatomy. Then, we present our novel, data-driven hierarchical organisation of sulcal stability.
To conclude, we summarise the implication of our method within the current field, as well as our overall contribution to the field of brain mapping.

Université Paris-Saclay
Espace Technologique / Immeuble Discovery
Route de l'Orme aux Merisiers RD 128 / 91190 Saint-Aubin, France